National Aeronautics and Space Administration

Changes on Titan’s Earth-like surface

Principal Investigator: Anezina Solomonidou (3220)

R.M.C. Lopes (3220); **A. Coustenis** (Observatory of Paris, FR); **S. Rodriguez** (AIM Laboratory, FR); **M. Malaska** (3227); **C. Sotin** (4000); **K. Lawrence** (4000); **M. Janssen** (1191); **R.H. Brown** (University of Arizona, USA)

Introduction & Problem

Titan, Saturn’s largest satellite, has a complex atmosphere and surface, making it a key area for planetary research.

Understanding the interplay of geologic processes on Titan is important for:

- ✧ **modelling the interior-surface-atmospheric interactions**
- ✧ **finding the CH_4 source**
- ✧ **climate evolution**
- ✧ **Unveiling surface compositions**
- ✧ **constraining habitability**

Geologically active areas could be utilized as future mission landing sites

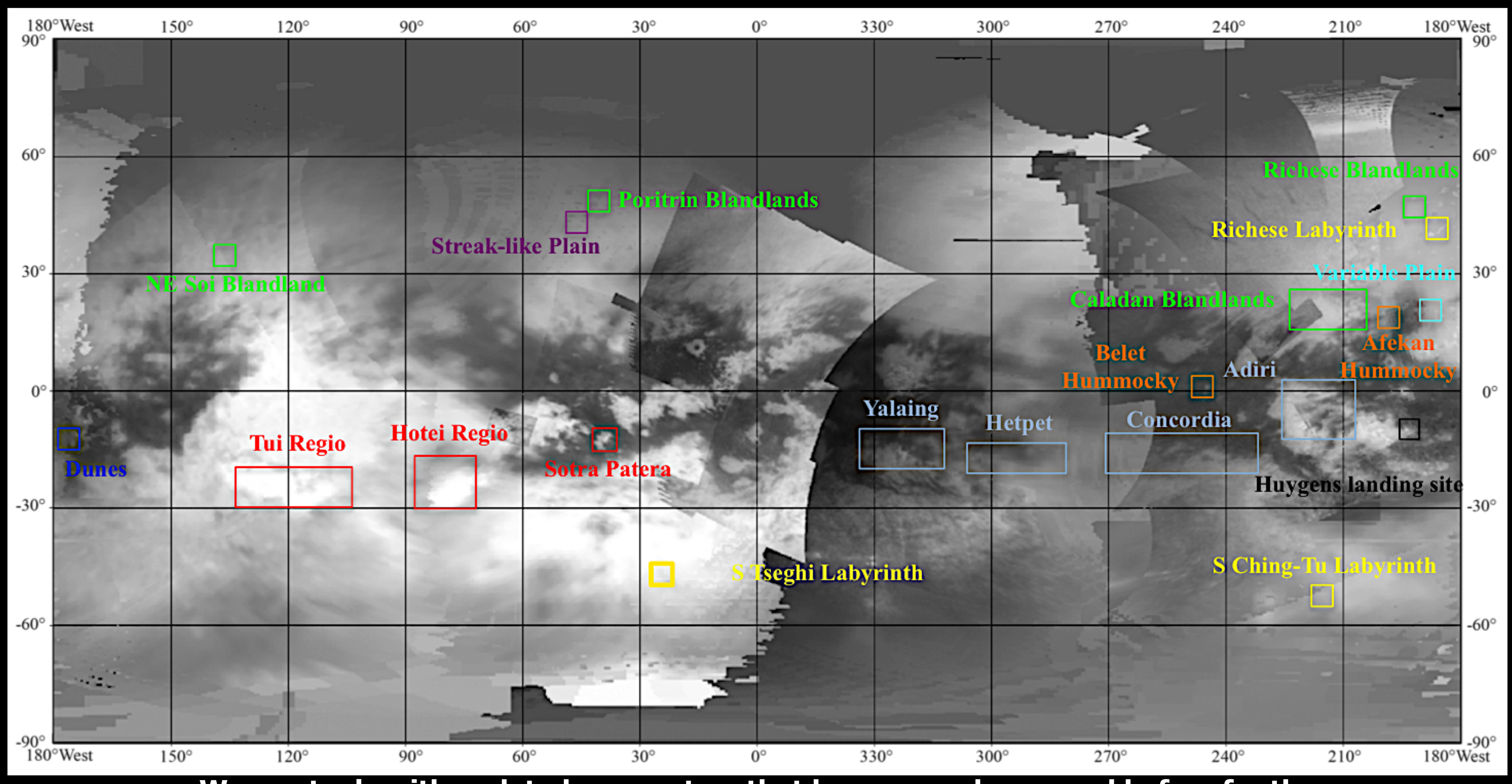

We use tools with updated parameters that have never been used before for the investigation of Titan’s surface.

Data & Method

Studying Titan’s surface requires specific tools

VIMS processed with Radiative Transfer code

✧ **aerosol and methane opacity characteristics**

All inferences of surface properties need to first account for the atmospheric contribution to the data.

We evaluate whether surface features change appearance with time accounting for

- ✧ **atmosphere**
- ✧ **surface albedo**
- ✧ **Changes indicate active processes (possibly endogenic)**

Solomonidou et al. (2014; 2015)

Temporal Evolution Of Surface Albedo (Wrt To HLS)

Geomorphic Unit Groups

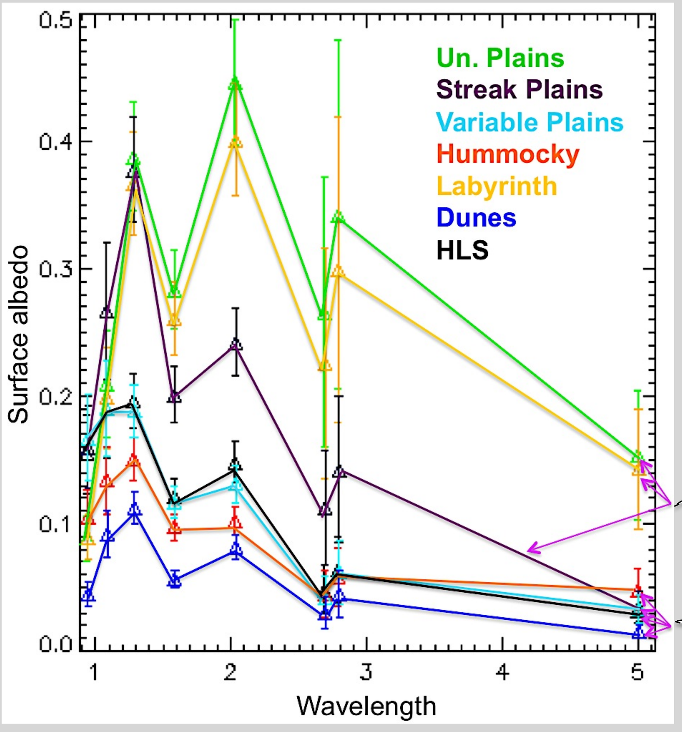

Based on surface albedo extractions

Group A:
Un. Plains
Labyrinth
Streak Plains

Group B:
Hummocky
Variable Plains
HLS
Dunes

RESULTS

Group A: ***Tholin-like material***

Group B: ***Very dark material***

Albedo As A Function Of Time

We tested the temporal evolution of:

Un. Plains
Cryo candidates
Dunes
Surrounding

Blandlands (2010-2012)
Hotei Regio (2005-2009)
Tui Regio (2005-2009)
Sotra Patera (2004-2006)
Test cases (dunes)

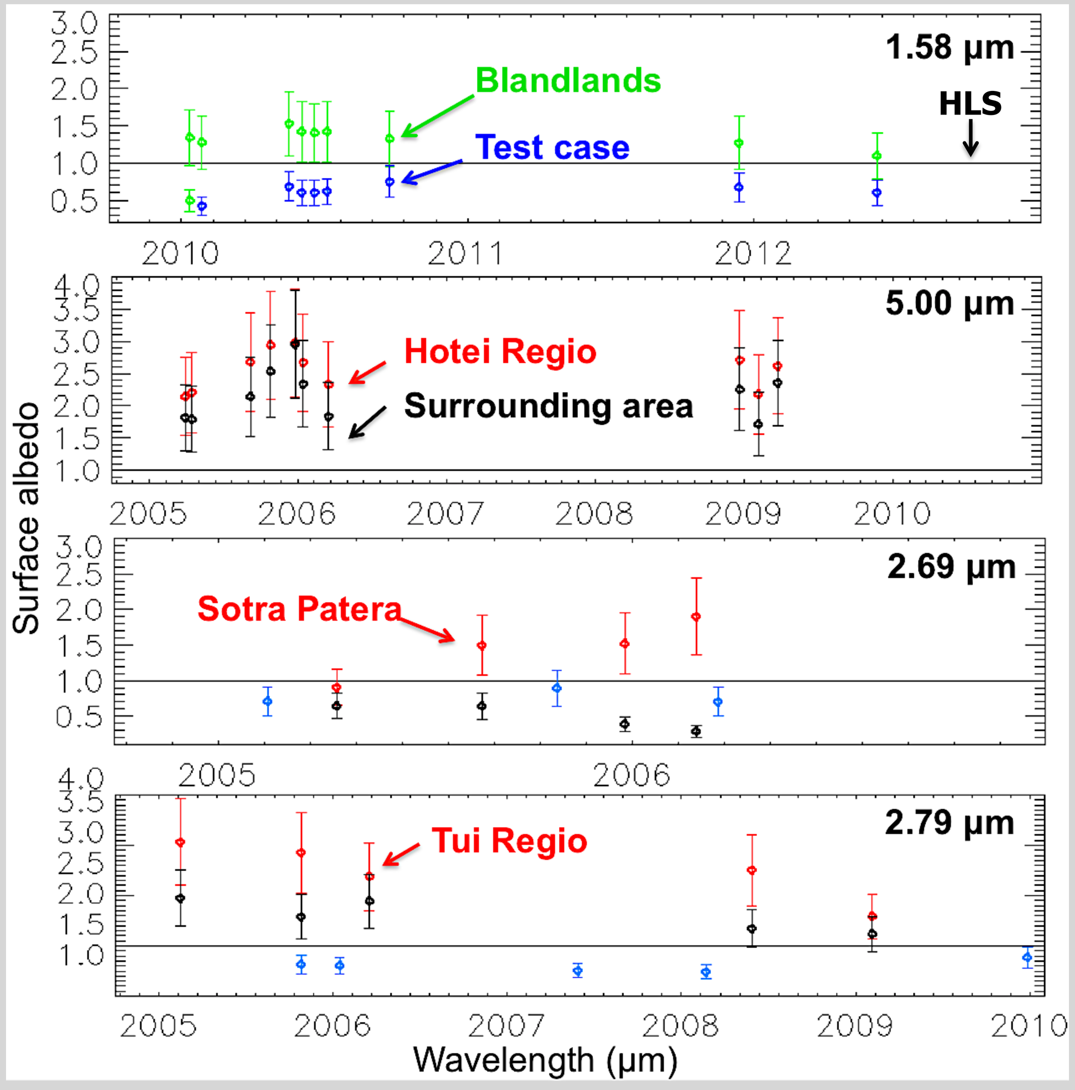

RESULTS
Blandlands **NO CHANGE**
Hotei Regio **NO CHANGE**
Tui Regio **50% DARKER**
Sotra Patera **2x BRIGHTER**

From Solomonidou et al. (2015); Sotin et al. (2015)

Conclusions and Next Steps

Tested areas	Change in albedo	Possible chemical compound
Tui Regio (2005-2009)	✓ (Solomonidou et al. 2015)	CO_2 (disappearance of CO_2 due to methane rainfall and cover up)
Hotei Regio (2004-2009)	✗ (Solomonidou et al. 2015)	-
Sotra Patera (2005-2006)	✓ (Solomonidou et al. 2015)	Deposition or exposure of bright material
Blandlands (2010-2012)	✗ (Solomonidou et al.; Lopes et al. 2015)	50-75% Tholin material
Test cases A,B,C (dune fields 2005-2012)	✗ (Solomonidou et al. 2015)	Bitumen material
Labyrinth, Streak Plains, Variable Plains Hummocky	Ongoing (Solomonidou et al. in prep.)	60-80% Tholin material 55% Tholin material 50-70% Bitumen material 40-65% Bitumen material
Evaporitic candidates (Yalaing, Hetpet, Concordia, Adiri)	Ongoing (Solomonidou et al. in prep.)	-
HLS (2004-2012)	ongoing (Sotin et al. in prep.)	-

ONGOING

The results of this analysis will shed light on geological process origination causing albedo changes with time.

Exogenic Processes

- ✧Evaporitic, fluvial, or lacustrine deposits
- ✧no connection to the interior
- ✧precipitation of methane rain and/or tholins

Endogenic Processes

- ✧Cryovolcanic deposits
- ✧Brightening or darkening due to resurfacing of an initially cryovolcanic terrain

IMPORTANCE

-energy
-methane reservoir
-interior/surface/atmosphere exchanges
-support for life

National Aeronautics and Space Administration

Jet Propulsion Laboratory
California Institute of Technology
Pasadena, California

www.nasa.gov

This research was supported by an appointment to the NASA Postdoctoral Program at the Jet Propulsion Laboratory, administered by Oak Ridge Associated Universities through a contract with NASA.

Papers from this work while at JPL:
1. **Solomonidou et al.** *(2014).* Surface albedo spectral properties of geologically interesting areas on Titan. JGR, 119, 1729-1747.
2. *Sohl,* **Solomonidou et al.** *(2014).* Structural and tidal models of Titan and inferences on cryovolcanism. JGR, 119, 1013-1036.
3. **Solomonidou et al.** *(2015).* Temporal variations of Titan’s surface with Cassini/VIMS. Published at Icarus, available online.
4. *Lopes,* **Solomonidou et al.** *(2015). Nature, Distribution, and Origin of Titan’s Undifferentiated Plains. Sibmitted at Icarus.*
4. *Sotin,* **Solomonidou et al***. (2015). In preparation.*

Poster No. P-2

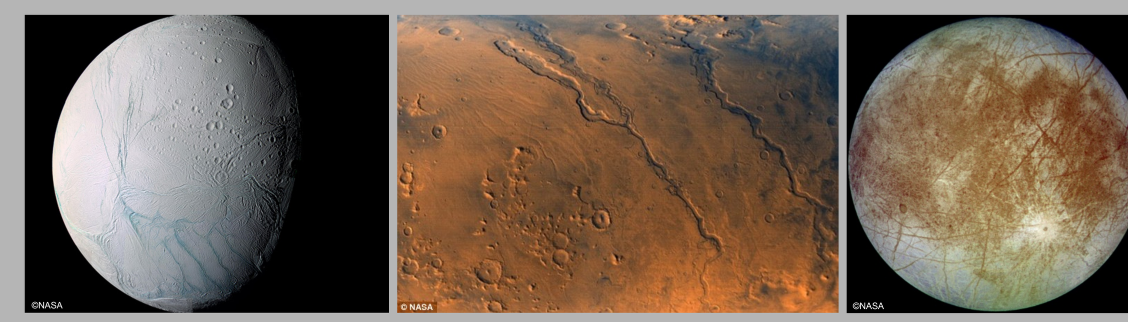

National Aeronautics and Space Administration

Development of a Chiral Amino Acid Separation by Microchip Electrophoresis for Analysis of Extraterrestrial Samples

Principal Investigator: Jessica S. Creamer (389K)
Maria F. Mora (389K) and Peter A. Willis (389K)

Objective

To develop a method for measuring the chiral distribution of at least twenty different amino acids in a soil, water, or ice sample with limits of detection at 1 part per billion (ppb) or lower.

Background

- The search for life in our Solar System is one of the highest priorities at NASA
- Amino acids are one of the building blocks of life that can be used as specific biomarkers
- Determining the chirality of amino acids can determine the biotic or abiotic origin of the sample

<u>"The Lego Principle"</u>

- Abiotic processes generally produce samples containing smooth distributions of molecular properties
- Biotic processes only use specific subsets of these distributions

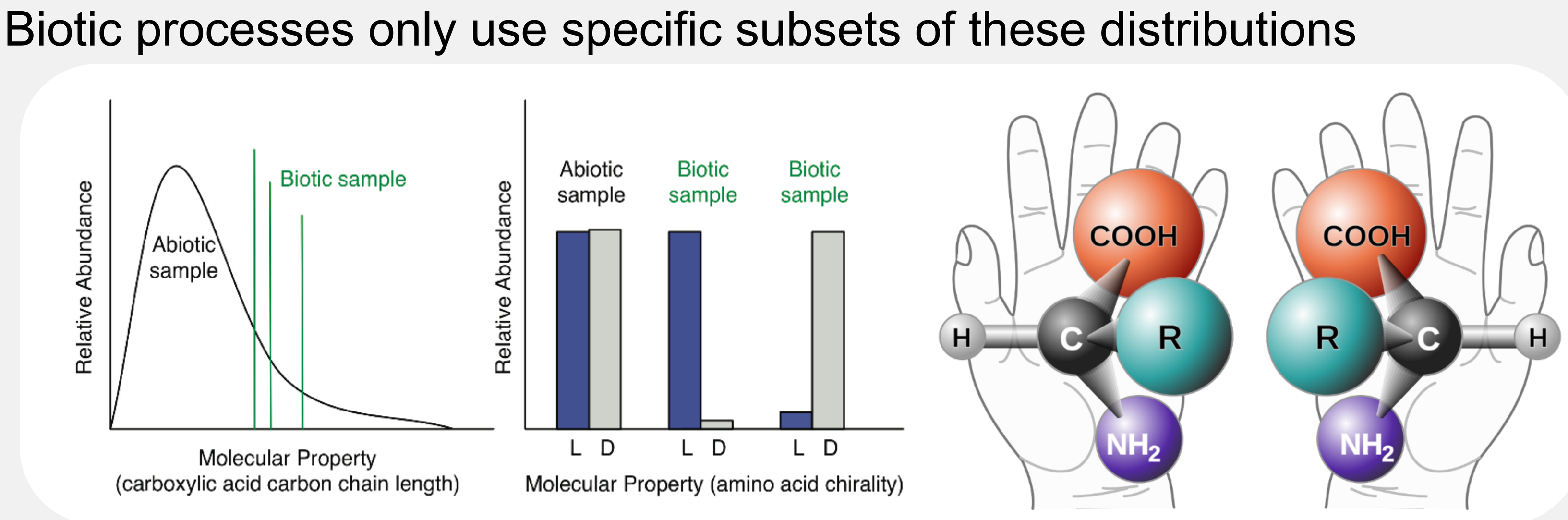

- Utilizing gas chromatography can have significant challenges getting small polar molecules into the gas phase

"… the influence of the mineral matrix and chemical composition on organic-compound derivatization, especially the presence of hydrated minerals and oxides in Martian samples, will likely be a major constraint in the ability for SAM to detect amino acids and carboxylic acids …" (Stalport et al.)

- New instruments capable of preforming aqueous analysis of samples *in situ* are needed

Methods

Microchip electrophoresis (ME) with laser induced fluorescence detection (LIF) allows analysis of polar organics without ever leaving the aqueous phase

1) Amino acids are labeled with fluorescent tag for high-sensitivity LIF detection
2) Labeled sample is delivered to separation channel
3) Analytes separated by ME based on their mobility (μ) which is proportional to their mass-to-charge ratio

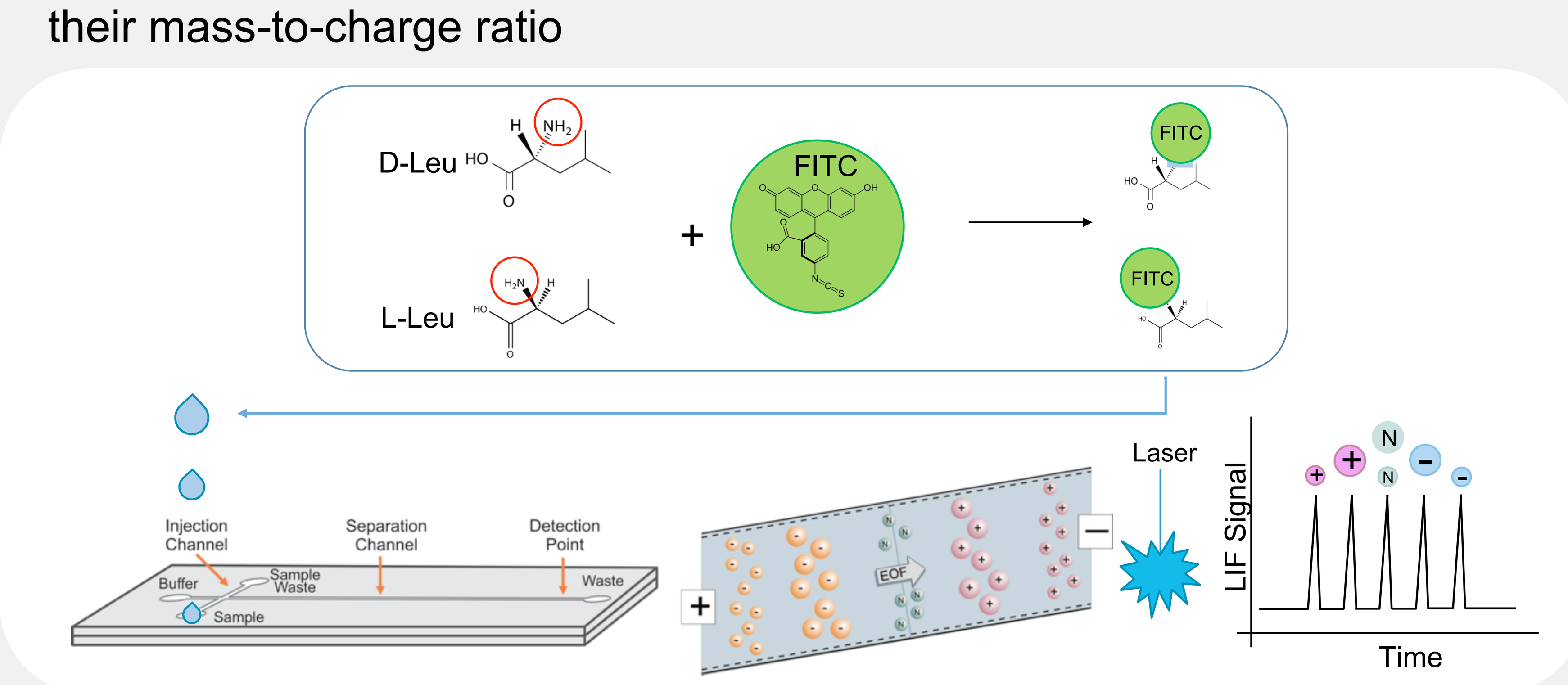

The Challenge

Enantiomers have identical mass-to-charge ratios, making them indistinguishable by ME without further optimization of the background electrolyte with chiral selectors (CS)

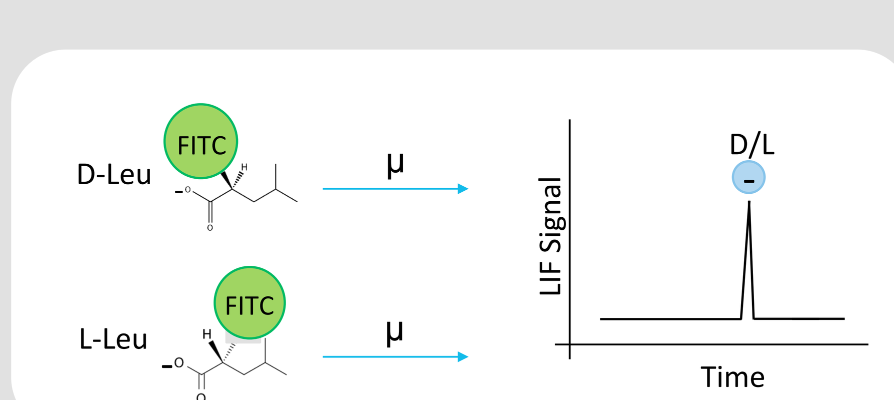

Results

Previous work by Lu et al. determined a cooperative effect between chiral selectors β-cyclodextrin and sodium taurocholate

<u>β-Cyclodextrin</u>

- Interaction with D-amino acids

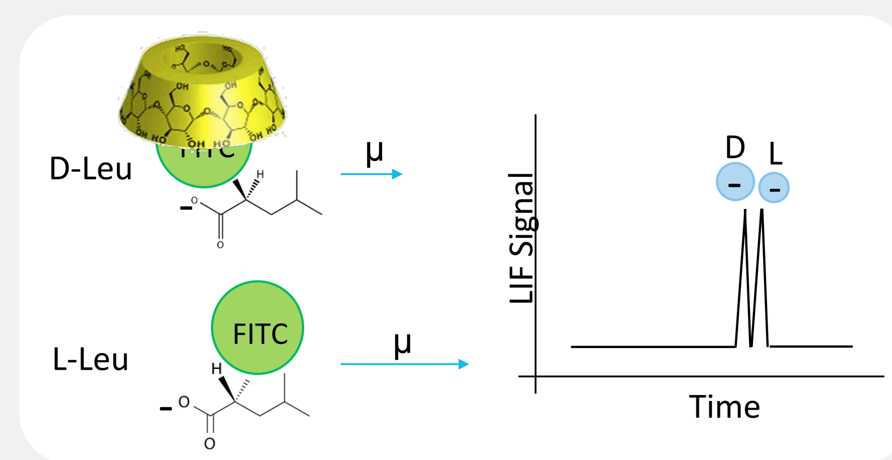

<u>Sodium taurocholate</u>

- Interaction with L-amino acids

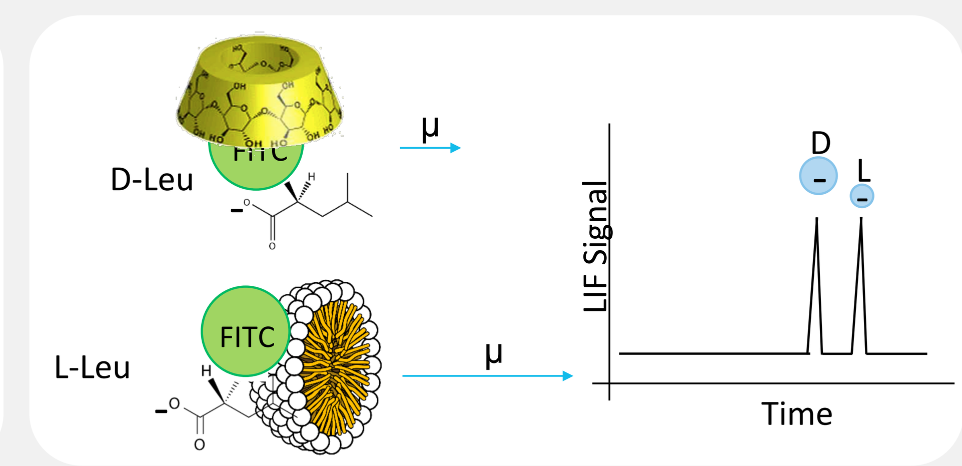

<u>Further optimization</u>

To influence the interaction between the amino acids and the CS the temperature and the polarity of the BGE were optimized to resolve five pairs of enantiomers

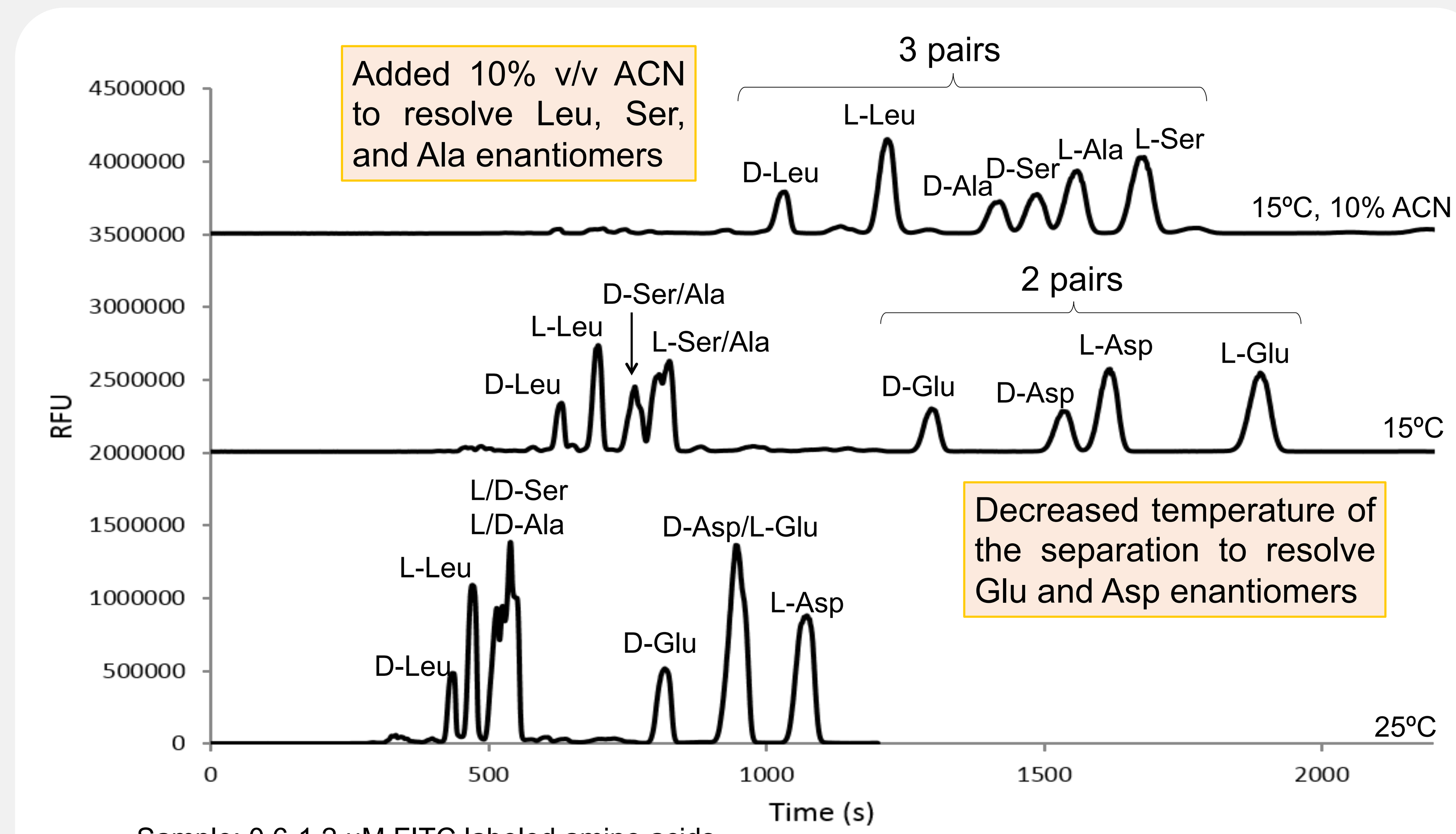

Sample: 0.6-1.2 μM FITC labeled amino acids
BGE: 80 mM borate pH 9.3, 20mM β-CD, 30mM STC

Conclusions

- Using two separation conditions it is possible to resolve 5 pairs of enantiomers on a 20 cm separation channel
  1) Lowered the temperature to resolve Glu and Asp
  2) Added acetonitrile to resolve Leu, Ala, and Ser
- This separation improves upon previous work in which Ala and Ser enantiomers were co-migrated

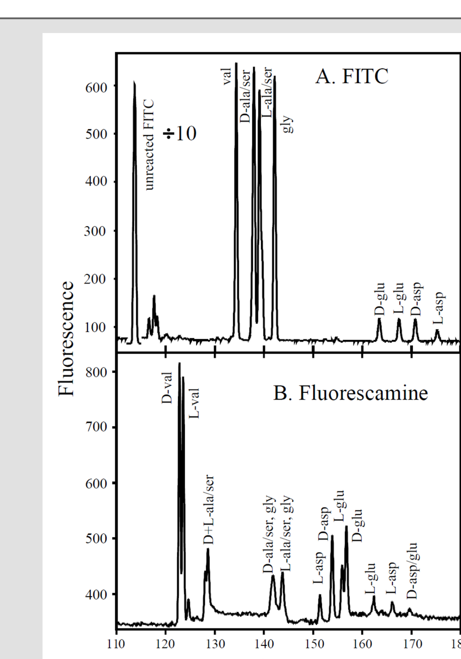

Future directions

- Increase amount of enantiomers separated
- Transfer the method to the Chemical Laptop, an instrument developed in the Willis group that houses the electronics and optics needed to perform sample handling and analysis by ME-LIF

Acknowledgements

- The Peter Willis Group
- The NASA-PICASSO Program funding for the "Microfluidic Life Analyzer" project

The NASA Postdoctoral Program

- This work was carried out at the Jet Propulsion Laboratory, California Institute of Technology, under contract with NASA.

National Aeronautics and Space Administration

Jet Propulsion Laboratory
California Institute of Technology
Pasadena, California

www.nasa.gov

Poster No. P-4

National Aeronautics and Space Administration

Metastable Oxygen Production by Electron Impact

Jeffrey D. Hein (3227-Caltech)
Charles P. Malone (3227), Paul V. Johnson (3227), Isik Kanik (3227)

Summary

We study metastable $O(^1S)$ and $O(^1D)$ fragments produced by electron-impact excitation of oxygen-containing gas targets:

Dissociative Excitation:

$$e^-(E) + N_2O \longrightarrow e^-(E-\Delta E) + N_2 + O(^1S)$$

Direct Excitation:

$$e^-(E) + O(^3P) \longrightarrow e^-(E-\Delta E) + O(^1S)$$

Fundamental measurements of cross sections and collision dynamics
- Challenge to experimentally measure (low internal energy, long life)
- Accurate determination is required for the reliable interpretation and modeling of natural phenomena and mission data
  - Atmospheric interactions/dynamics with electrons
    - Metastable species act as energy reservoir
  - Observation of emissions serve to characterize composition [McKay 2015; Raghuram 2013; Zhang 2005]

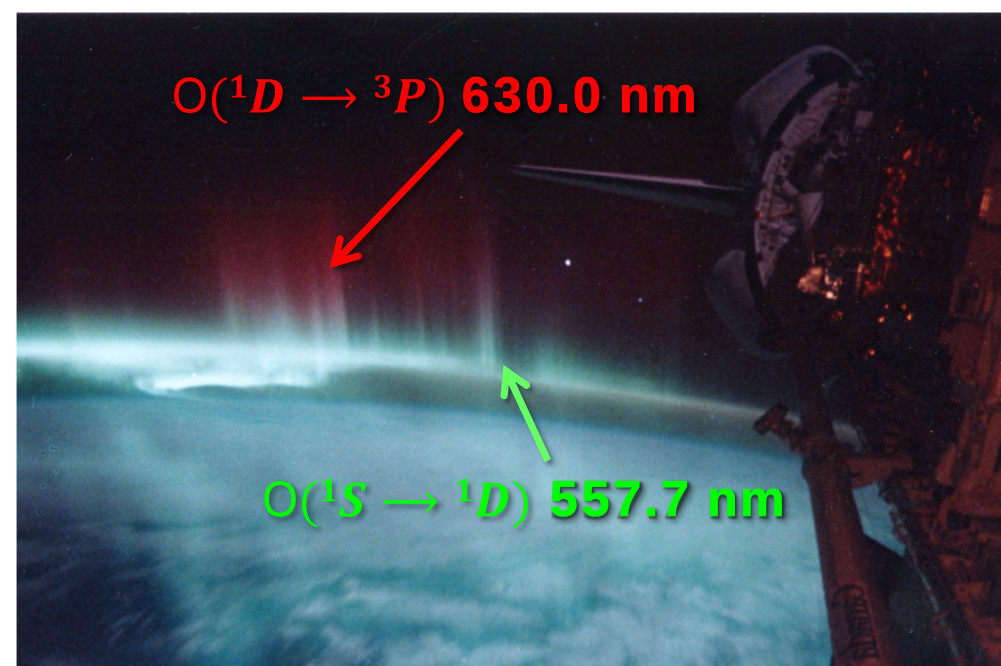

Aurora Australus observed from STS-39.

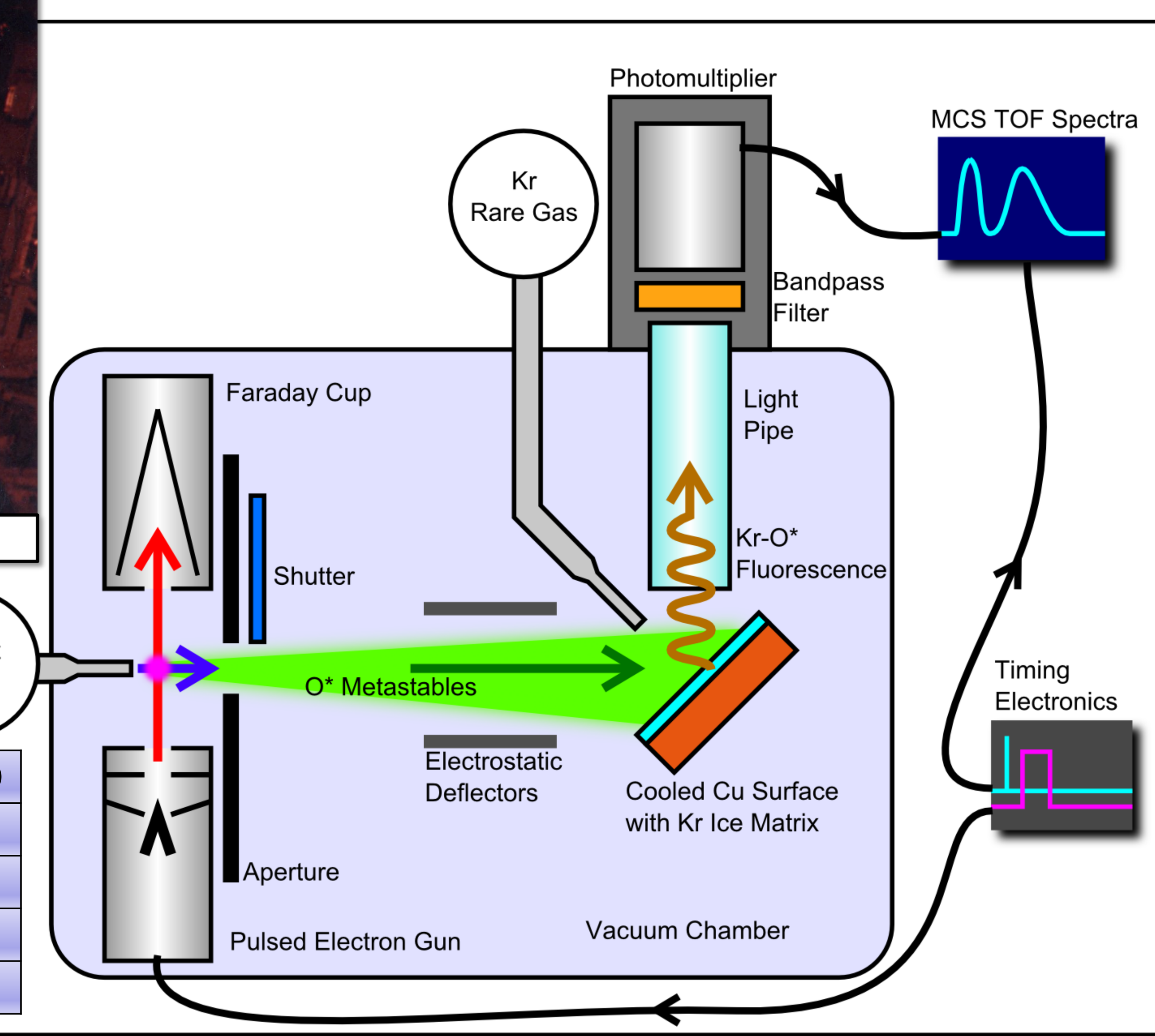

Metastable Species	$O(^1S)$	$O(^1D)$
Internal Energy (eV)	4.19	1.96
Lifetime (s)	0.8	116
Suitable Detector	Kr	Ne
Emitted wavelength (nm)	570	635

Figure 1: Overview of experiment for measuring metastable oxygen produced by electron impact. Photons detected by exciplex emission serves as an indirect observation of metastable production

Measurement

Metastable oxygen particle detection using ***Rare Gas Conversion Technique***
- Pulsed electron beam produces metastable O fragments at interaction region
- Metastables drift and impinge on rare gas ice formed on a cooled (~ 5 K) surface
- RG-O* exciplexes form and rapidly (~ 1 μs) de-excite, producing photons
  - Wavelength filtering isolates desired metastable species
- Time-resolved photomultiplier signal: cross section and dissociation dynamics
  - Prompt signal: photons from interaction region during electron pulse
  - Metastable signal: exciplex emission

Rare Gas Conversion:

$$\underbrace{O(^1S)}_{\text{metastable}} + Kr(^1S) \longrightarrow \underbrace{Kr{-}O^*}_{\text{exciplex}} \longrightarrow O(^3P) + Kr(^1S) + \underbrace{h\nu}_{\text{detected by PMT}}$$

Results

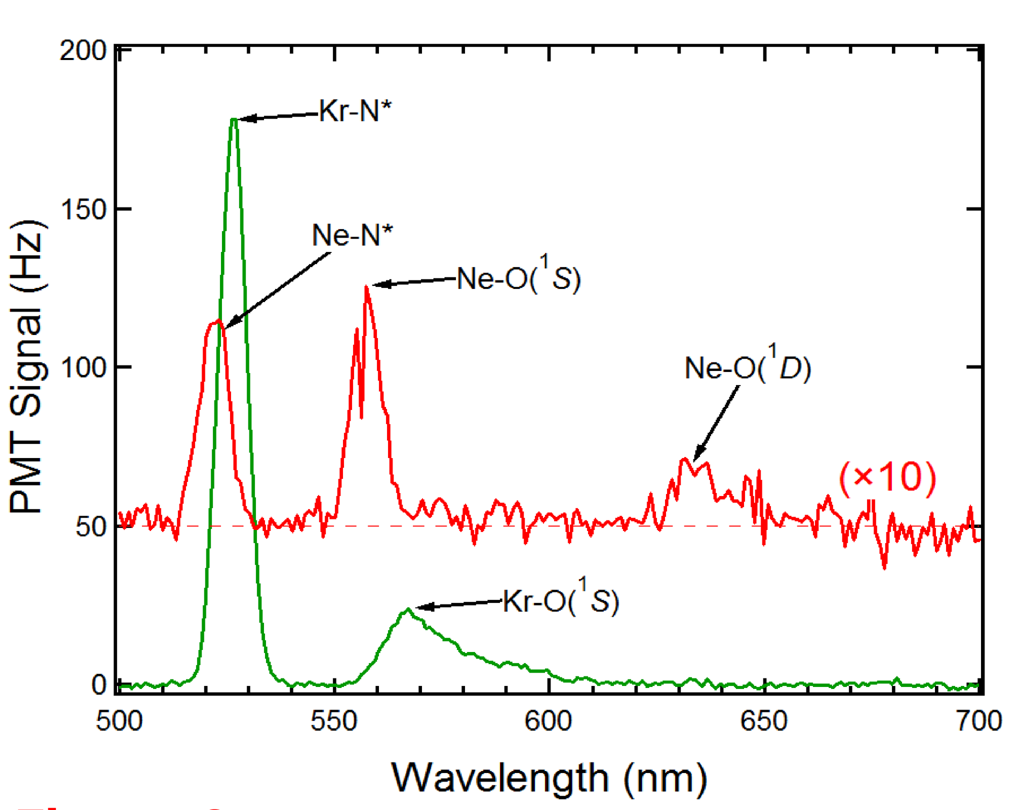

Figure 2 Fluorescence spectra for **krypton ice** and **neon ice**, with identified exciplex emissions, measured using a 6 nm FWHM monochromator for wavelength selection. **Neon spectrum** is offset and scaled for clarity. Bandpass filters are chosen to isolate the exciplex emission of interest.

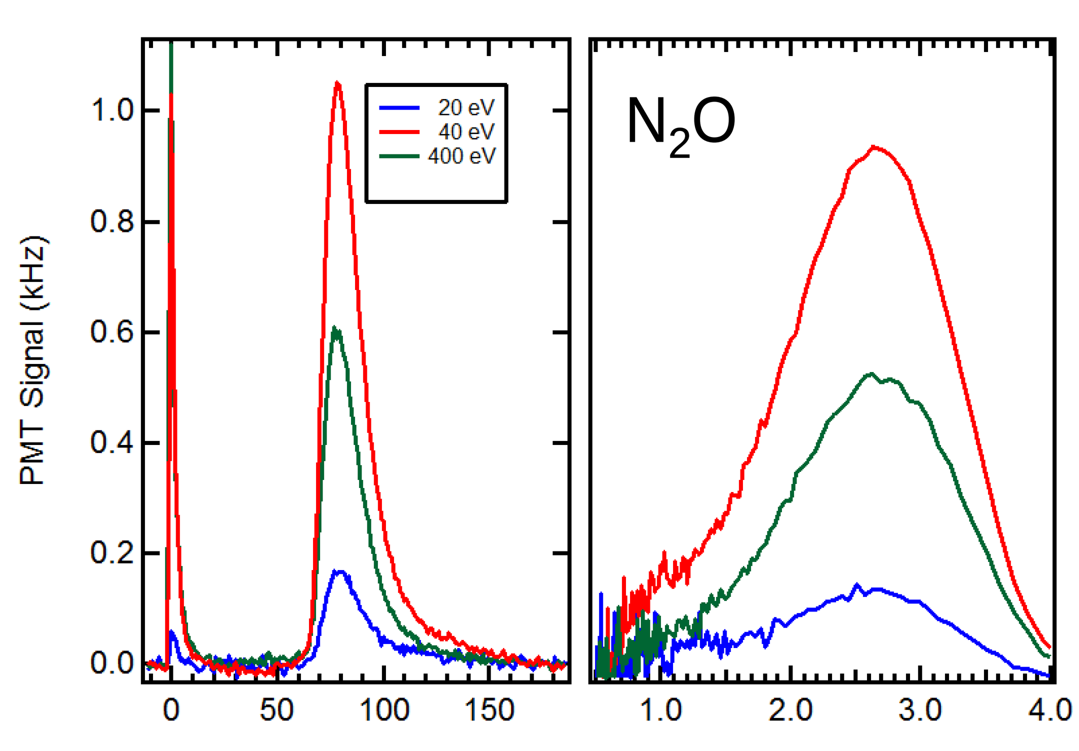

Figure 3 Time-of-flight (TOF) and kinetic energy released (KER) spectra for $O(^1S)$ production from N_2O, for 20, 40, and 400 eV electron impact energy. KER indicates a single dissociation channel, suitable for absolute cross section normalization shown in **Figure 5**.

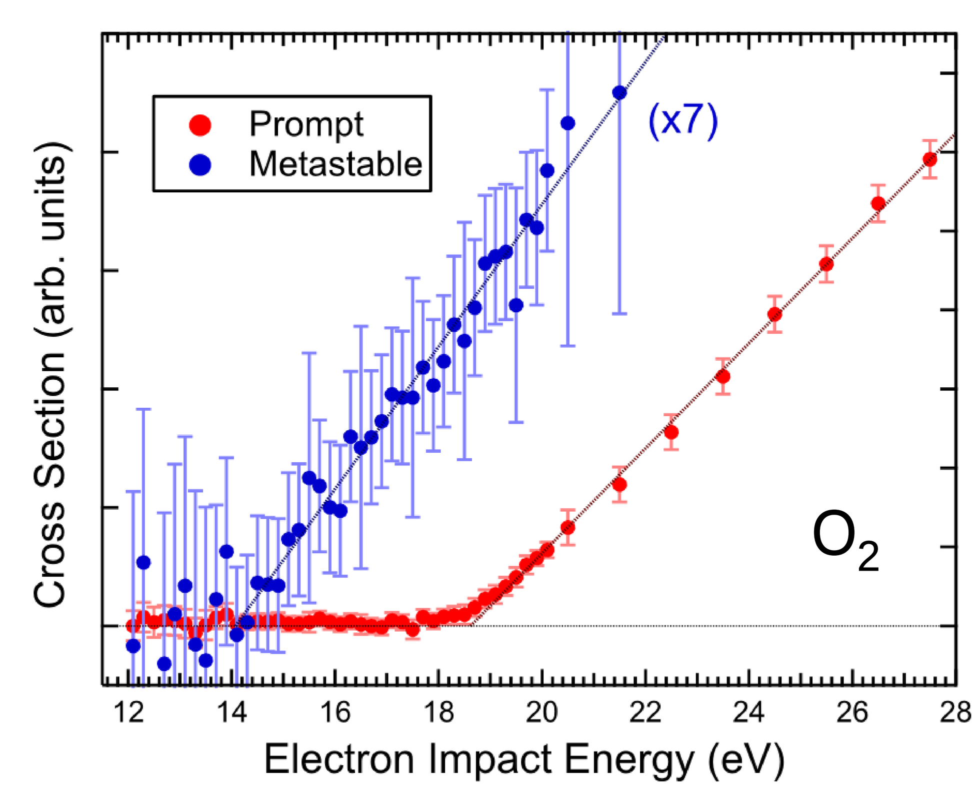

Figure 4 Threshold excitation function spectra for O_2. **Prompt signal** from $O_2^+(b\,4\Sigma_g^- \longrightarrow a\,4\Pi_u)$ with a 18.62 eV threshold [LeClair 1993]. This calibrates the impact energy scale, and gives $O(^1S)$ **metastable signal** threshold of 14.07 ± 0.13 eV, consistent with [LeClair 1993].

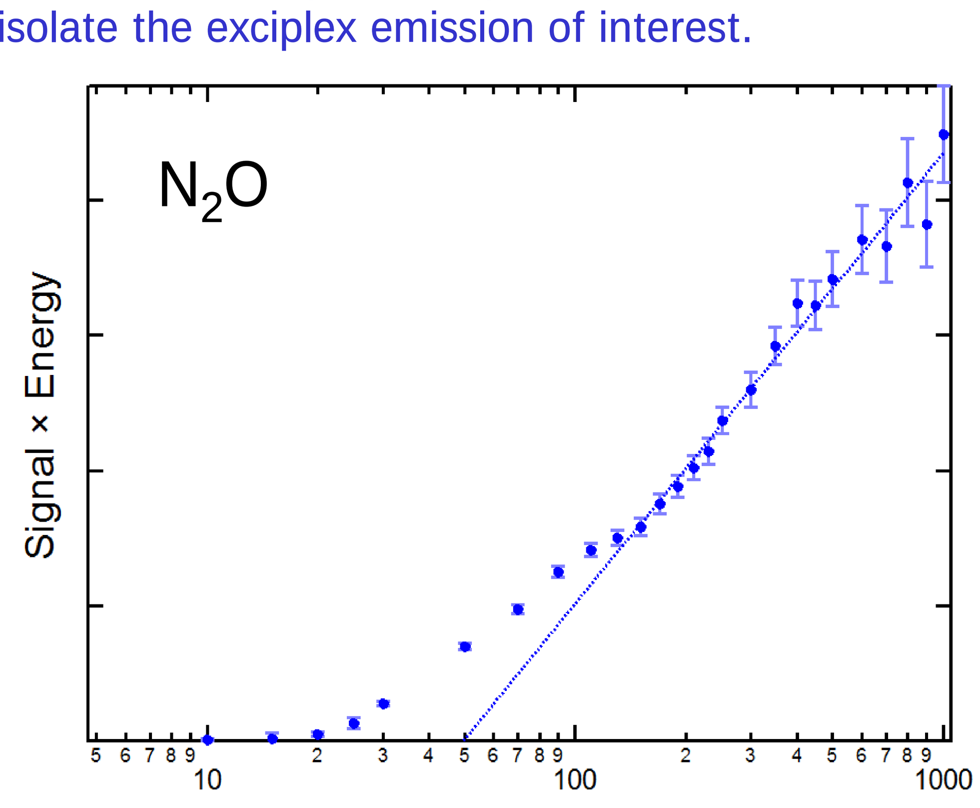

Figure 5 Bethe-Born plot of $O(^1S)$ production from N_2O. Signal goes as $\ln E/E$ for high E, and the absolute cross section $\sigma(E)$ is determined by:

$$\sigma(E) = \frac{4\pi a_0{}^2 R^2 f}{E_{th} E} \ln\left(\frac{4CE}{R}\right)$$

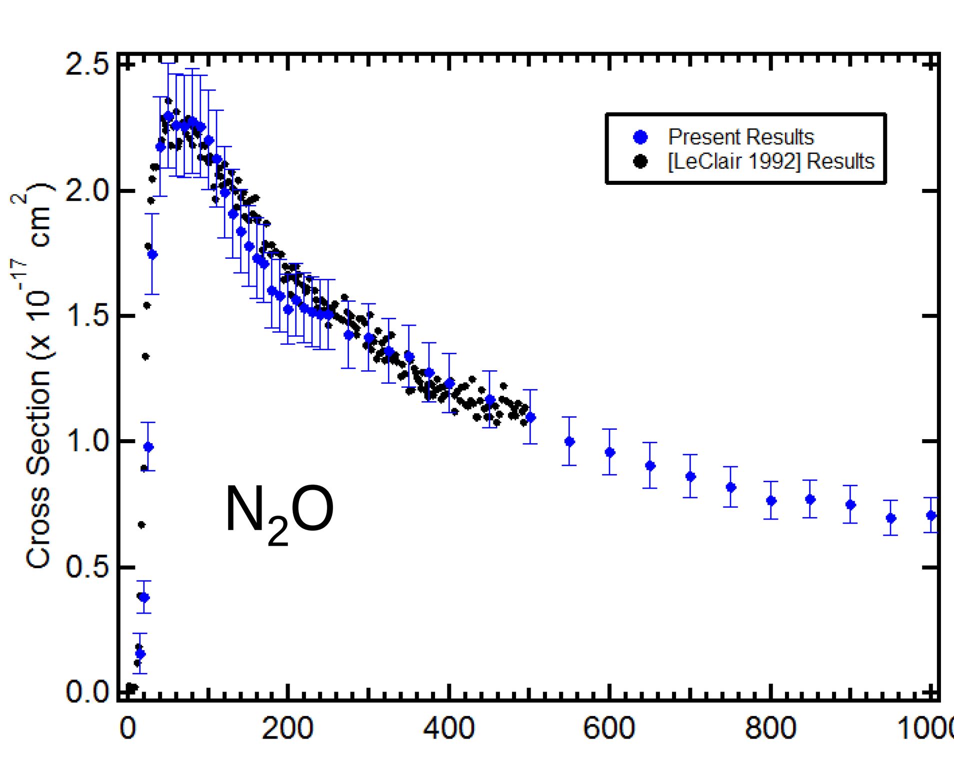

Figure 6 Absolute excitation function for $O(^1S)$ production from N_2O using Bethe fit in **Figure 5**. Impact energy is calibrated using threshold measurements of O_2 as described in **Figure 4**. **Measured results** show very good agreement with **previous results** from [LeClair 1992].

Future Work

The absolute electron-impact dissociative excitation cross section for $O(^1S)$ production from N_2O (shown in **Figure 6**) serves as a calibration standard for all atmospherically-relevant species currently under investigation, including O_2, CO_2, CO, H_2O, and atomic O targets.

The capability of preparing a neon ice matrix was recently achieved through the installation of a ColdEdge 101E cryostat capable of achieving a steady 5 K surface temperature. The detection of $O(^1D)$ fragments is possible (see **Figure 2**), and measurements are currently underway.

References

LeClair L R, Corr J J, and McConkey J W, (1992) *J. Phys. B*, **25**, L647.
LeClair L R and McConkey J W, (1993) *Chem. J. Phys.*, **99**, 4566.
McKay A J *et. al*, (2015) *Icarus*, **250**, 504.
Raghuram S and Bhardwaj A, (2013) *Icarus*, **233**, 91.
Zhang S P and Shepherd G G, (2005) *J. GeoPhys. Res.*, **110**, A03304.

National Aeronautics and Space Administration

Jet Propulsion Laboratory
California Institute of Technology
Pasadena, California

www.nasa.gov

Poster No. P-5

National Aeronautics and Space Administration

Kinetics of Methane Clathrate Formation and Substitution with Ethane – Implications for Outgassing on Titan

Principal Investigator: Tuan H. Vu (3227)
Co-Investigator: Mathieu Choukroun (3227)

Introduction

- Titan's atmospheric methane is constantly depleted through complex photochemical reactions. Replenishment processes must take place to explain present-day abundance.
- Total amount of liquid hydrocarbons detected on surface lakes alone cannot account for replenishment. Impacts and/or cryovolcanism (consistent with release of ^{40}Ar) are required.
- Titan's interior crust is believed to contain stable layers of methane clathrates that may serve as internal methane reservoir.
- …es and …uld …of …

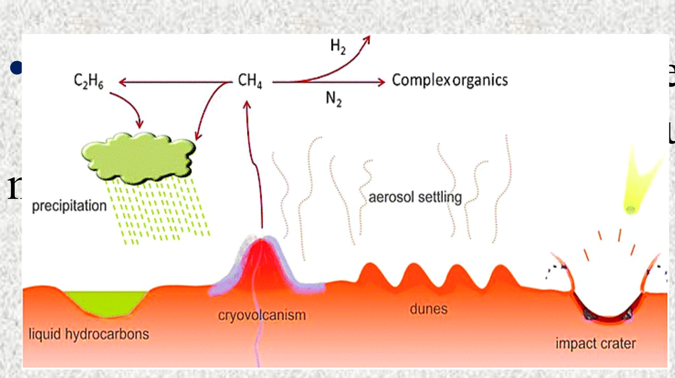

Raulin et al. *Chem. Soc. Rev.* **2012,** 41, 5380

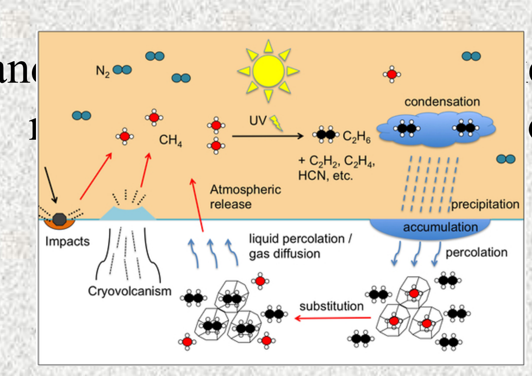

Choukroun, Sotin. *GRL* **2012,** 39, L04201

What are clathrate hydrates?

- A type of solid inclusion compounds containing small hydrocarbons trapped inside symmetric cages of water ice, also known as "burning ice."
- Conditions for formation and structures of the cages depend largely on the size of the guests.
- Titan's surface conditions (1.5 bar, 90 - 94 K) … within the stability zones for many clathrates.

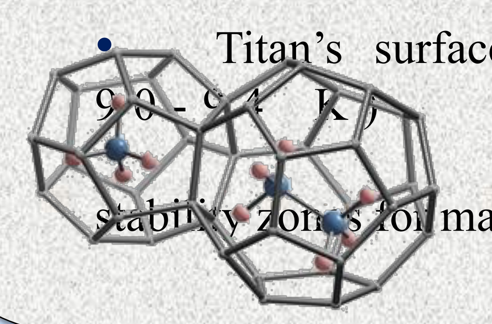

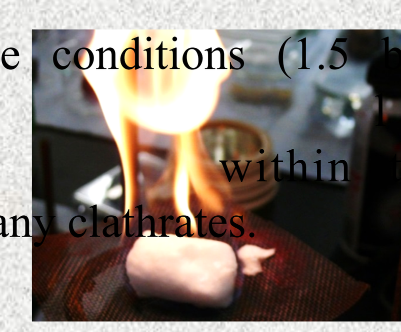

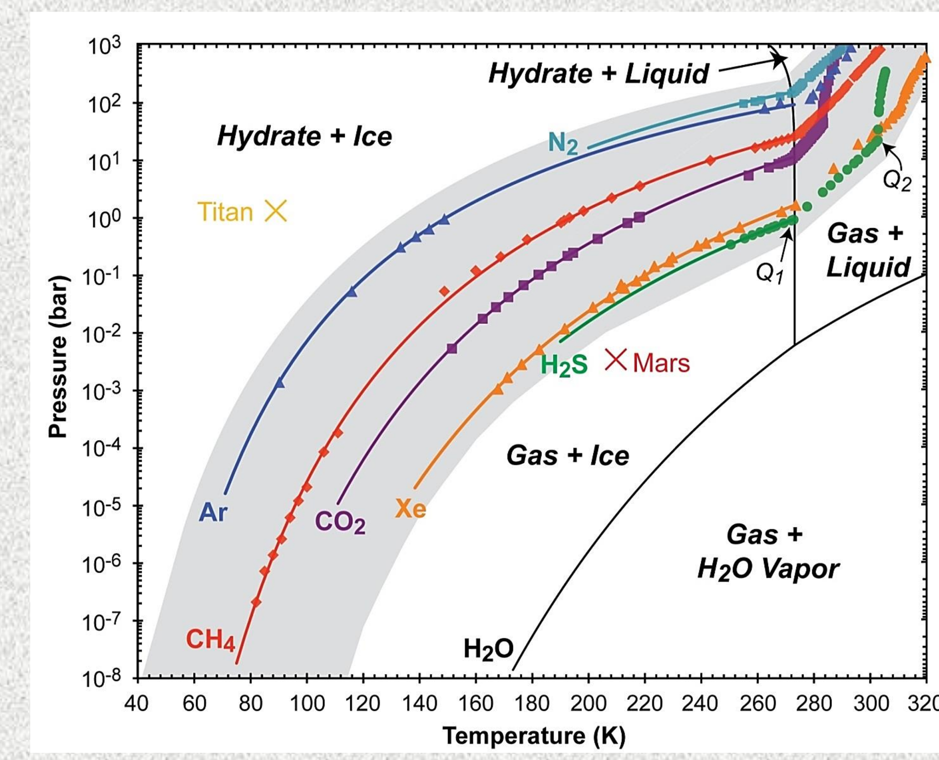

Choukroun et al. *The Science of Solar System Ices*; Springer, 2013, pp. 409

Kinetics of Formation

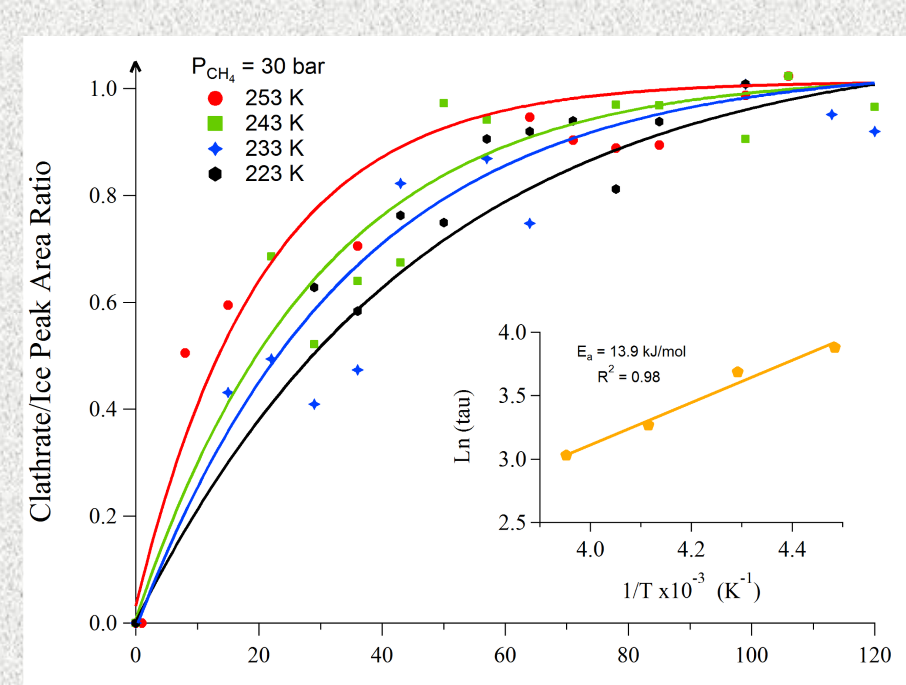

- Pressurization of small ice deposits inside the capillary tube with 30-40 bar of CH_4 at 223-253 K results in clathrate formation within minutes.
- Clathrate growth proceeds faster at warmer temperatures and higher pressures. Growth is monitored by the ratio of peak areas between the clathrate peak and ice peak at ~3120 cm^{-1}.
- Arrhenius plot (inset) yields an activation energy of 12.3 kJ/mol for methane clathrate formation at 40 bar and 13.9 kJ/mol at 30 bar.

Experimental Setup

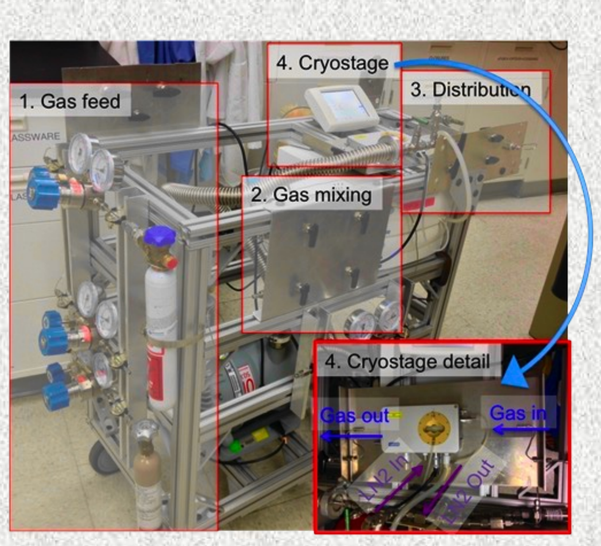

- A high-pressure apparatus (up to 200 bars) is developed for studying clathate kinetics.
- Methane clathrate samples are synthesized *in situ* at 223-253 K and 30-40 bars in a temperature-controlled Linkam CAP 500 cryostage.
- Kinetics of formation are monitored via changes in the microscopic images and in the Raman spectral features as a function of time until equilibrium is reached.

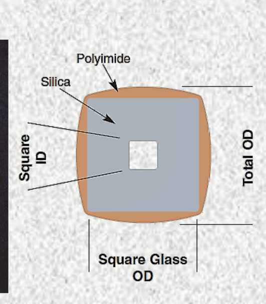

Photograph of the Linkam CAP 500 high-pressure cryostage. The capillary has a square cross-section and is guided to the optical area (#9) after locking (#7).

Ethane Substitution

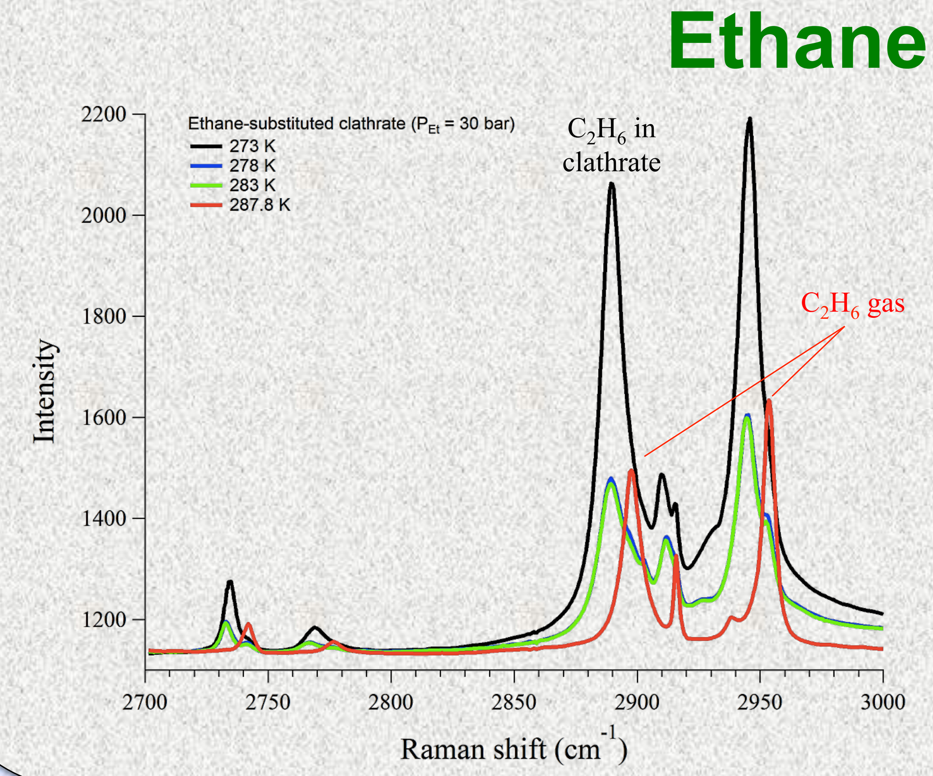

- Following clathrate formation, excess methane gas is removed from the system and methane clathrates are exposed to 30 bar of ethane at 273 K for 1 hr.
- Raman signatures point to the presence of a mixed methane-ethane clathrate after gas exchange.
- A dissociation temperature of 287.8 K is found for the substituted product, indicating a composition of 1.6% methane mole fraction.

Micro-Raman Observation

Methane Clathrate Formation at 40 Bar

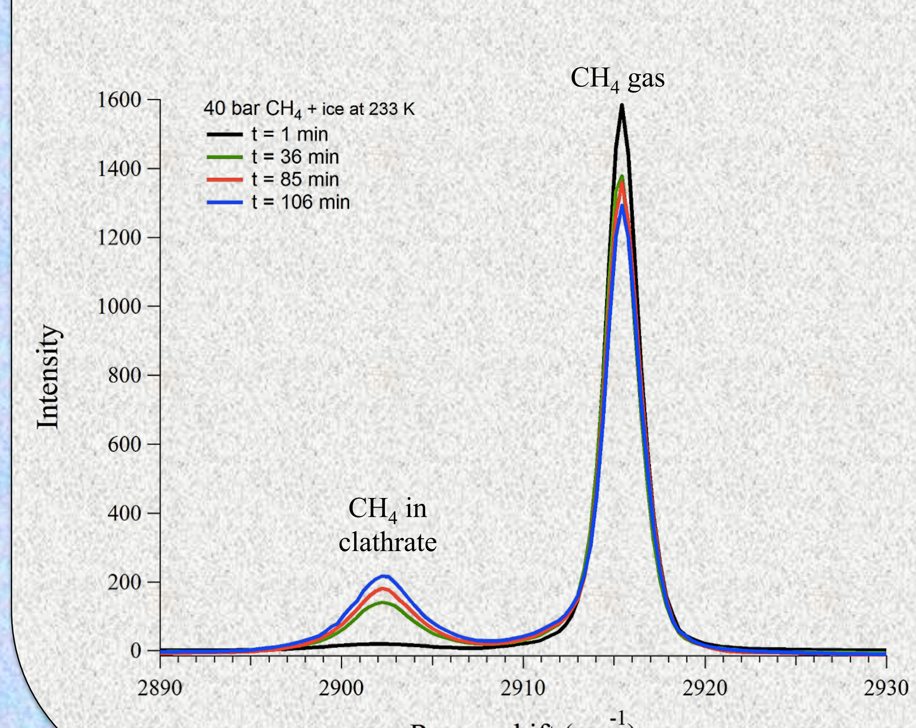

Raman spectra (left) show evolution of the 2903 cm^{-1} peak, characteristic of the υ_1 symmetric stretch of enclathrated CH_4, over time. Note the morphological change in the ice textures in the corresponding microscope images.

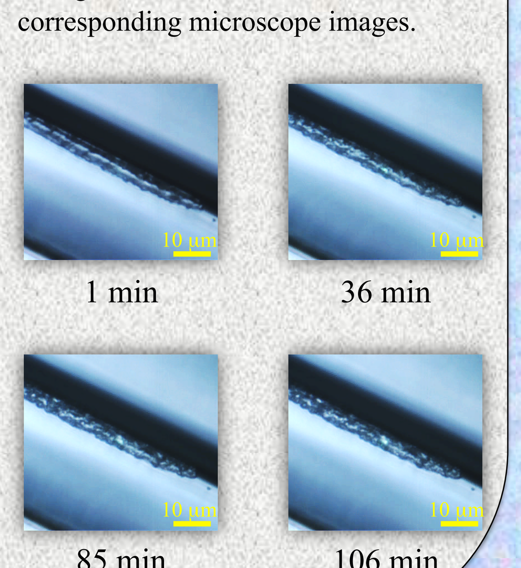

Conclusion

- High-pressure experiments have been conducted to measure the kinetics of clathrate formation and guest exchange, bringing forth new information on the timescales that would be required for these processes to occur at Titan's conditions.
- Preliminary results suggest that, for small particle size with high surface areas, both formation and substitution processes take place on a rather fast timescale (on the order of minutes).
- Subsequent work will examine formation and exchange kinetics at other pressures and temperatures to determine activation energies, thereby providing constraints for current geophysical/outgassing models.

Acknowledgements

This work was conducted at the Jet Propulsion Laboratory, California Institute of Technology, under contract with NASA. Support from the NASA Outer Planets Research Program and government sponsorship are gratefully acknowledged.

National Aeronautics and Space Administration
Jet Propulsion Laboratory
California Institute of Technology
Pasadena, California

www.nasa.gov

Poster No. P-6

National Aeronautics and Space Administration
Jet Propulsion Laboratory
California Institute of Technology
Pasadena, California

www.nasa.gov

National Aeronautics and Space Administration

Support of the Juno mission: IRTF-TEXES observations of Jupiter's polar aurorae

James Sinclair[1]
Glenn Orton[1], Thomas Greathouse[2], Leigh Fletcher[3,4], Pat Irwin[3]
[1]Division 3222, Jet Propulsion Laboratory, [4]Southwest Research Institute, San Antonio, [3]University of Oxford [4]University of Leicester

P-7

Jupiter's aurorae in the Infrared

- Air glow seen at shorter wavelengths (Figure 1a) is produced when energetic solar wind particles bombard atmospheric gases.
- The atmosphere also acts a resistor to these particles producing Joule heating, which yields *auroral hotspots* observed in the thermal infrared (Figure 1b).
- Influx of charged particles also modifies stratospheric chemistry.

(a) Ultraviolet (b) Infrared

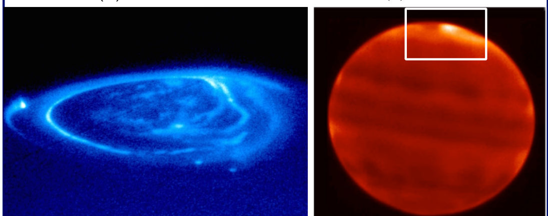

Figure 1: (a) UV image of Jupiter's auroral emission (http://juno.wisc.edu/Images/using/Science/Objectives/Jupiter_Aurora.jpg), (b) Jupiter at 7.8-µm (stratospheric CH_4 emission) from Subaru-COMICS.

Ground-based support of Juno mission

- Juno spacecraft arrives at Jupiter in July 2016.
- Auroral emission and deep atmosphere to be studied using UV, Near-Infrared, Microwave and Radio instruments on payload.
- BUT, Juno has no thermal infrared instrument (5- to 25-µm) capable of determining temperature and composition.
- Need ground-based thermal infrared observations to complement/set context for Juno observations in other wavelength ranges.

The TEXES spectrograph on NASA's IRTF

- The **T**exas **E**chelon **Cross** **E**chelle **S**pectrograph on NASA's **I**nfra**r**ed **T**elescope **F**acility (3 m telescope at Mauna Kea, HI).
- Measures spectra from 5- to 25-µm at a very high spectral resolving power ($\nu/\Delta\nu$ = 85000).
- High spectral resolution sounds Jovian atmosphere over much larger altitude range (10 to 0.001 mbar) compared to Cassini-CIRS (Figure 2).

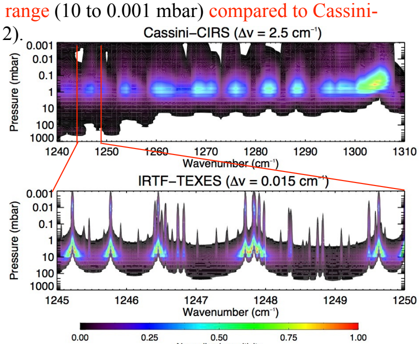

Figure 2: The normalised sensitivity to temperature as a function of pressure (or decreasing height) and wavenumber for Cassini-CIRS (top) and IRTF-TEXES (bottom).

IRTF-TEXES observations during solar maximum

- Observations acquired on Dec 11th 2014 close to solar maximum as test of future TEXES observations during Juno mission.
- Spectra measured of H_2 S(1), CH_4, C_2H_2, C_2H_6, and C_2H_4 emission at Jupiter's high latitudes.
- Brightness temperature maps show northern auroral hotspot centred on 62°N (planetographic) and 180°W (System III Longitude.

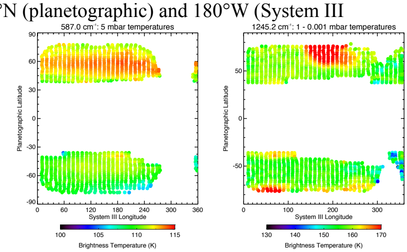

Figure 3: Brightness temperature maps of H_2 S(1) (587.0 cm^{-1}) and CH_4 (1245.2 cm^{-1}) emission.

Retrieval analysis

- Vertical temperature profile at 62°N, 100°W (quiescent) and 180°W (on-aurora) retrieved using NEMESIS (a radiative transfer retrieval code).
- Using H_2 S(1) and CH_4 emission as temperature metrics.

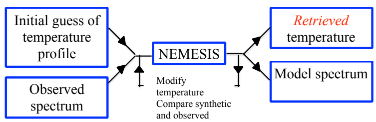

Results/Conclusions

- Aurora has little effect on temperatures at pressures higher than 0.1 mbar.
- Largest retrieved temperature difference of 18.9 ± 2.8 K at 6-µbar between 100°W and 180°W.

⟹ Auroral heating strongest at 6-µbar?

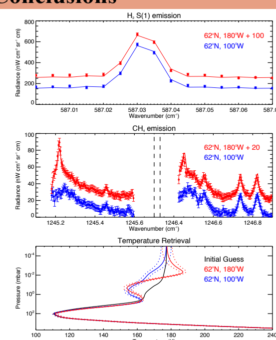

Figure 4: Observed (points,error bars) and modelled (solid) spectra at 62°N, 100°W (blue), 180°W (red) and corresponding retrieved temperature profiles.

Next steps

- Perform subsequent retrievals of C_2H_2, C_2H_4 and C_2H_6 to quantify auroral effects on composition.
- Correlate with H_3^+ auroral emission at 3-µm.
- Perform similar observations/analysis during Juno mission.
- Use Gemini North (8 m telescope) for higher spatial resolution.

National Aeronautics and Space Administration

Energetic Processing of Astrophysical Ice Analogs, Investigated via Two-Step Laser Ablation and Ionization Mass Spectrometry

Bryana L. Henderson (3227)
Murthy S. Gudipati (3227)

Bryana L. Henderson, Caltech Postdoctoral Scholar
Email: Bryana.L.Henderson@jpl.nasa.gov

Motivation: *Astrophysical Ices Exposed to Radiation*

Can complex chemistry occur at 100 K? At 5 K?

Which reactive intermediates are important? How might these reactions affect the emergence or survival of life?

Method: (1) Recreate these processes in the lab.
(2) Detect reaction products and intermediates with a novel mass spectrometry technique that allows for low-temperature analysis.

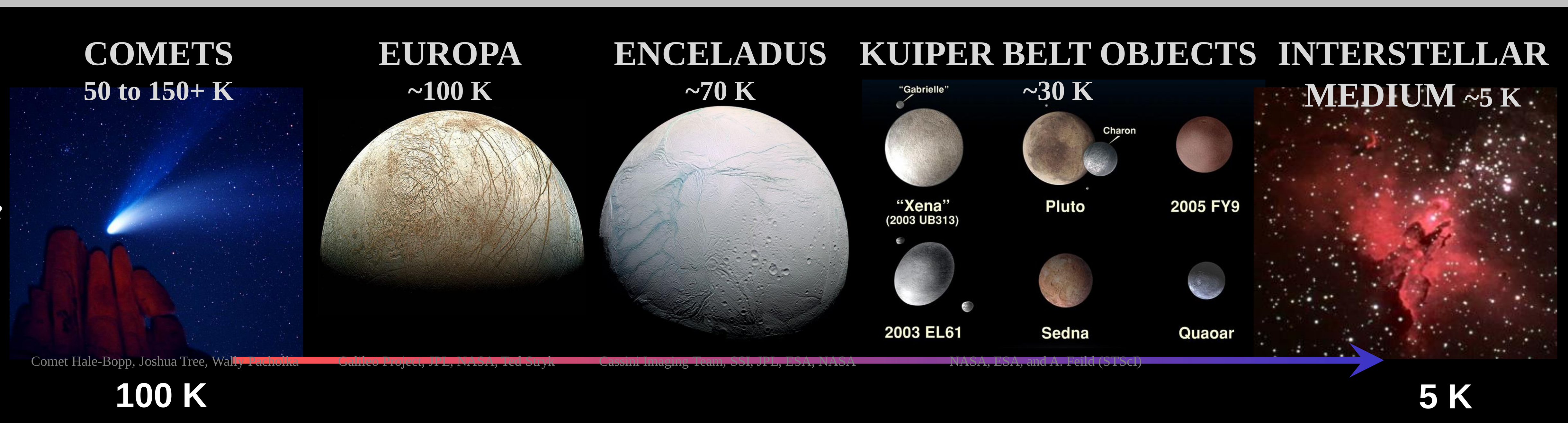

1. Prepare Ice Analogs and Expose to Space-Like Radiation

Comets and the interstellar medium (ISM) have similar compositions. During a typical lab experiment, we deposit and irradiate water ices containing relevant proportions of CO, CO_2, CH_4, CH_3OH, H_2CO, and/or NH_3 at temperatures <100 K.

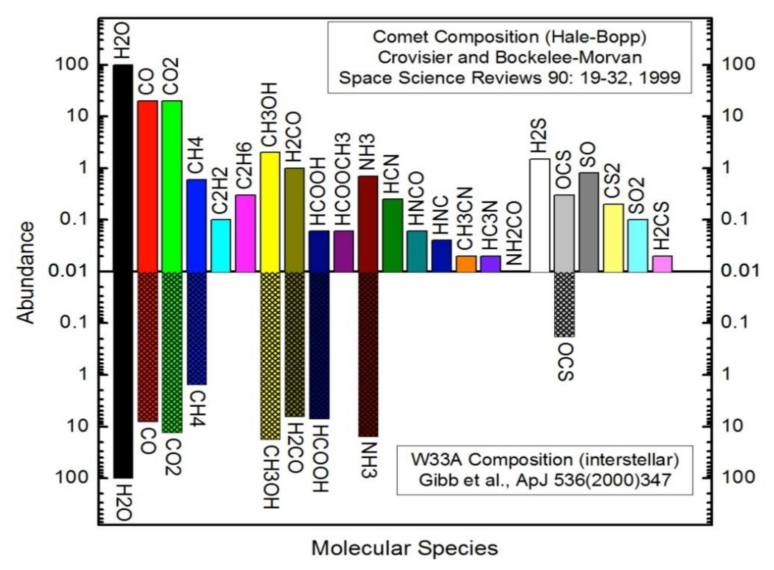

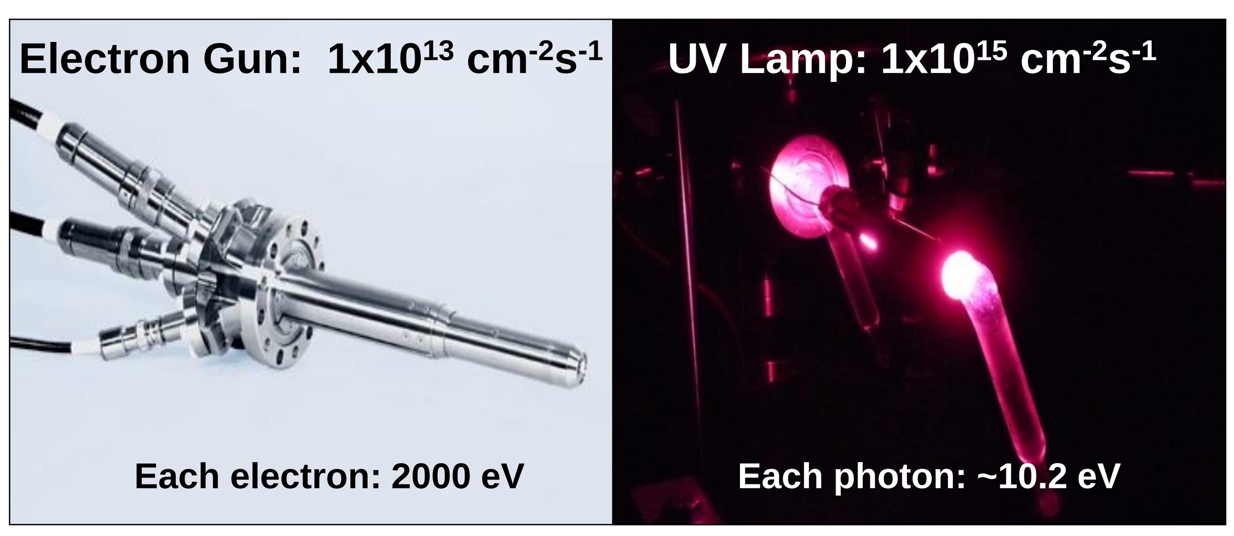

2. Detect Radiation Products Using Laser Ablation/Ionization Mass Spec.

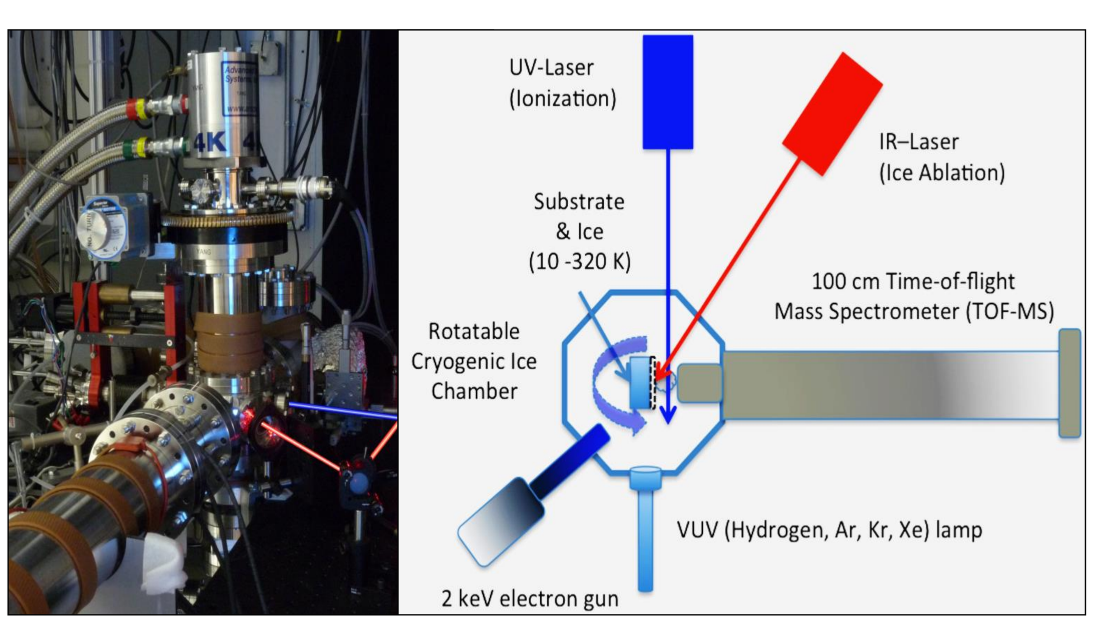

Also see Gudipati, M.S. & Yang, R. 2012, *ApJ*, 756, L24.

Our novel two-laser ablation and ionization mass spectrometry technique has several advantages:

- Enables *in situ* mass spectrometry at low temps for more direct analysis (other mass spec methods rely on sample warming and processing).
- Complements and extends IR spectroscopy (where spectral congestion leads to uncertain assignments).

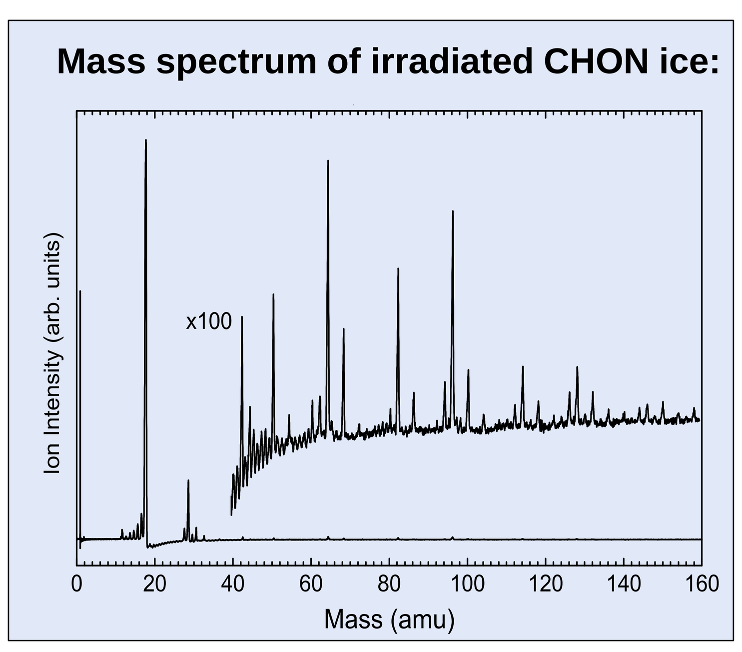

3. Assignment of Radiation Products

Verification by Isotope Exchange

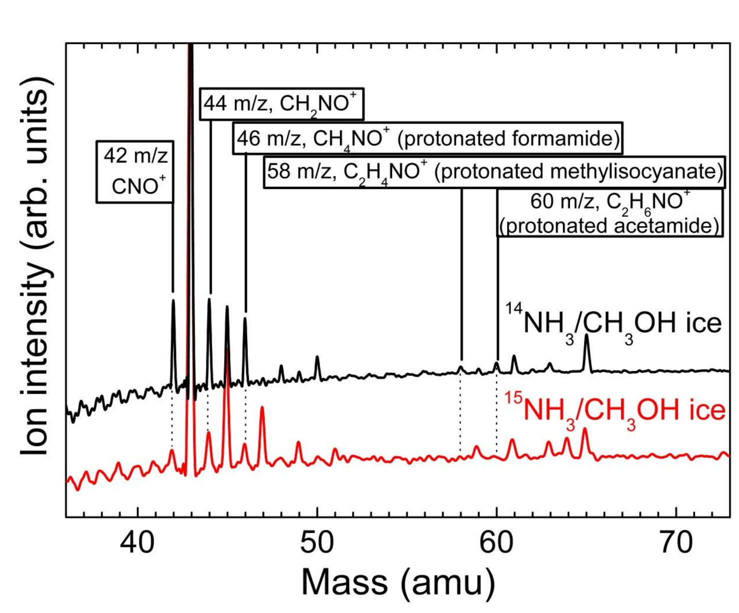

We have identified several new CH_xNO^+ species by comparing $^{14}NH_3$ (top trace) and $^{15}NH_3$ precursors in methanol ice samples (bottom trace).

Henderson, B.L. & Gudipati, M.S. 2015, *ApJ* 800.1, 66.

Verification by Volatility Analysis

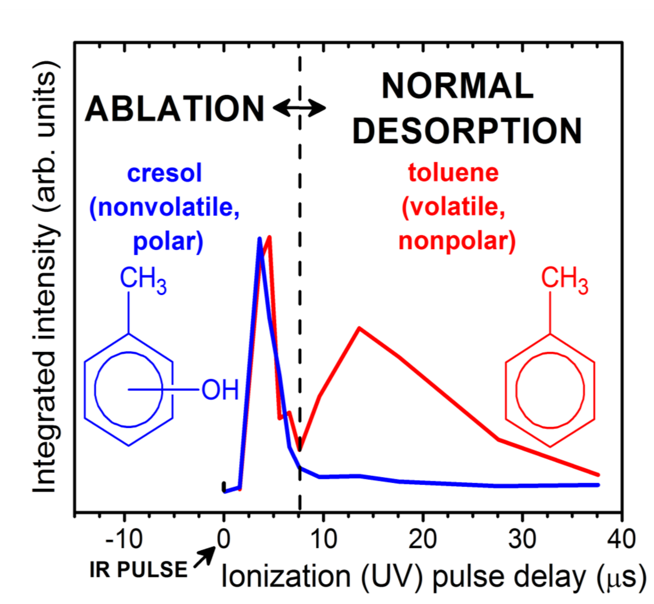

Non-volatile species are found only in the initial ablative ejection (2-8 μs). Products found later in the plume's evolution must be volatile (i.e. small or relatively nonpolar). **Our technique can provide structural information for ambiguous mass fragments!**

Henderson, B.L. and Gudipati, M.S. 2014, *JPC A*, 118.29, pp. 5454-5463.

4. Summary of UV and e^- Radiation Products of CHON Ices at 5 K

Using the techniques above, we find that even simple ices containing only ammonia and methanol produced many new complex organics upon exposure to electron radiation at 5 K.

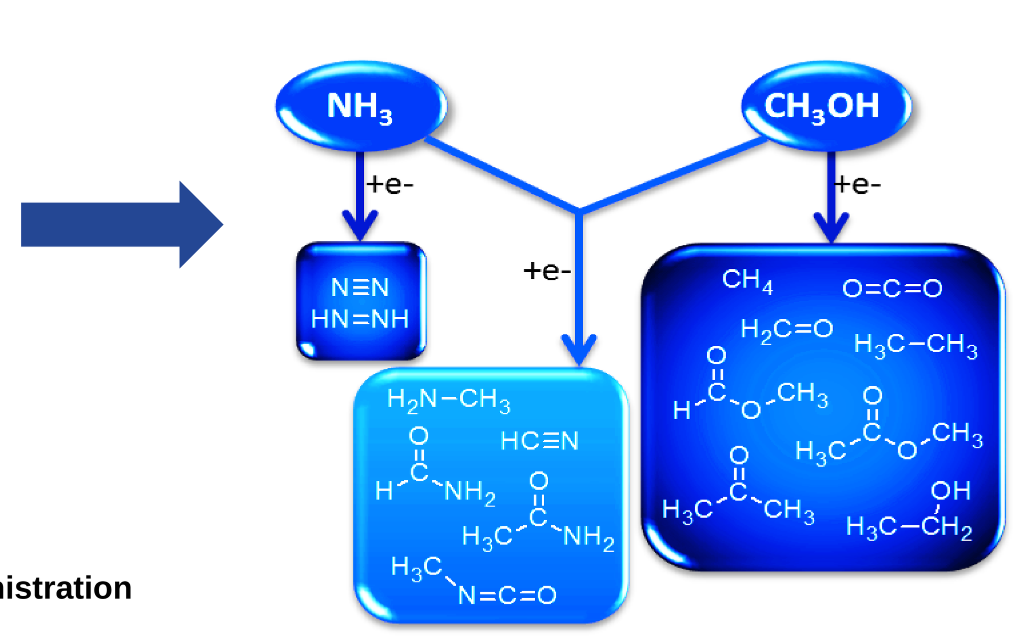

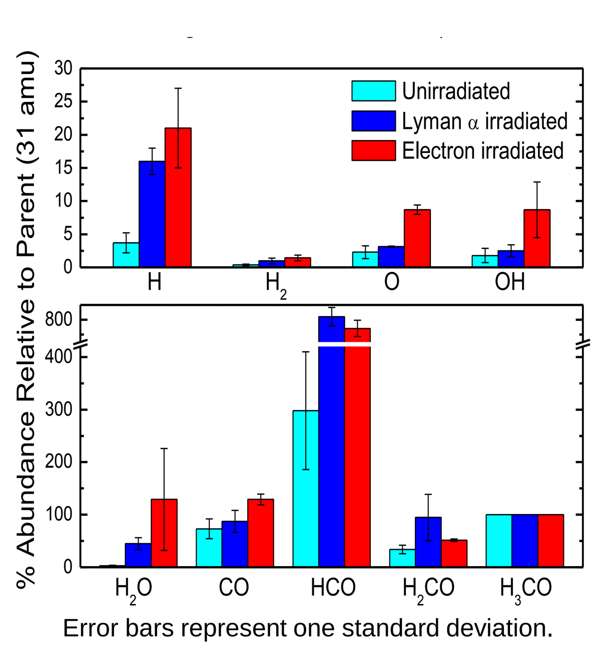

Both UV and electron radiation sources led to the same reaction products in methanol ices, although e^- radiation generally led to more H_2O and CO and UV irradiation produced more HCO and H_2CO.

Compare With Observational Data

Most of our detected species have been observed in space, but several have not yet been identified in comets. Our findings will help to guide future astronomical observations and investigations of viable low-temperature reaction pathways in astrophysical ices such as comets, KBOs, and other planetary and interstellar ices.

Complex Organics		ISM	Sgr B2	Comets	Meteorites
Formaldehyde	$H_2C{=}O$	x	x	x	x
Methylamine	$H_2N{-}CH_3$	x	x	x	x
Formamide		x	x	x	?
Acetone		x	x	?	?
Acetamide		x	x	?	?
Methyl Formate		x	x	x	?
Methyl Acetate		x	x	?	?

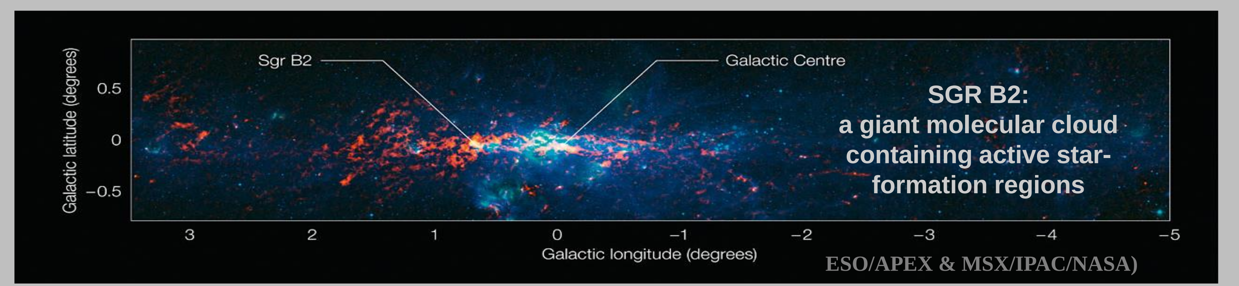

Compare With IR Spectroscopy Data: HCO^+ and CH_3CO^+ Are Key Intermediates

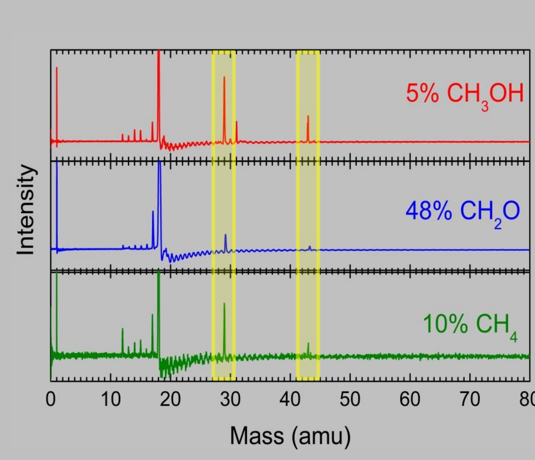

All of our carbon-containing precursors generated HCO^+ and CH_3CO^+ when embedded in water ices. HCO^+ and CH_2OH^+ /OCH_3^+ (29 and 31 m/z) have long been identified as important intermediates in these ices (see diagram below), but **our low-temperature experiments suggest that CH_3CO^+ (43 m/z) plays a more important role than currently thought**.

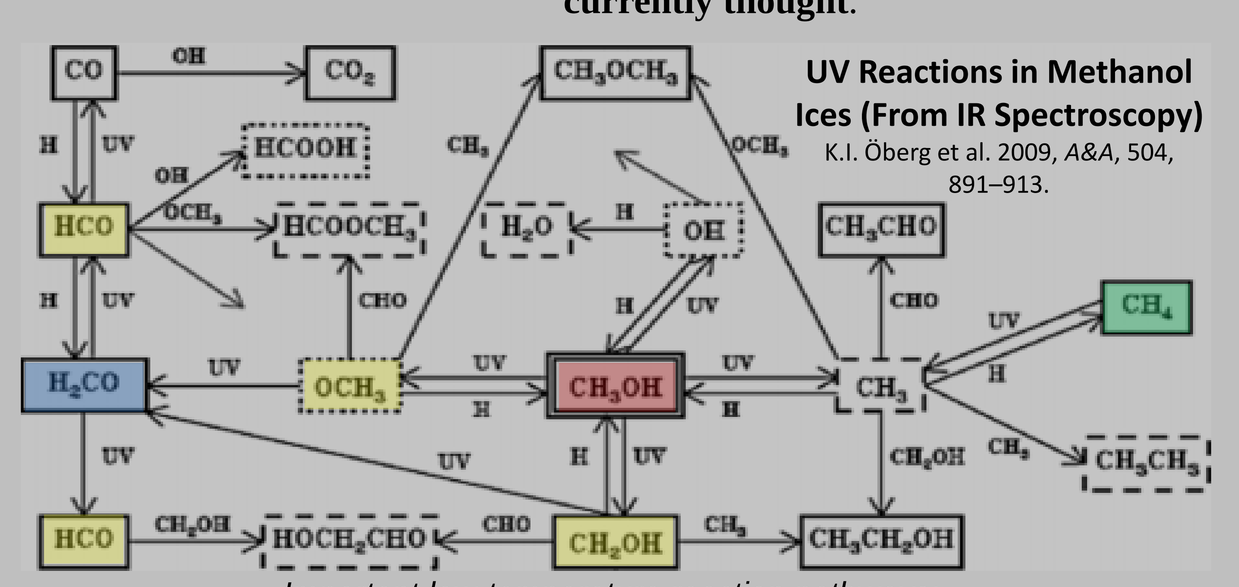

Important low-temperature reaction pathways: how does the CH_3CO^+ (43 m/z) intermediate fit into this scheme?

Is CH_3CO^+ Also a Key Amino Acid Intermediate? (Work in Progress)

We have recently obtained the first mass spectrum of an amino acid encased in ice (right). Exposure to 2h of electron radiation led to a strong signal at 43 m/z. Is this signal due to CH_3CO^+ as seen above, or to $HCNO^+$, which is commonly observed in space? Isotopic verification of the assignment is currently underway.

This work will facilitate further observational searches for prebiotically-relevant species and will help to define the conditions required for synthesis and survivability of complex organics in space.

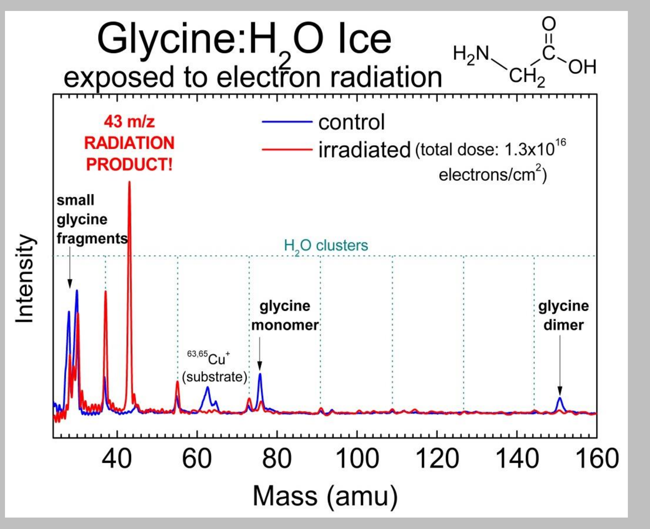

First ever mass spectrum of glycine encased in ice, 30 K. 43 m/z appears as a major radiation product – is it CH_3CO^+ or $HCNO^+$?

National Aeronautics and Space Administration

Jet Propulsion Laboratory
California Institute of Technology
Pasadena, California

www.nasa.gov

Poster No. P-8

National Aeronautics and Space Administration

Electron irradiation and thermal driven chemistry on H_2S-CH_3OH-NH_3-H_2O and CH_3OH-NH_3-H_2O ices: application to Jupiter Trojans

Principal Investigator: Ahmed MAHJOUB (3227)

M. Poston (Caltech), K. Hand (4000), M. Brown (Caltech), J. Blacksberg (389K), J. Eiler (Caltech), R. Hodyss (3227), R. Carlson (3227), B. Ehlmann (3220-Caltech), M. Choukroun (3227)

Overview: Jupiter Trojan asteroids display two distinct populations that contrast in color: "Less-Red Trojans" and "Red Trojans". Why do objects belonging to the same group present this bimodal spectral distribution? This question is linked to the history and evolution of these objects and the solar system as predicted by dynamical models such as the ''Nice'' model where the Jupiter Trojans are predicted to have formed in the Kuiper belt region and subsequently moved into their present orbits as result of a large scale solar system disruption. In one hypothesis, this red color reflects the formation of organic crust due to hundreds of millions years of space weathering. The color of this organic crust is believed to depends on the initial chemical composition of the icy surfaces of these objects. We investigate here the difference between objects formed outside and inside the stability line of H_2S in terms of color and chemical composition. The main outcome of this laboratory work is a prediction of detectable molecules and signatures that could serve as target molecules for future mission to Jupiter Trojans.

Colors and size distribution of Jupiter Trojans:

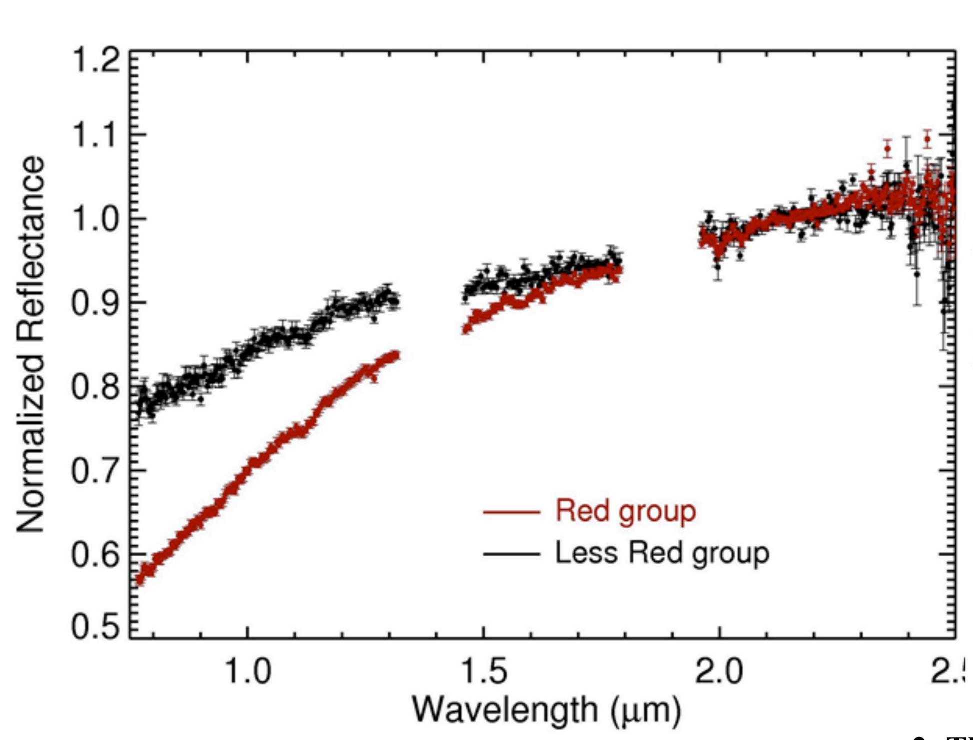

1- Two distinct populations with different Vis-NIR spectra (Emery et al. 2011)

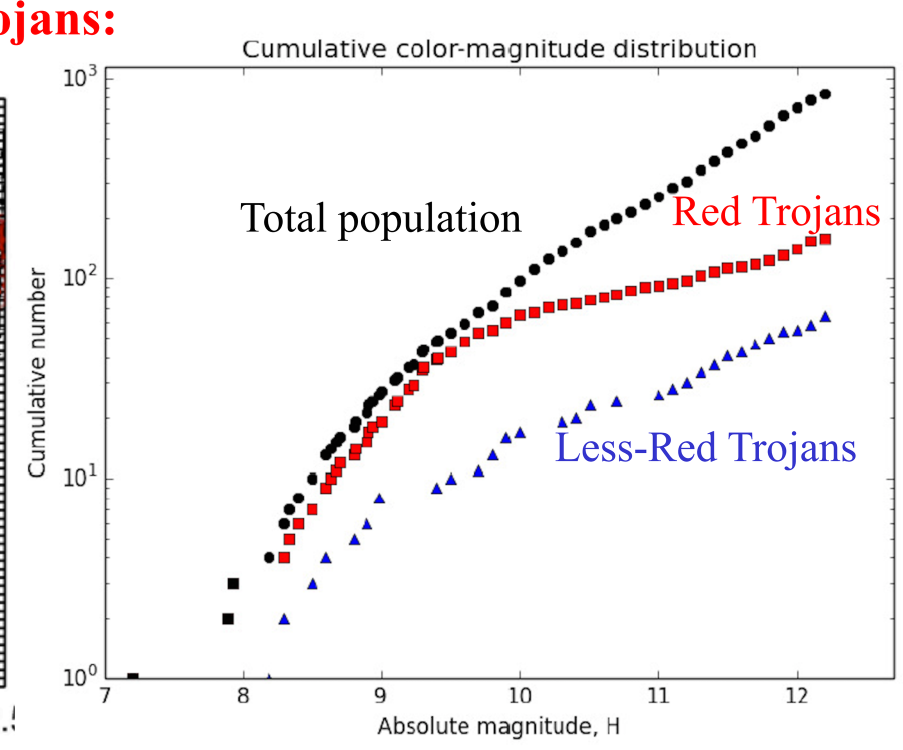

2- The two sub-populations differ strongly in their size distributions, they may come from distinct source populations (Wong et al. 2014).

Hypothesis:

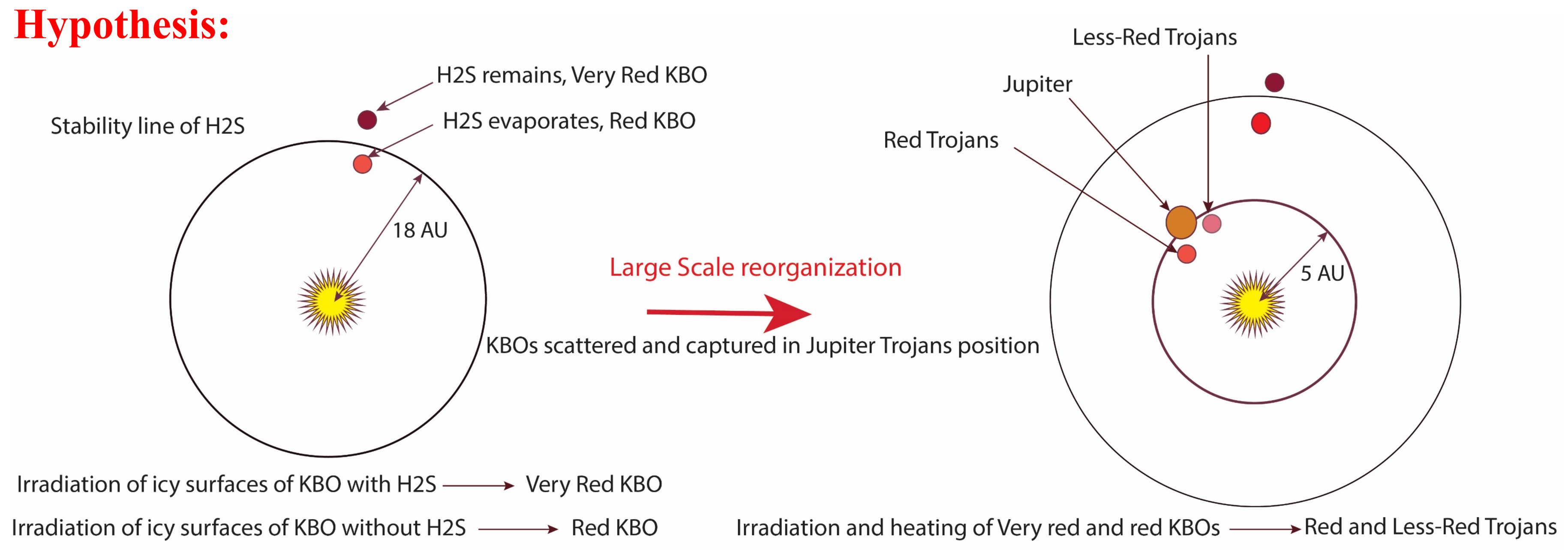

Hypothetical scenario explaining the origin of the two color groups of Jupiter Trojans

Hypothesis testing: Laboratory simulation

By submitting ice mixtures, with and without H_2S, to irradiation and heating we simulate the surface weathering which is responsible for color bi-modality in our hypothesis. The experimental setup is a high vacuum chamber fitted with a closed cycle He Cryostat, FTIR, RGA mass spectrometer and an electron gun. Ice films are deposited at T = 50 K and irradiated for ~ 20 h with 10 KeV electrons. The deposited fluence is ~ 2 10^{21} eV cm^{-2}. The sample is then heated to 120 K at 0.5 K/min and kept at this temperature for one hour while irradiated. The sample is then heated to 300 K.

Two mixtures studied to understand the role of H_2S in the reddening
3-ice mixture: 2:2:1 CH_3OH-NH_3-H_2O
4-ice mixture: 3:3:3:1 H_2S-NH_3-CH_3OH-H_2O

IRRADIATION CONDITIONS FOR ICE MIXTURES

Electron Fluence	Corresponding solar e^- irradiation time at 15 AU	Corresponding solar e^- irradiation time at 5 AU
~ 2 x 10^{21} eV/cm²	~ 200,000 Yrs	~ 1.8 Million Yrs

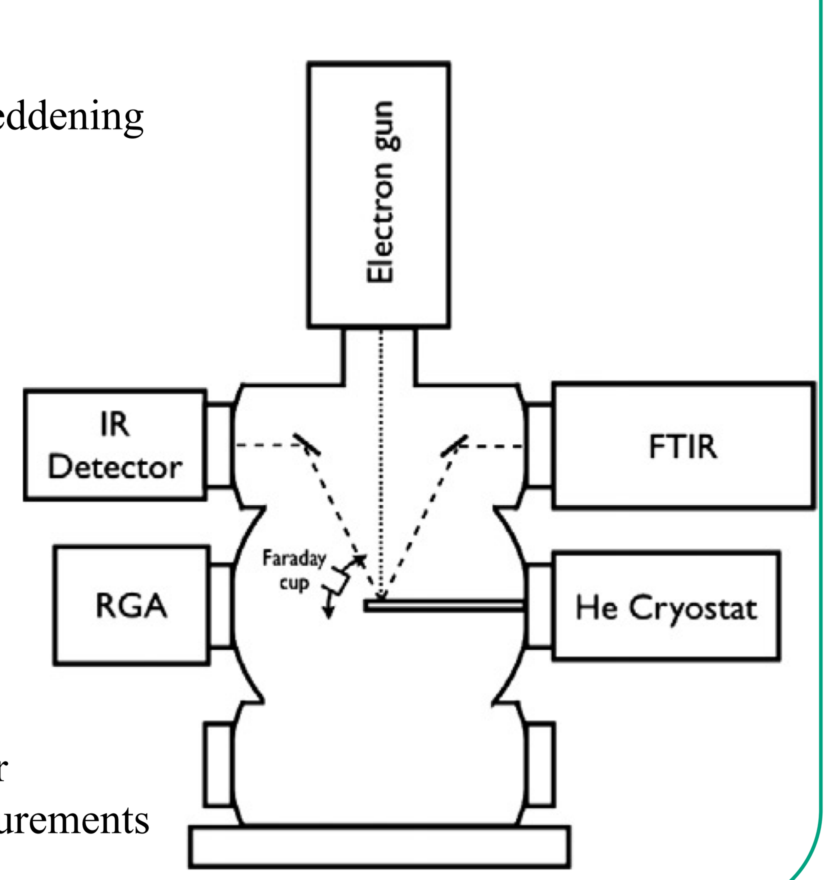

Diagnostic techniques:
- Chemical characterization: FTIR and Mass spectrometer
- Optical characterization: Vis and NIR reflectance measurements

Impact to JPL

(1) We address fundamental questions of solar system origins
(2) We search target molecules that can serve as markers for future missions or observations.
(3) We support the development of targeted instrumentation for answering key origins questions

Results:

Optical Characterization (Vis-NIR spectroscopy)

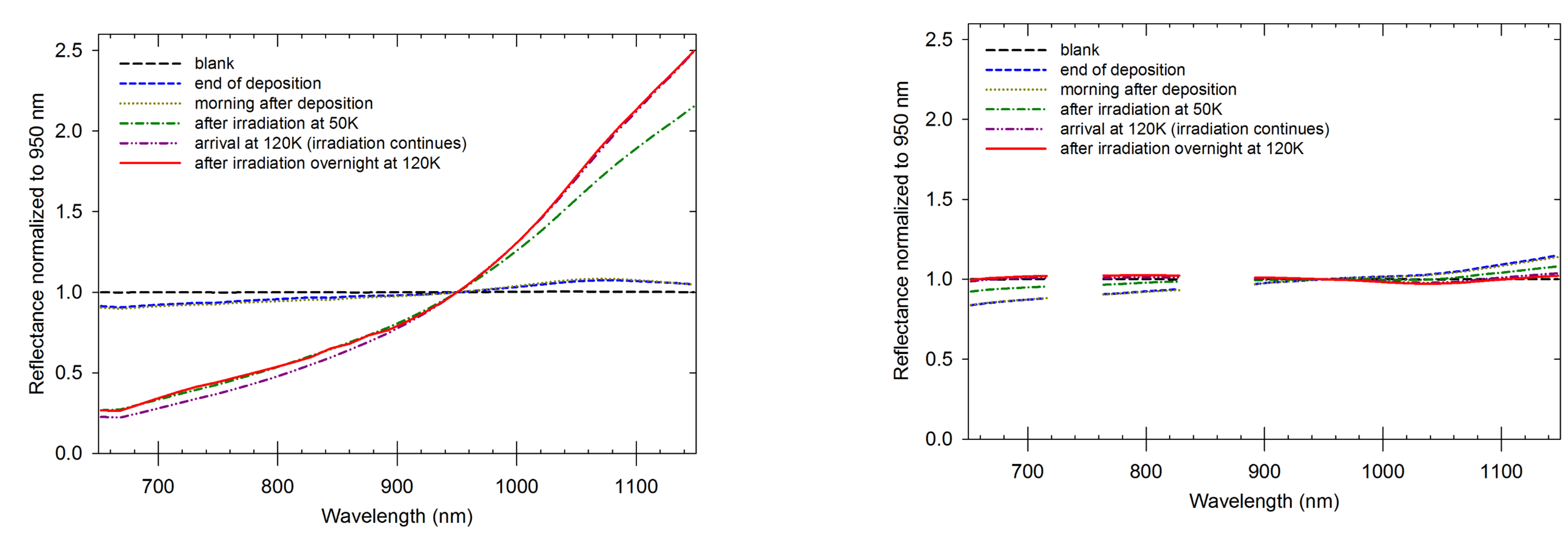

The Vis-NIR spectra show a clear reddening (positive slope) induced by irradiation of ice with and without H_2S. The reddening slope is much more important when the initial mixture contains H_2S.

Chemical Characterization (Mid-IR spectroscopy)

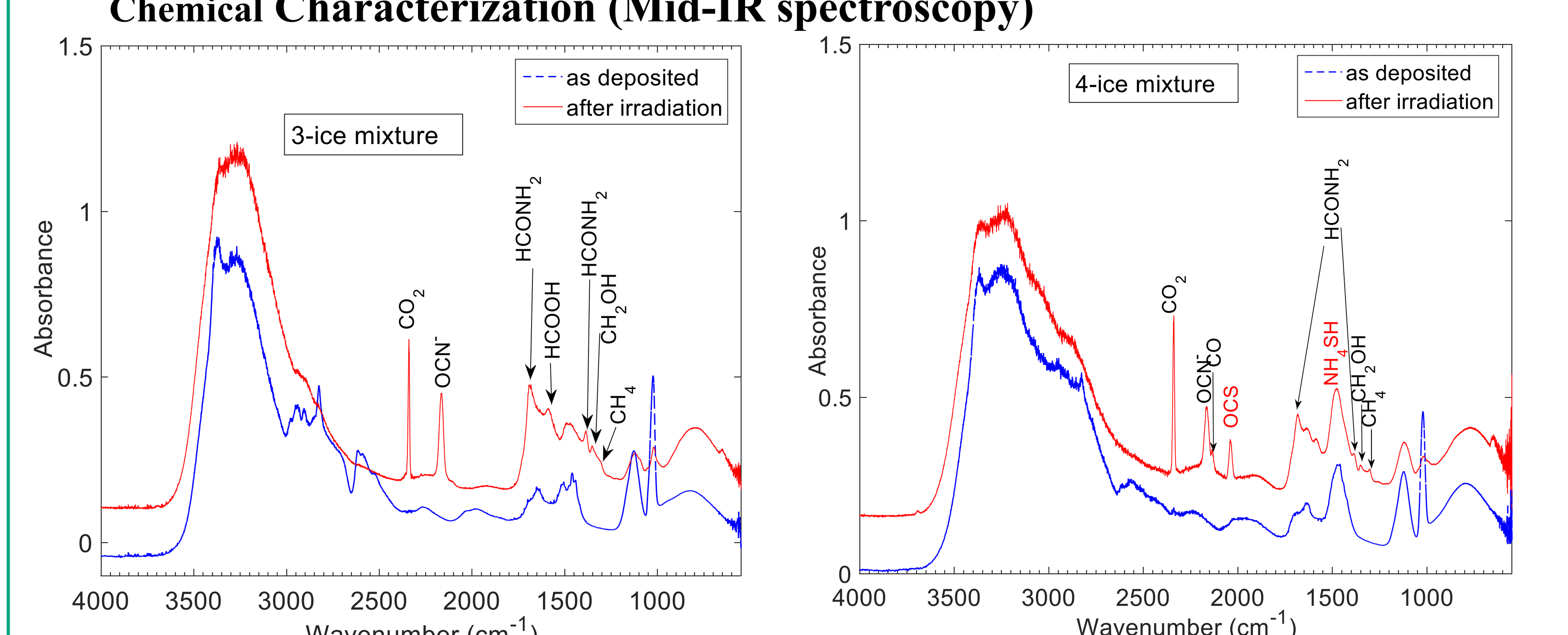

Different chemistry in the 3-ice and 4-ice mixture. OCS and NH_4SH produced only in 4-ice mixture.

New bands appeared when the irradiated 4-ice mixture warmed up. These new products indicate the occurrence of a thermal driven chemistry. These bands are assigned to CS, CS_2 and SO_2. This assignment is supported by mass spectroscopy.

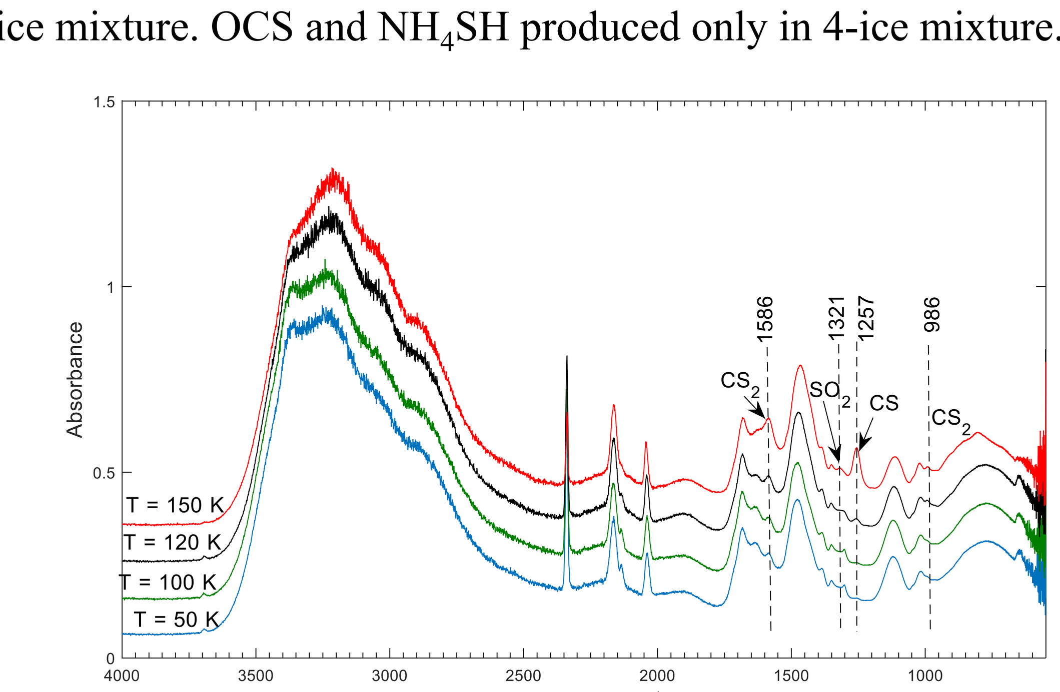

About 70 % of the initial amount of OCS remained after heating the system to 120 K while continuing electron irradiation. This amount remains stable during the test period where the temperature is fixed at 120 k for 16 h.

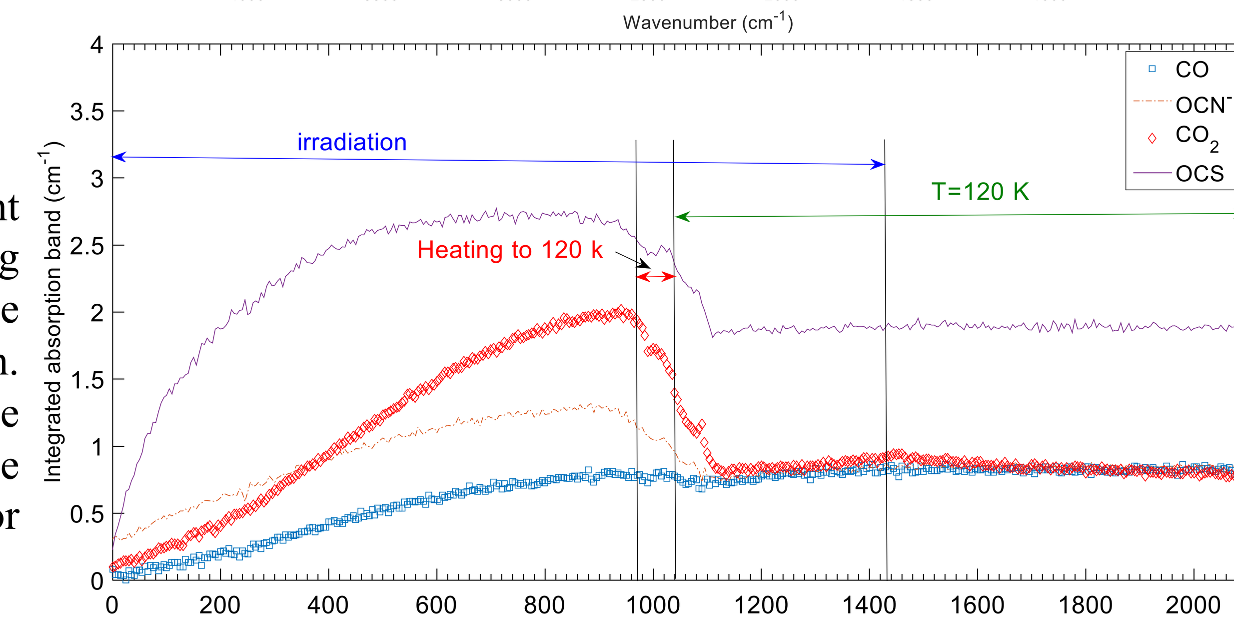

Conclusion: Irradiation of ice films with and without H_2S leads to a reddening and darkening observed in NIR spectra. The reddening is much more pronounced in the case of mixture with H_2S. Space weathering of H_2S containing surfaces could lead to darker and redder objects. The red color is due to a complex chemistry leading to the formation of organic polymers. The generation of S containing molecules like OCS, NH_4SH,CS_2 and SO_2 and their stability under irradiation and heating can be helpful for choosing target molecules for potential future missions to the Jupiter-Trojan asteroids as well as telescope observations with high signal to noise.

The research described here was carried out at the Jet Propulsion Laboratory, California Institute of Technology, under a contract with the National Aeronautics and Space Administration (NASA), and at the Division of Geological and Planetary Sciences at the California Institute of Technology.

Poster No: P-10

National Aeronautics and Space Administration

Measurements of self and foreign broadening coefficients using Tunable Laser Diode Spectrometer for Mars-TLS specific lines

Esha Manne (3225) and Christopher R. Webster (3200)

INTRODUCTION

This laboratory investigation supports and refines the data analysis of measurements made by the Tunable Laser Spectrometer (TLS) in the Sample Analysis on Mars (SAM) suite on the Mars Science Laboratory (MSL) Curiosity rover.

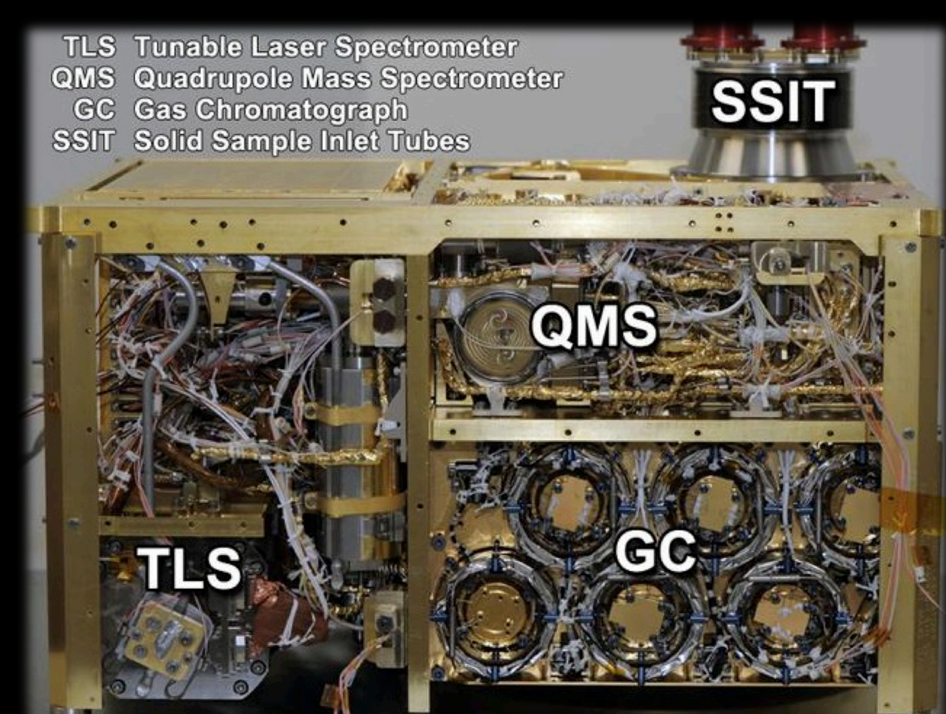

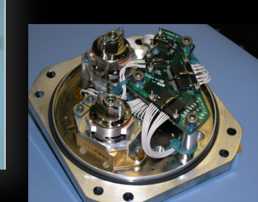

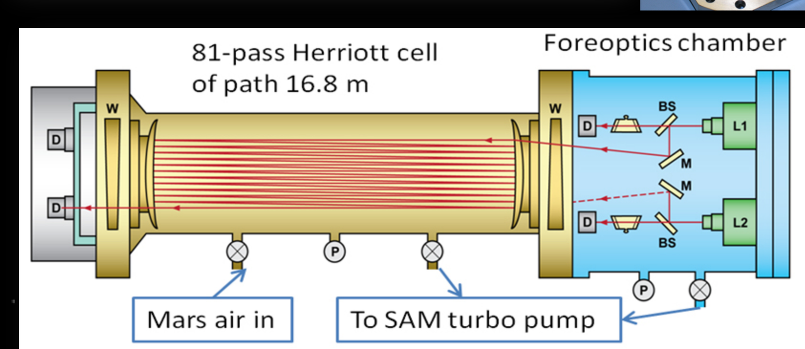

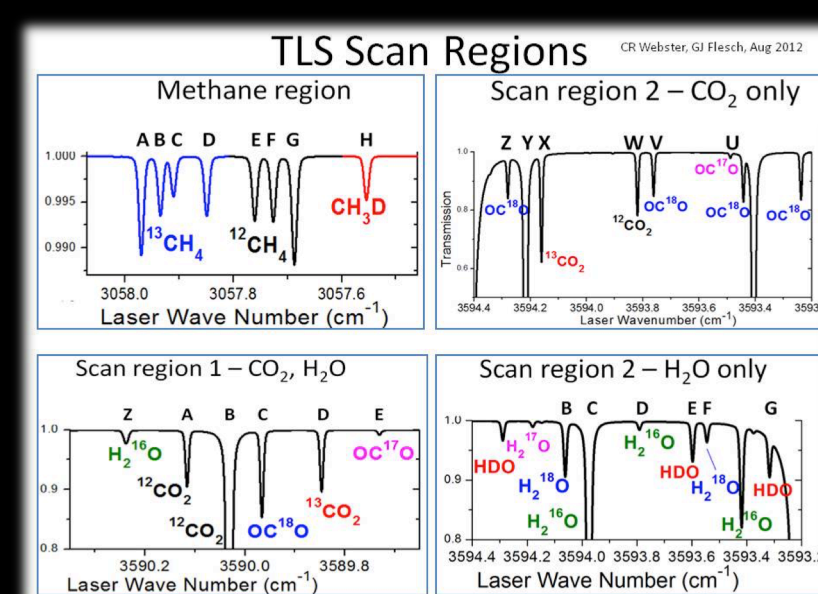

TLS has 2 channels and detects gases both in the atmosphere and evolved from rock pyrolysis:

Methane trace gas detection (3.27μm)

- Also measures $\delta^{13}C$ in methane evolved from rocks.

Isotopic ratios (2.78 μm)

- Water evolved from rocks: δD, $\delta^{18}O$, Atmospheric CO_2: $\delta^{13}C$, $\delta^{18}O$, $\delta^{17}O$, $\delta^{13}C^{18}O$

MOTIVATION: TLS-SAM instrument has been collecting data on gas abundances and isotope ratios [1-3], both from the Mars atmosphere and gases evolved from the pyrolysis of rock samples. These two applications of Mars atmosphere and pyrolysis in a helium flow present the need to quantify self- and foreign-broadening coefficients at higher accuracies than those provided by the HITRAN 2012 [4] linelist. Moreover, HITRAN's foreign-broadening listing is only for air.

METHODS

The spectrometer is a similar setup to the existing TLS instrument on Mars, based on Tunable diode laser absorption technique. Direct absorption technique is used for these studies. One laser source is a near-IR tunable diode laser at 2.78 μm that can scan two spectral regions containing CO_2 and H_2O isotopic lines. The second laser source is a diode laser at 3.27 μm for methane detection.

$$I = I_0 \exp(-\alpha d)$$

Fast current tuning 1-2 cm-1

Laser source → α, N (d) → Detector

α:Absorption coefficient=σ×N
σ:Absorption cross-section cm²
N: Number density /cm³

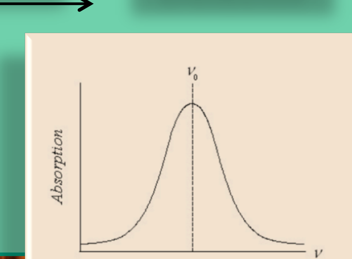

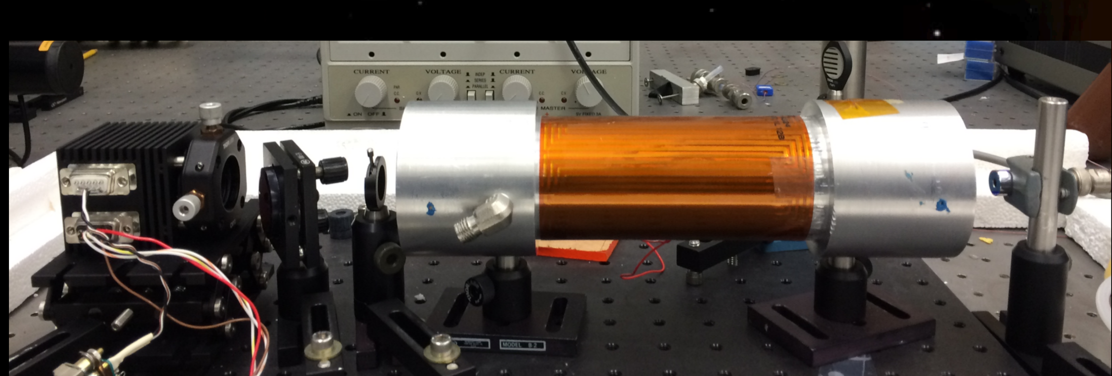

Tunable **lasers** 2.78, 3.27 μm

Gas cell

Detector

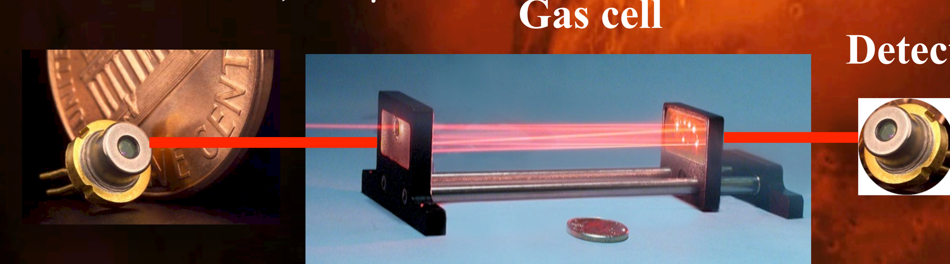

RESULTS

Direct absorption spectrum

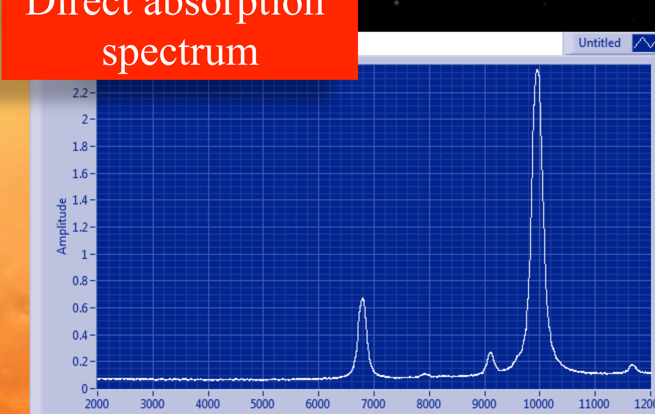

Wavelength calibration

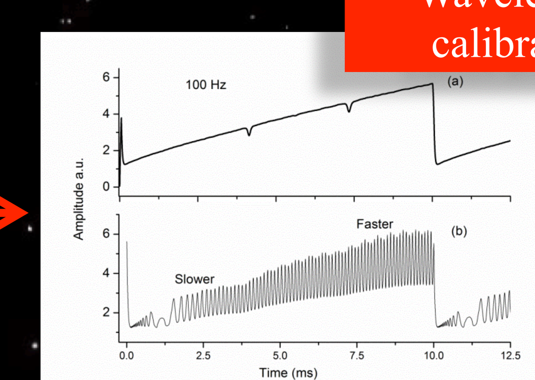

Voigt profile

$$I_V(\omega) = \frac{1}{\sqrt{\pi}\Delta\omega_D} \mathrm{Re}[w(x,y)]$$

$$w(x,y) = \frac{i}{\pi}\int_{-\infty}^{+\infty} \frac{e^{-\tau^2}}{x-\tau+iy} d\tau$$

Complex probability function

$$x = \frac{\omega-\omega_0-\Delta}{\Delta\omega_D},\ y = \frac{\Gamma}{\Delta\omega_D}$$

ω:Angular frequency,
Doppler width
Lorentzian width

Line profile fitting

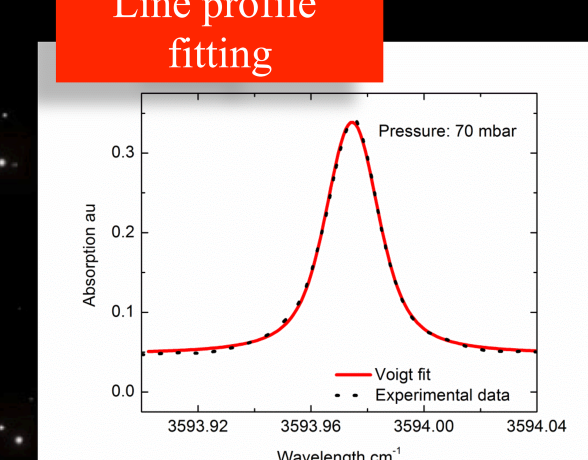

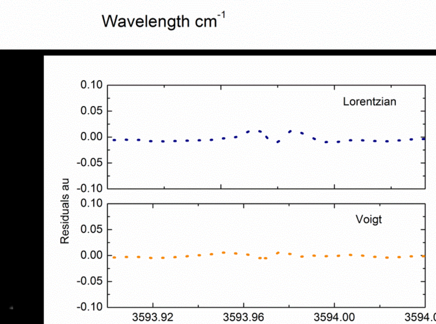

Line profiles used : Gaussian, Lorentzian, and Voigt
Ongoing work : Speed dependent Voigt, Rautian, and Galatry etc

CH$_4$ lines	γ_{N_2} (cm^{-1}/atm)		γ_{He}/γ_{N_2}	$\gamma_{CO_2}/\gamma_{N_2}$
	This work	HITRAN-12	This work	This work
E	0.06288 ± 0.0005	0.0645 (≥20%)	.6209	1.192
F	0.0609 ± .00071	0.0598 (≥20%)	.6448	1.295
G	0.06225 ± .00043	0.0609(10-20%)	.707	1.285

^{13}CH$_4$ lines	γ_{N_2} (cm^{-1}/atm)		γ_{He}/γ_{N_2}	$\gamma_{CO_2}/\gamma_{N_2}$
	This work	HITRAN-12	This work	This work
A	0.0583± 0.0005	0.0588 (≥20%)	.763	1.41
B	0.0633 ± .00071	0.065 (≥20%)	.711	1.291
C	0.05561 ± .00043	0.056 (≥20%)	.629	1.384
D	0.062550.00072	0.0611 (≥20%)	.702	1.38

Line (CO_2)	γ_{Self} (cm^{-1}/atm)		γ_{N_2} (cm^{-1}/atm)		γ_{He} (cm^{-1}/atm)
	This work	HITRAN-12	This work	HITRAN-12	This work
A (CO_2)	.094 ± .0013	.09 (1-2%)	.0655 ± .001	.0689 (1-2%)	.0217 ± .00055
C ($OC^{18}O$	.0955 ± .001	.092 (1-2%)	.066 ± .0012	.0692 (1-2%)	.0193 ± .00043
D ($^{13}CO_2$)	.073 ± .0008	.076 (1-2%)	.0658 ± .0009	.0675 (1-2%)	.0259 ±.00046

Line (Water)	γ_{Self} (cm^{-1}/atm)		γ_{N_2} (cm^{-1}/atm)		γ_{He} (cm^{-1}/atm)
	This work	HITRAN-12	This work	HITRAN-12	This work
B ($H_2{}^{18}O$)	0.433 ± 0.005	0.456 (2-5%)	.0903± 0.00146	.1034 (2-5%)	.0120 ± .00022
C (H_2O)	0.62 ± .0071	0.611 (≥20%)	.0826 ± 0.001	.0843 (1-2%)	.0114 ± .00013
E (HDO)	0.375 ± .0043	0.368 (5-10%)	.0756 ± .00095	.0741 (5-10%)	.0119 ± .00015

Measurement errors are within 5% for self- and pressure- broadening coefficients. Differences in experimentally-measured N_2 broadening coefficients from that listed in HITRAN-12, are <5%. For TLS, differences in reported isotope ratios between HITRAN 12 and our results are only ~70 per mil for δD values close to 3500 per mil, ~2 per mil for $\delta^{18}O$ in water, and ~4-5 per mil for $\delta^{13}C$ and $\delta^{18}O$ in CO_2.

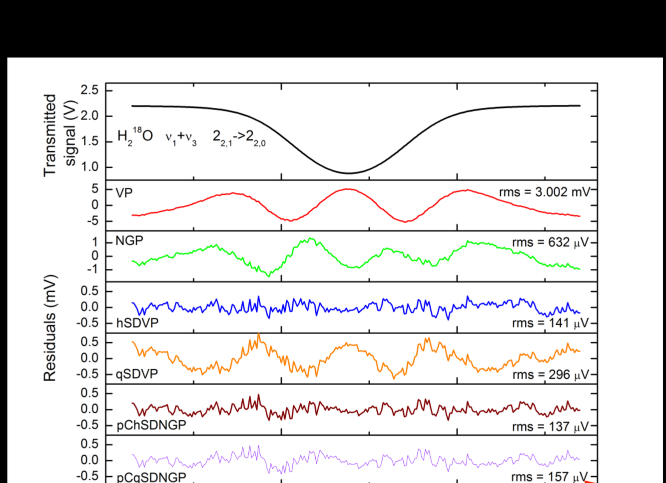

Conclusions: We report experimental measurements of self- and pressure- broadening coefficients for the spectral lines targeted by TLS on Curiosity rover. A tunable diode laser spectrometer operating near 2.78 μm and 3.27 μm has been implemented for these studies. The experimental parameters have been compared with values from the HITRAN-12 database.

Future Work: (Left Figure) Comparison of line-shape fits to the $H_2{}^{18}O$ absorption feature at 7222.29 cm^{-1} measured at a pressure of 2.70 Torr and a temperature of 273.16 K (De Vizia *et al.* 2012).

References

[1] C. R. Webster *et al.*, Science **341** 260 (2013).
[2] P. R. Mahaffy *et al.*, Science **341**, 263 (2013).
[3] C.R. Webster, Applied Optics **44**, 1226 (2004).
[4] L.S. Rothman et al., J. Quant. Spectrosc. Radiat. Transf. **130**, 4 (2013).

Acknowledgements: The research described here was carried out at the Jet Propulsion Laboratory, California Institute of Technology, under a contract with NASA. J. Manne also acknowledges support from NASA in the form of a postdoctoral fellowship.

Jet Propulsion Laboratory
California Institute of Technology
Pasadena, California
www.nasa.gov

P-11

National Aeronautics and Space Administration

Chemical environments in extremophile-rich sulfide caves as analogs for Europa's subsurface ocean.

Michael J. Malaska[1] (3227), Hilary S. Kelly[2], Penelope J. Boston[2], Mike Spilde[3], Laura Rosales-Lagarde[4]

[1] Jet Propulsion Laboratory / California Institute of Technology, Pasadena, CA. [2] New Mexico Institute of Mining and Technology, Socorro, NM. [3] University of New Mexico, Albuquerque, NM. [4] Georgia Southern University, Statesboro, GA.

What is relevance of Cueva de Villa Luz to Europa's subsurface ocean?

Both have H_2S – O_2 gradient systems – environments with potential chemical gradients for metabolism

Europa H_2S - O_2 gradient

Ice photolysis and subduction injects O_2 into ocean
Hydrothermal vents inject H_2S into ocean base

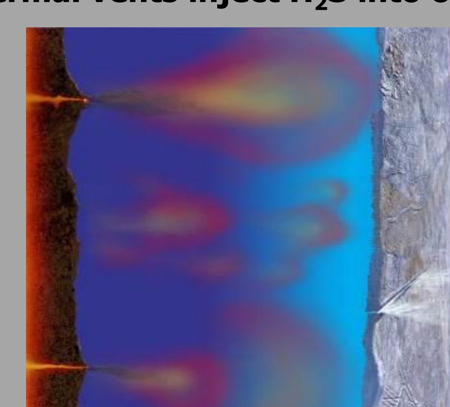

H_2S-rich waters
Oxygen-rich waters

Cueva de Villa Luz H_2S - O_2 gradient

Meteoric flux brings in O_2-rich waters
Subsurface springs inject H_2S – rich waters

H_2S-rich waters
Oxygen-rich waters

Colony sampled from where waters mixed

Extremophile life

thrives in Cueva de Villa Luz H_2S - O_2 gradient

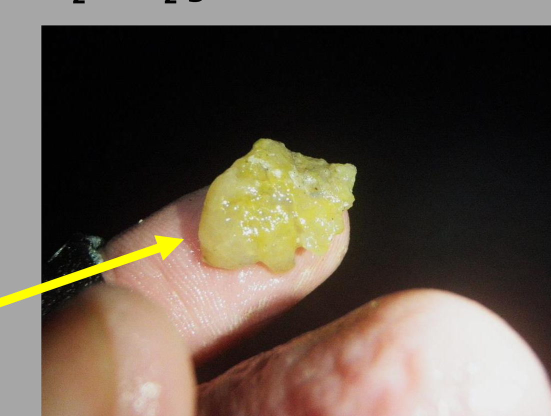

Thiobacillus spp. "phlegmball" metabolism: $H_2S + O_2 \rightarrow H_2SO_4$

Introduction

Cueva de Villa Luz is a flooded cave in southern Mexico containing H_2S-rich waters that mix with oxygenated waters. The cave hosts extremophile organisms that survive by metabolizing hydrogen sulfide (H_2S) into sulfuric acid (H_2SO_4).

The gradients and environments in Cueva de Villa Luz could be analogs for the chemical gradients that may exist in Europa's subsurface ocean.

Objective

Previous work sampled only 7 points and identified only two types of environments.

As part of a combined scientific expedition to study Cueva de Villa Luz, our goal was to fully map and identify the chemical environments in the cave.

The chemical environment maps will serve as a basemap for current and future geology and extremophile studies in Cueva de Villa Luz.

Methods

We systematically sampled cave waters using an EXO-1 chemical probe to measure:

- Temperature
- pH
- Oxidation-Reduction Potential (ORP)
- Dissolved Oxygen (ODO)
- Total Dissolved Solids (TDS)
- Turbidity

Cueva de Villa Luz sample locations (over 70 inside cave; 2 outside)

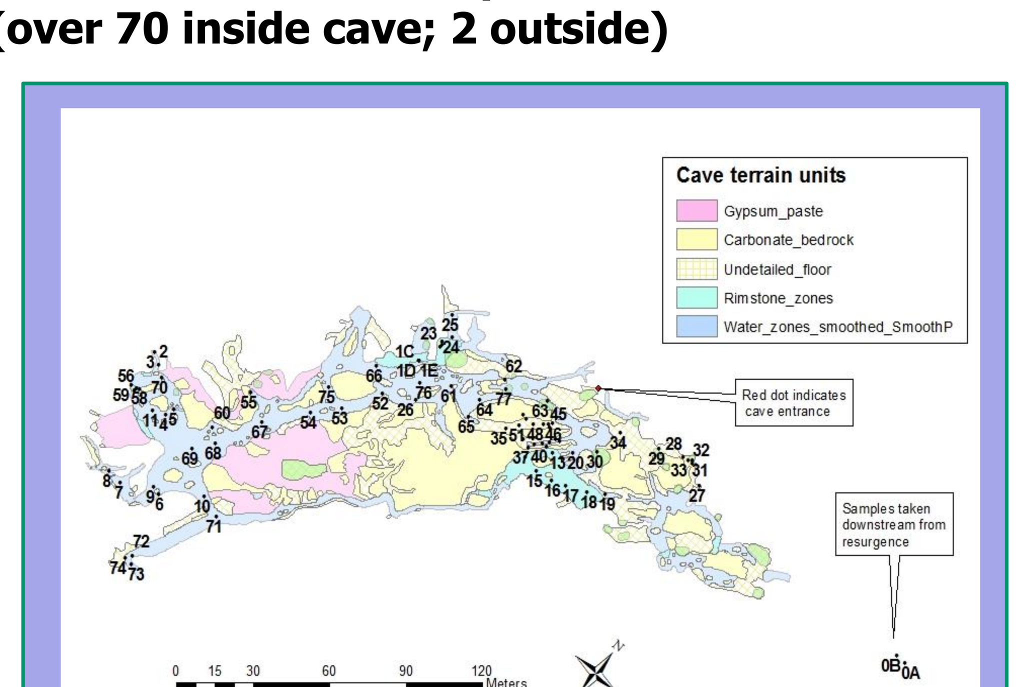

Results

Classification of environments using measured ORP and Turbidity

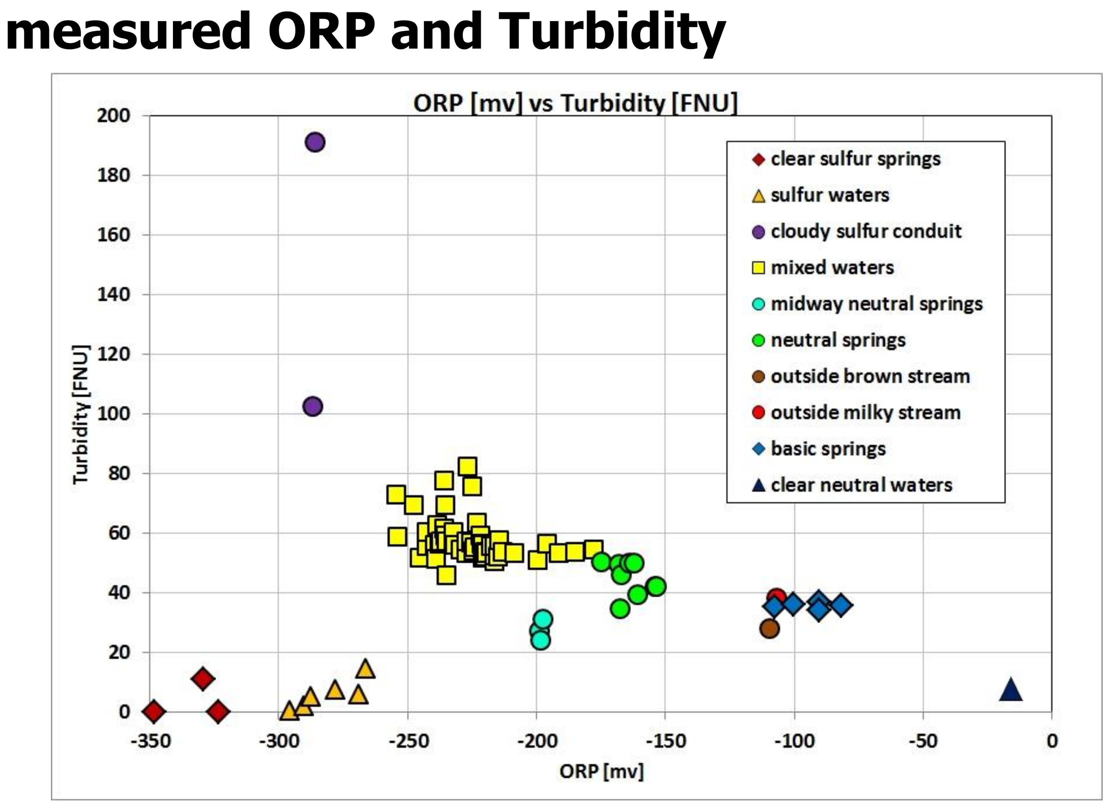

Map product showing Oxidation-Reduction Potentials of Cueva de Villa Luz

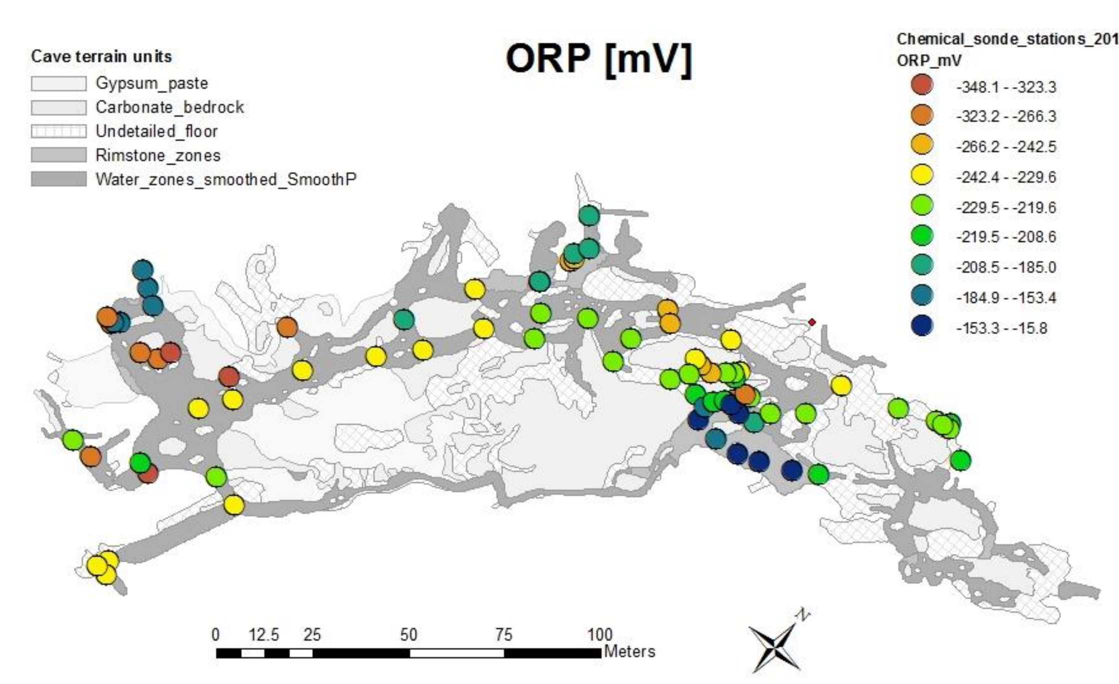

Spatial correlation of identified environments

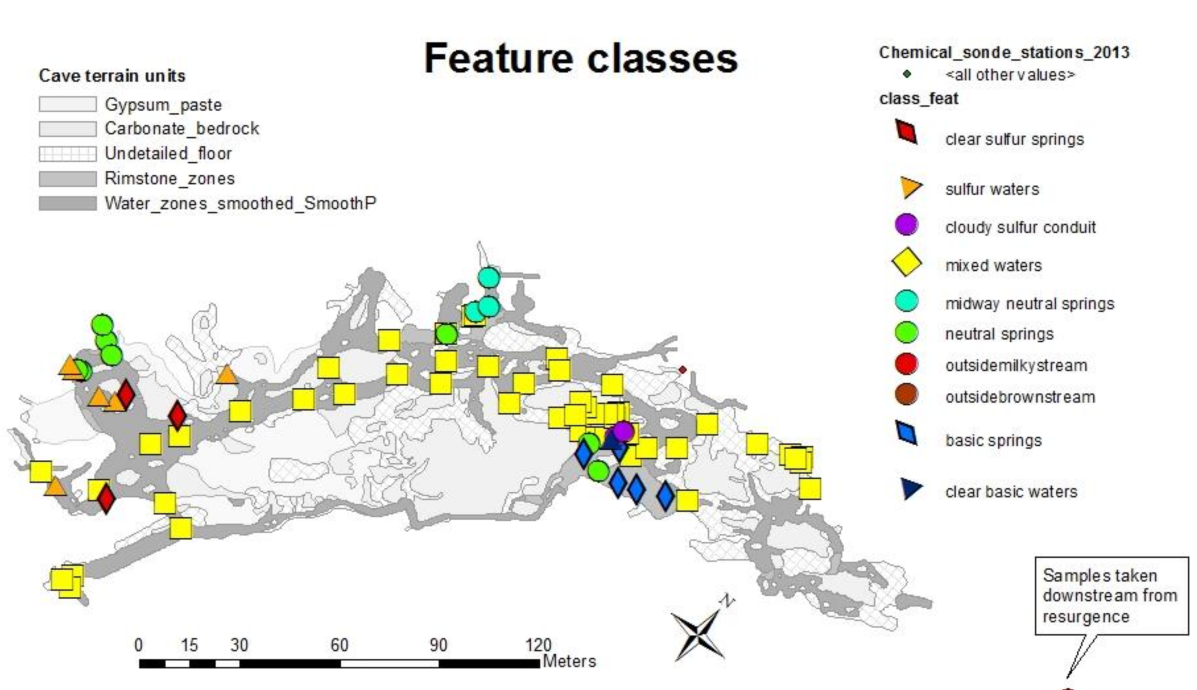

Cueva de Villa Luz environments align with putative Europa environments

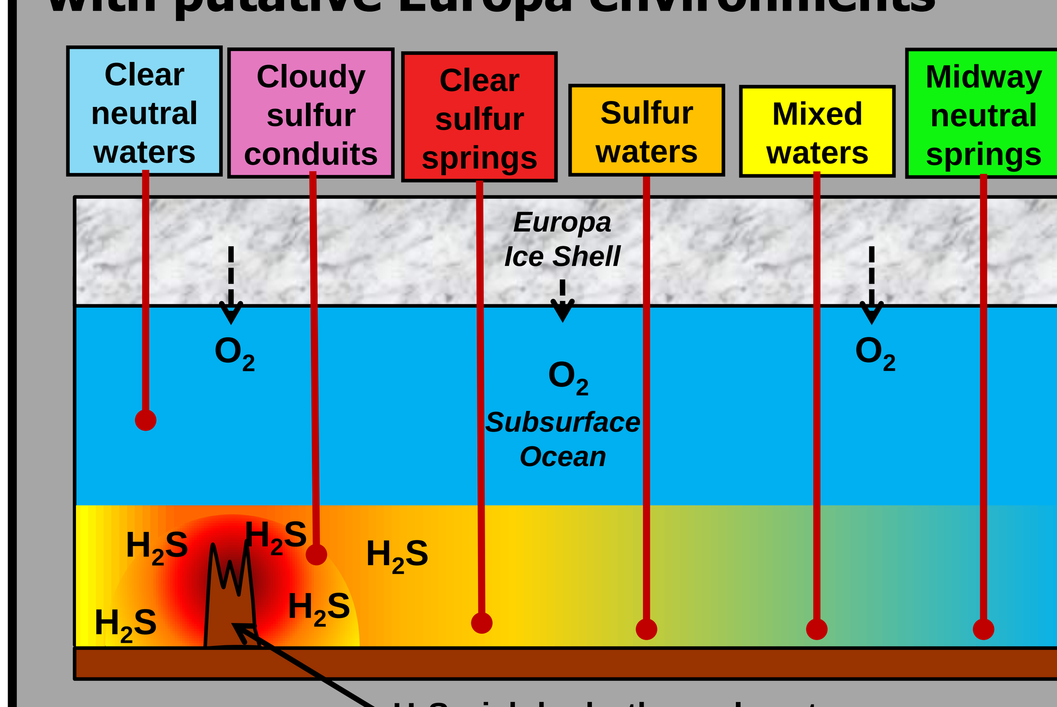

Examples of identified environments

Clear sulfur springs

Neutral springs

Cloudy sulfur conduit

Clear basic waters

Conclusions

- Chemical map of Cueva de Villa Luz
- Range of H_2S-rich aqueous environments
- 8 types of environments characterized
- Base map for extremophile studies
  - biology
  - geology
  - extremophile communities
- May serve as possible analogs for Europa

National Aeronautics and Space Administration

Jet Propulsion Laboratory
California Institute of Technology
Pasadena, California

www.nasa.gov

Poster No. P-12

National Aeronautics and Space Administration

Phase transitions and energy exchanges in the systems H_2O-THF-NH_3, H_2O-CH_4-NH_3 and H_2O-C_2H_6-NH_3 at Titan's crust conditions

V. Muñoz-Iglesias (3227)
T. H. Vu (3227), W. D. Smythe (3227), C. Sotin (4000) and M. Choukroun (3227)
Jet Propulsion Laboratory, California Institute of Technology, Pasadena, CA, USA

Introduction: Titan's upper layers

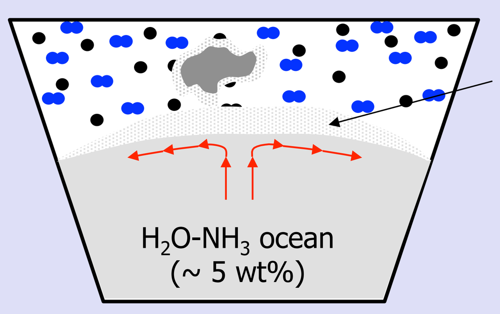

Crust (H_2O Ice, CH_4- and C_2H_6-clathrates, ammonia hydrates (AH)) melting zone due to contact with a warm plume of NH_3 aqueous solution

Conductive crust: Zones rich in AH also melt with the arrival of the plume to the bottom, resulting in moltens more NH_3 concentrated than the ocean, i.e. ~ 15 wt%

THF-clathrate: analogue CH_4-clathrate at lower pressures

Goal

Better understanding of NH_3—clathrate hydrates interactions

Method: Calorimetry

Setaram BT 2.15, Fixed Volume High Pressure Cells

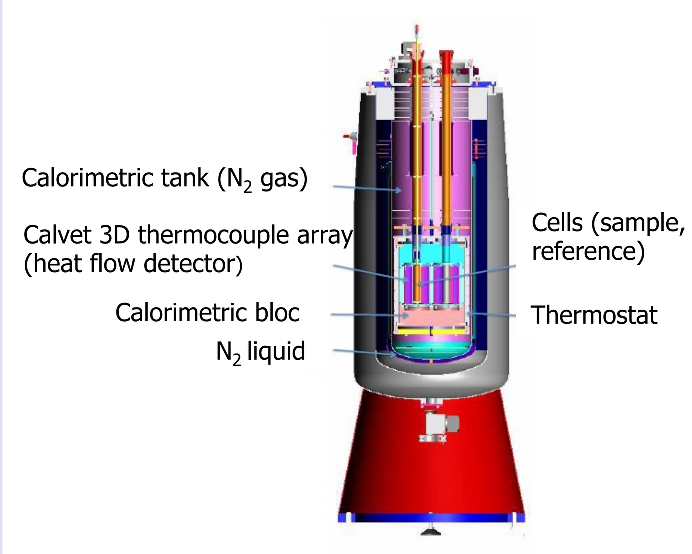

Cooling/Heating rate: 0.1 K.min^{-1}

Phase diagrams of the systems studied so far

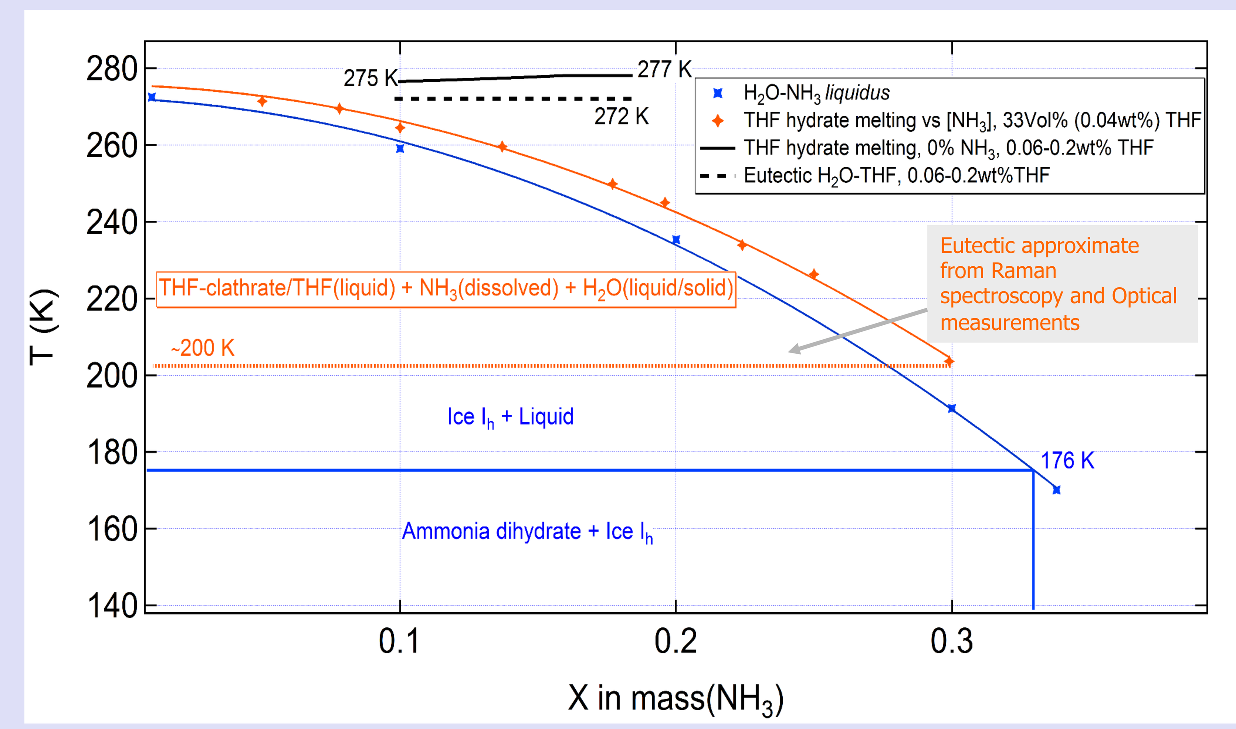

Calorimeter validation

H_2O-NH_3 29.3 wt%

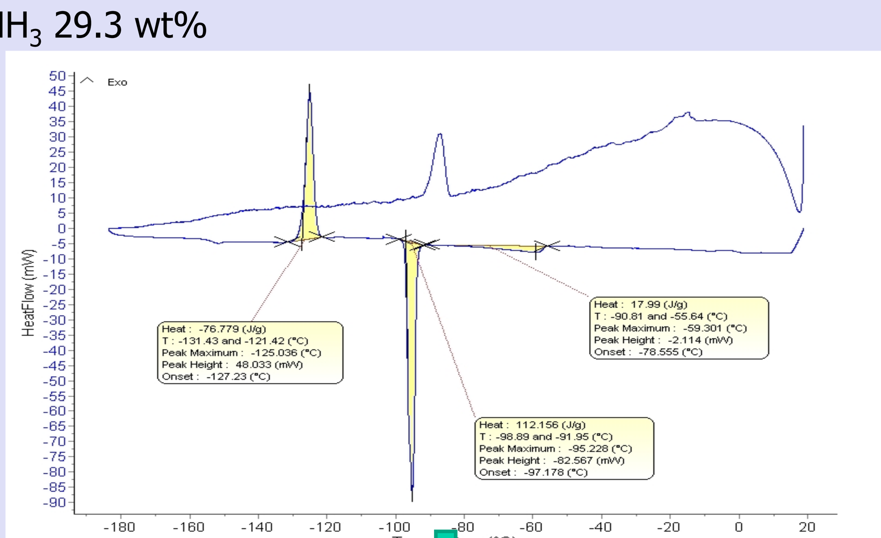

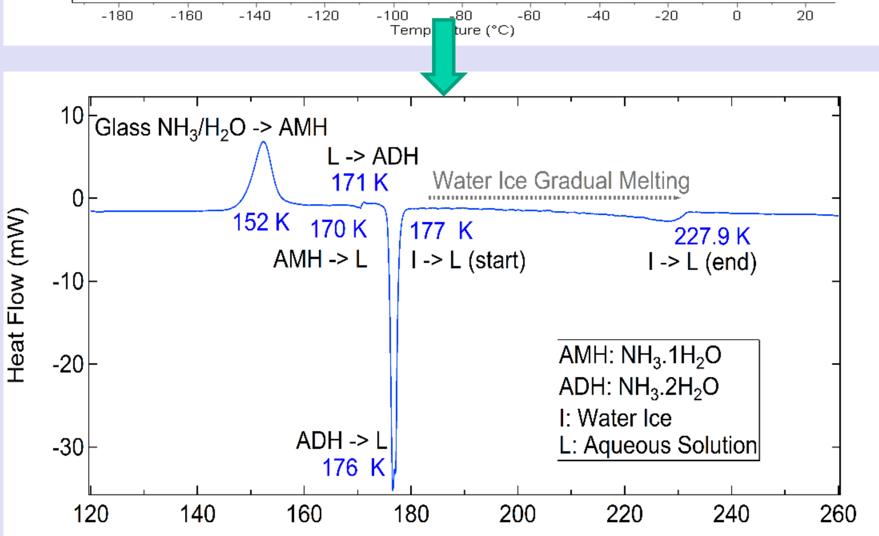

Complete agreement with previous works

Results: H_2O-THF-NH_3 system

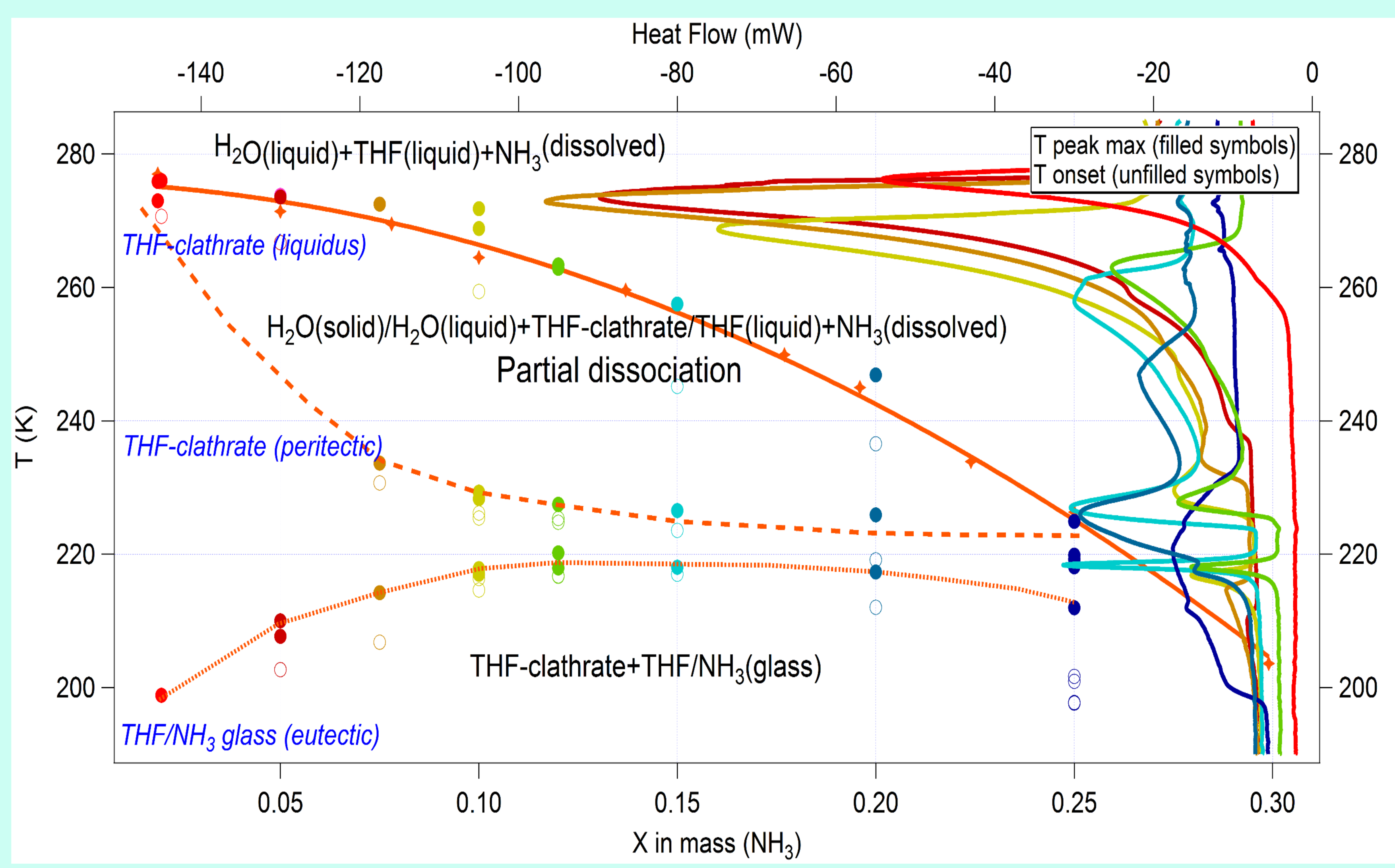

NH_3 causes:

a) Depression THF-clathrate equilibrium curve

b) THF-clathrate dissociation in steps (*partial dissociation*)

c) NH_3-THF bond below 220 K avoids AMH, ADH and/or pure NH_3 solid stabilization

Thermograms allow qualify and quantify these partial dissociations

In this case: 2 partial dissociations

↑ [NH_3] -> ↑ Heat flow 1st dissociation and ↓ Heat flow 2nd dissociation

Calorimetry: Higher accuracy for eutectic and partial dissociation determination

Next runs: H_2O-CH_4-NH_3 and H_2O-C_2H_6-NH_3 systems at pressures up to 10 MPa

NH_3 moves Water Ice melting to lower T:
5 wt% NH_3 → ΔT ~ 5 K
17.6 wt% NH_3 → ΔT ~ 30 K

Questions to answer:
1) Will NH_3 promote similar ΔTs in CH_4- and C_2H_6-clathrates equilibrium curves as it does with Water Ice and THF-clathrate?
2) Will NH_3 promote also clathrate partial dissociation as it does with THF-clathrate?

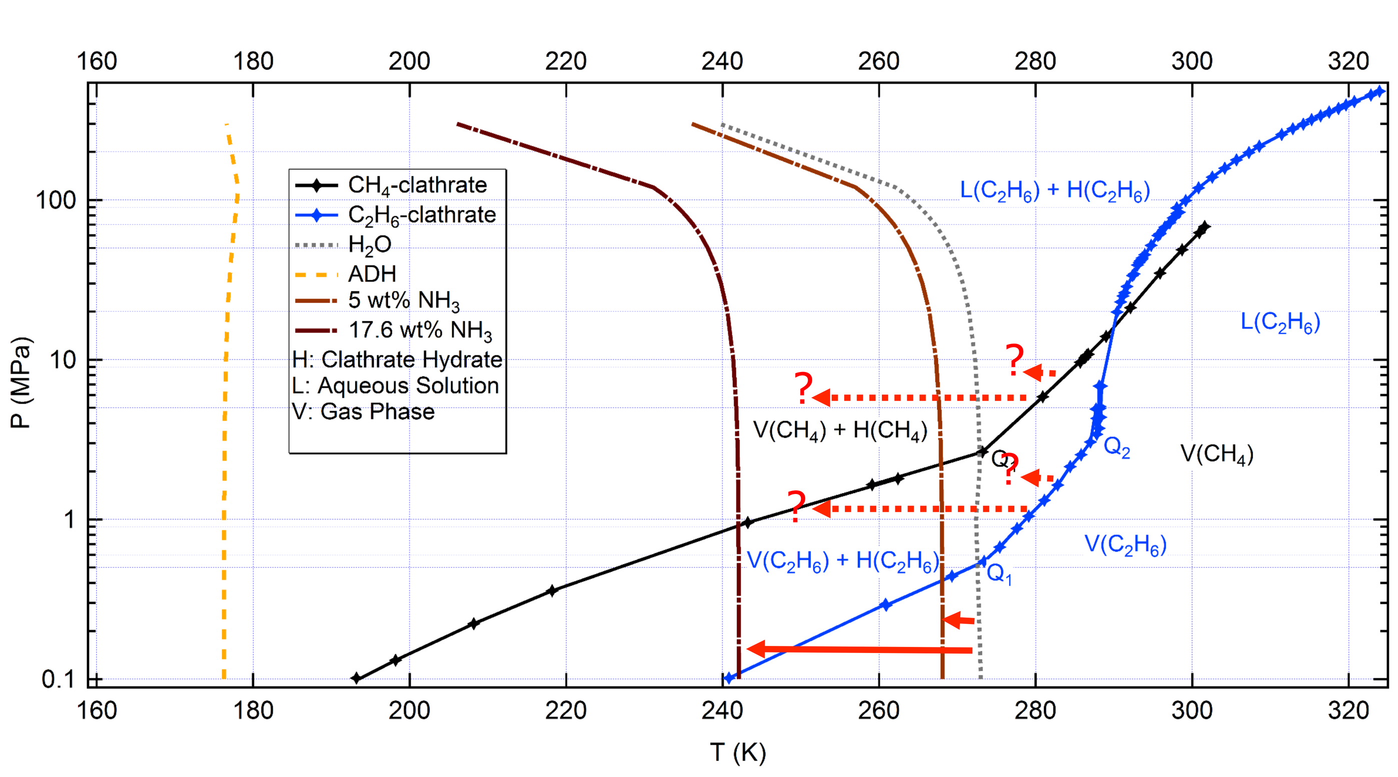

Run: H_2O-C_2H_6

Starting at 0.1 MPa

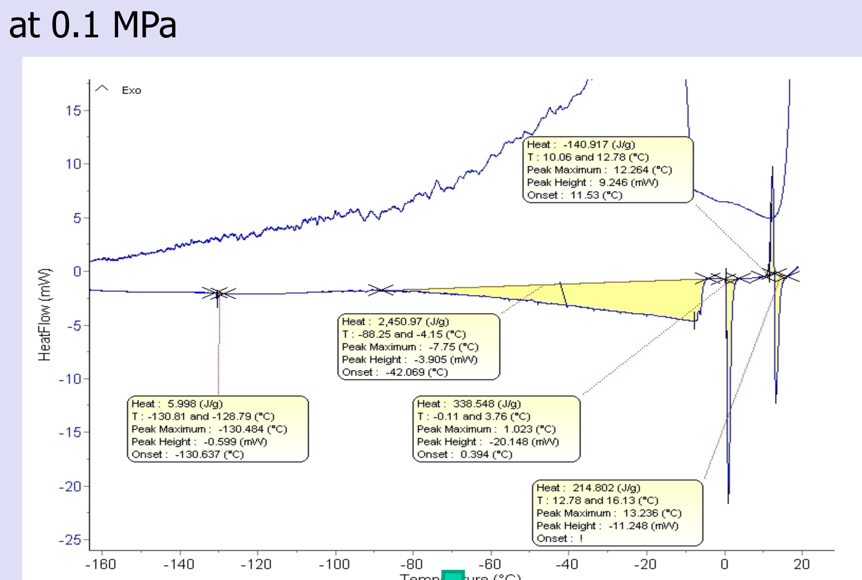

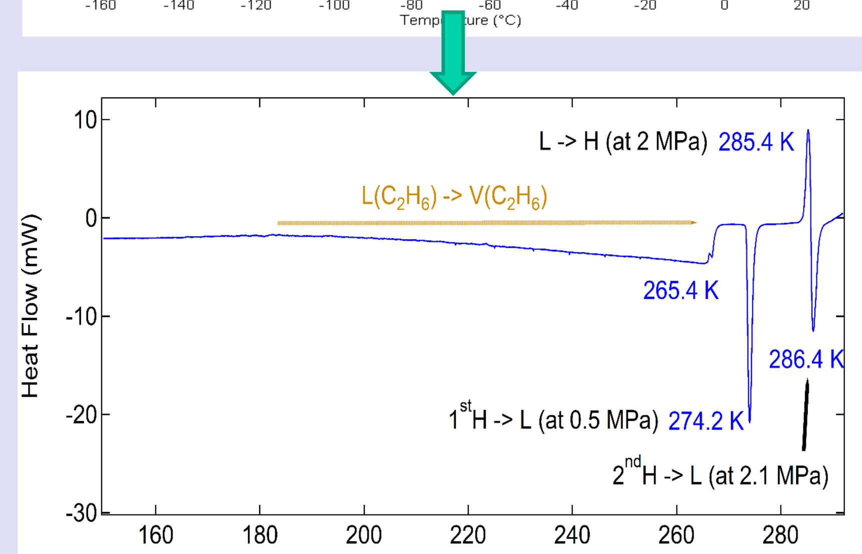

Before heating → 2 phases: L(C_2H_6) + C_2H_6-clathrate hydrate
180 K–265 K: L(C_2H_6) evaporates ⟶ pressure ↑ from 0.1 MPa to 0.5 Mpa
274 K: H dissociation ⟶ pressure ↑ from 0.5 MPa to 2 Mpa
285 K: Formation of a new H due to pressure ↑

Implications

Clathrate dissociation way and energy requirements necessary for:

1) Approach to current crust state

2) Better evaluation of the outgassing process from the crust to the atmosphere

References

[1] Choukroun, M., and Sotin, C.: Geophys. Res. Lett., 39, L04201, 2012.
[2] Mitri, G., et al.: Icarus, 236, 169-177, 2014.
[3] Fortes, A.D., and Choukroun, M.: Space Sci. Rev., 153, 185-218, 2010.
[4] Jones, C.Y., et al.: J. Thermodyn., 2010, 583041, 2009.
[5] Vu, T.H., et al.: J. Phys. Chem. B, 118, 13371-13377, 2014
[6] Yarger, J. et al.: J. Geophys. Res., 98, 13109-13117, 1993.
[7] Sloan, E.D., and Koh, C.A.: Clathrate Hydrates of Natural Gases, 3rd Ed., CRC Press, 2008.
[8] Hogenboom, D.L., et al.: Icarus, 128, 171-180, 1997.
[9] Leliwa-Kopystynski, J.: Icarus, 159, 518-528, 2002.

Acknowledgements

This research is supported by an appointment to the NASA Postdoctoral Program at the Jet Propulsion Laboratory, California Institute of Technology, administered by Oak Ridge Associated Universities through a contract with NASA. Support from the NASA Outer Planets Research program and government sponsorship acknowledged

National Aeronautics and Space Administration
Jet Propulsion Laboratory
California Institute of Technology
Pasadena, California

www.nasa.gov

Poster No. P-13

National Aeronautics and Space Administration

InSight and Impacts:
Geological Investigations of the InSight Landing Site Using Fresh Craters and Implications for Seismic Detection of Impacts

Ingrid J. Daubar (3223) and Matthew P. Golombek (3223)

Figure 1 (below): *496 new dated impact sites on a map of the TES Dust Cover Index (DCI) [9], a measure of the dustiness at the surface.*

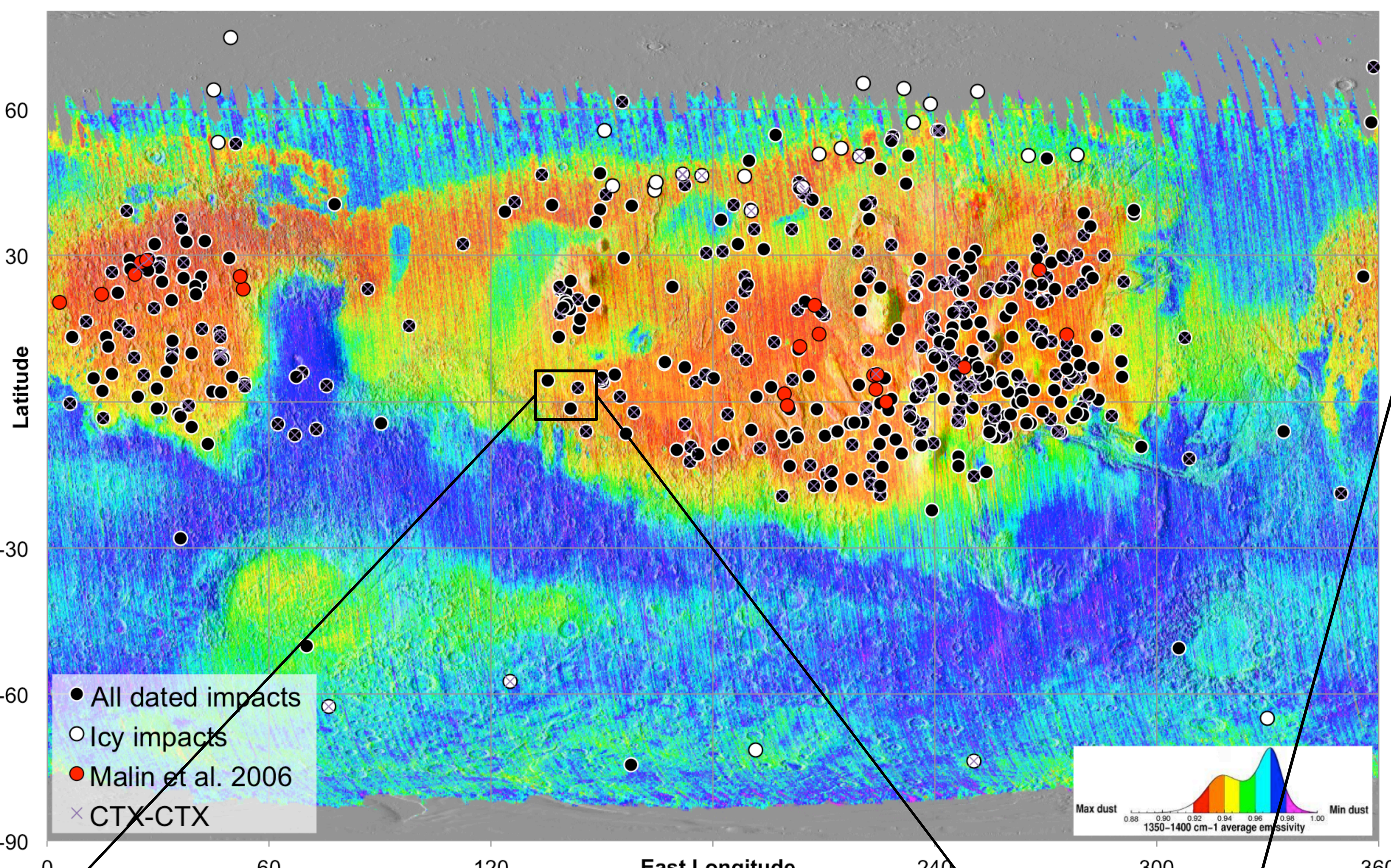

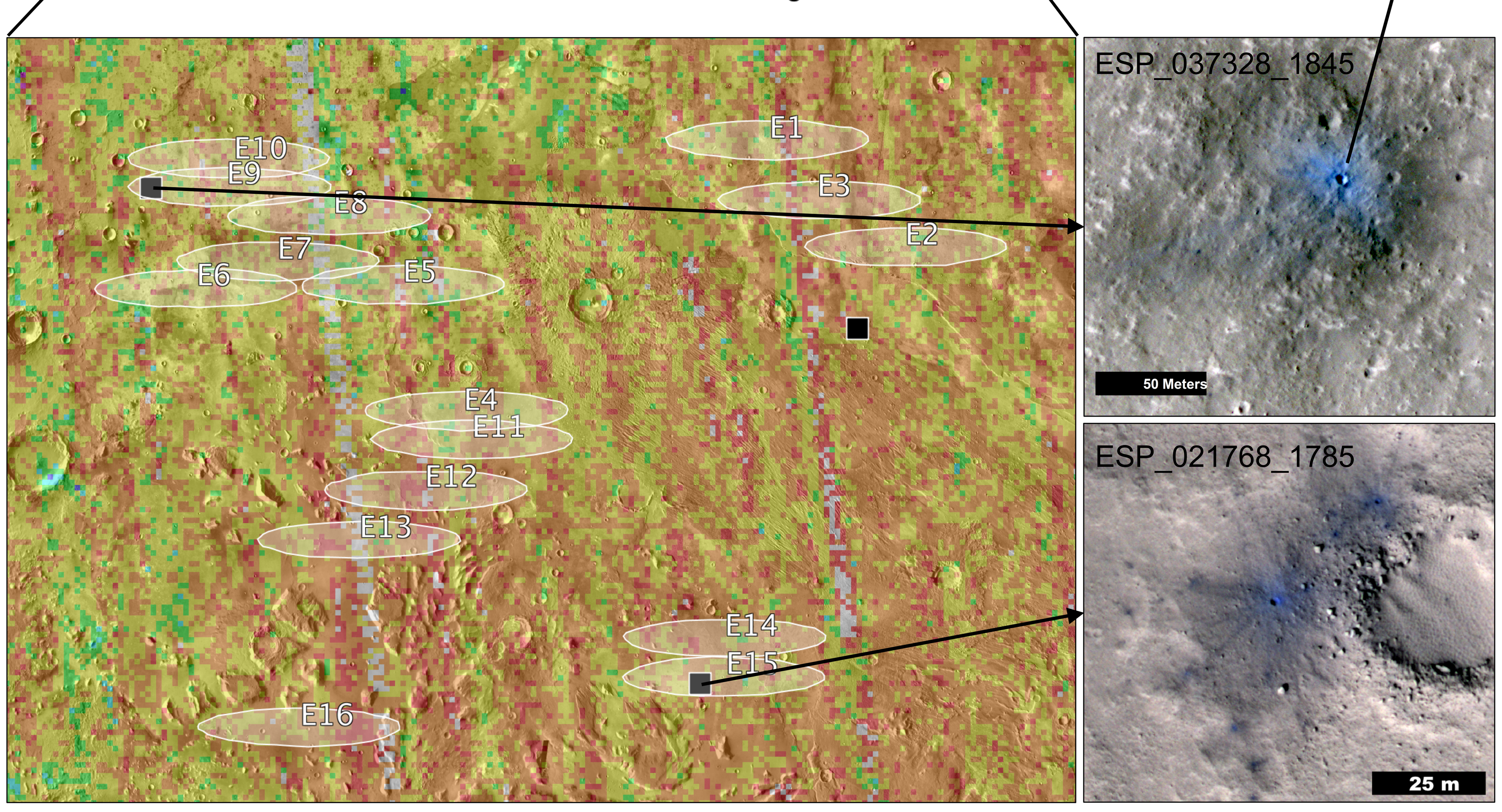

Figure 2 (above): Left: *Locations of new dated impacts (black squares) near proposed InSight landing ellipses (white; shown before downselection). Basemap is TES DCI [9] (same scale as Fig. 1) over THEMIS Day IR [15]. Lower dust cover to the west is likely contributing to fewer craters being found.* ***Right****: Two examples of new impacts near proposed InSight landing sites. HiRISE images credit: NASA/JPL/University of Arizona*

(Sub)surface properties and their importance to InSight

- New, small craters near InSight landing site (Fig. 2, left) expose properties of the surface and shallow subsurface
- Amount of surface dust and underlying albedo indicated by darkened "blast zones" around impacts (Fig. 2, right)
- Ejecta distributions and crater morphologies determined by target material strength, cohesion, and layering within depth of excavation (Fig. 3).

- **Relevance to HP[3] instrument:**
  - Mole hammering expected to similar depths, up to 5 m – soil penetrability
  - Surface albedo and dust covering – inputs to thermal models
- **Relevance to SEIS instrument:**
  - Propagation of seismic signals through a scattering regolith layer
  - Impact-induced seismic signals – frequency and detectability
- Regolith cohesion, material strength, surface dust cover, etc. also affects:
  - Instrument site selection and deployment
  - Surface ops, e.g. thermal radiometer surface brightness temperature measurements

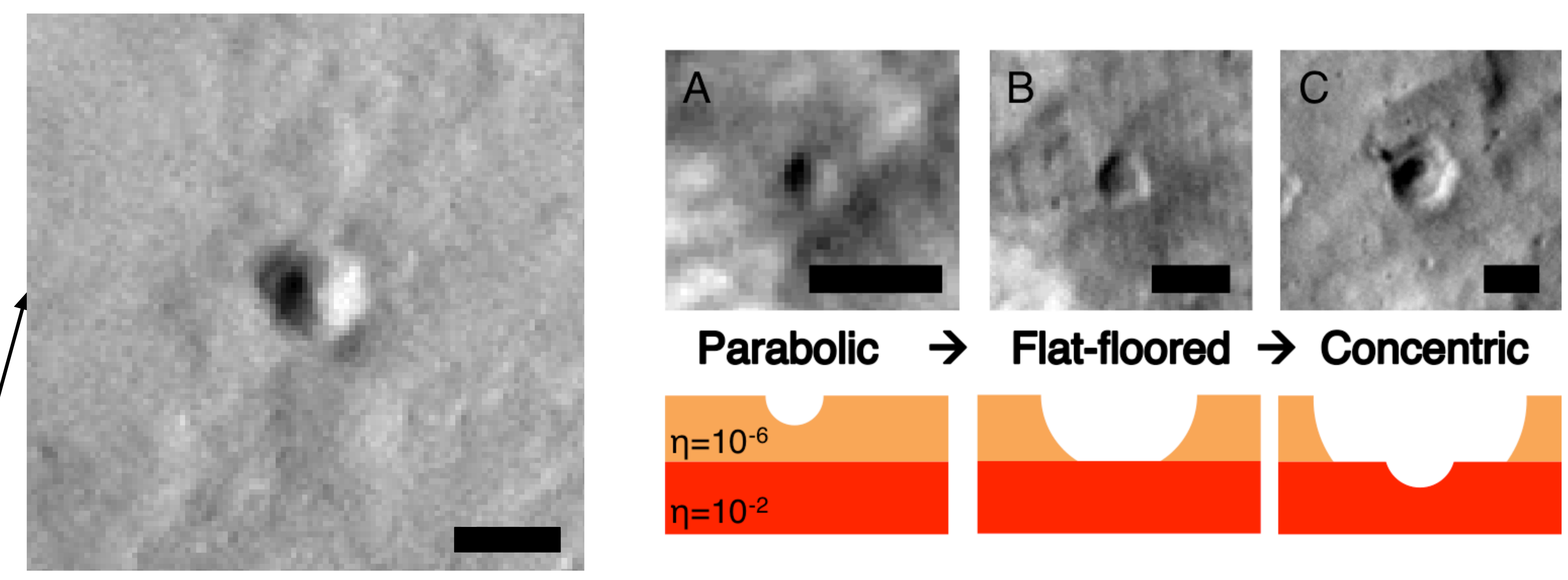

Figure 3 (above): Left: *Possible concentric/"nested" crater located in E09 landing ellipse.* ***Right:*** *Example cluster with schematic showing how varying crater morphology with size indicates subsurface layering with differing material strength. Cluster in HiRISE image PSP_010292_1785 (1.28ºS, 250.1ºE; scale bars are 5 meters.*

Current cratering rate: 1.8×10^{-6} $D_{eff}\geq3.9$ m/km^2/yr (cumulative)

- For D<50 m, observations are lower than models; when extrapolated to larger sizes, they are higher than models
  → Model ages higher by a factor of ~4 if using small diameters, or lower if extrapolated to larger sizes [*e.g.*, 10]
- **Commonly-used martian isochrons should be used with great caution for small craters**
- Dark blast zones key to identification → Spatial bias toward dustiest areas of Mars (Fig. 1)

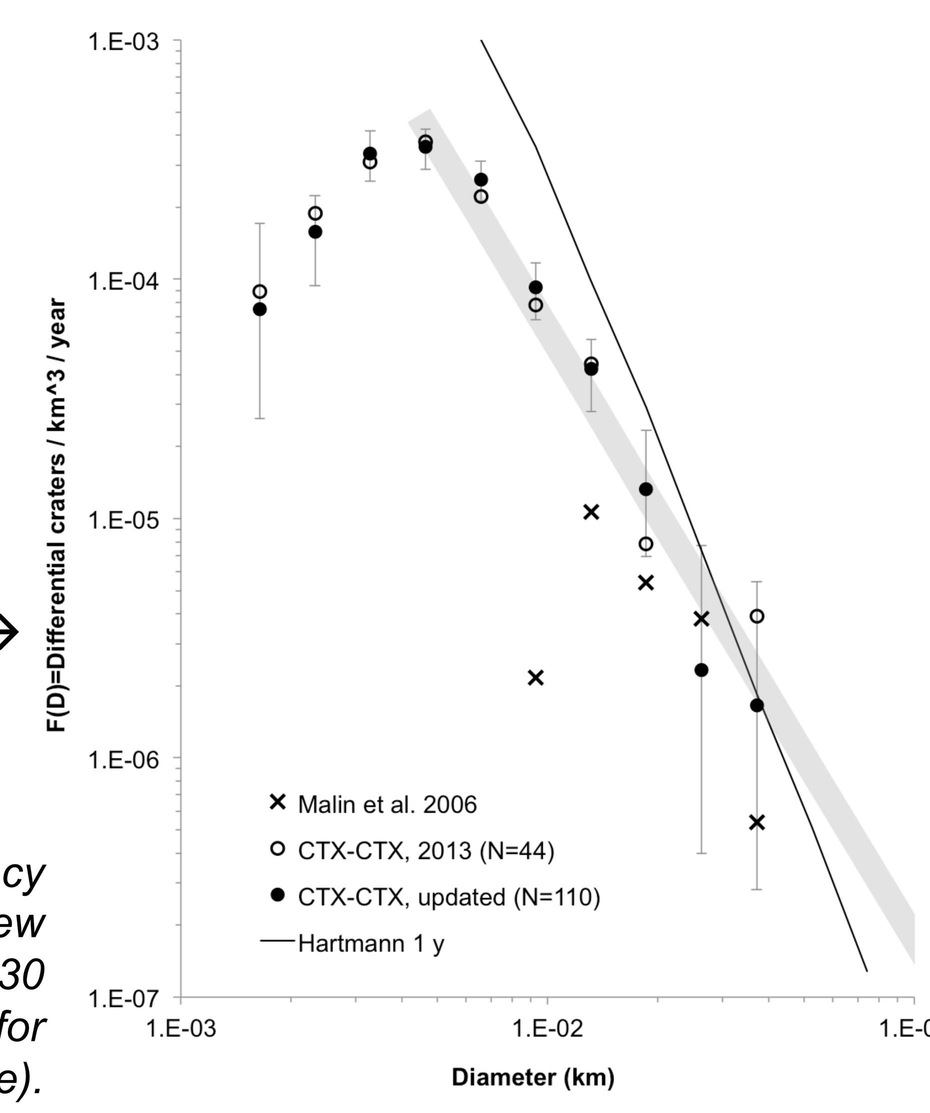

Figure 4 (right)*: Current crater size frequency distribution for a 1y production function using new dated craters [1, 2]. Shaded line is best fit for 4-30 m diam. Hartmann 2005 model [8] shown for comparison (solid line).*

Predicting InSight impact detections

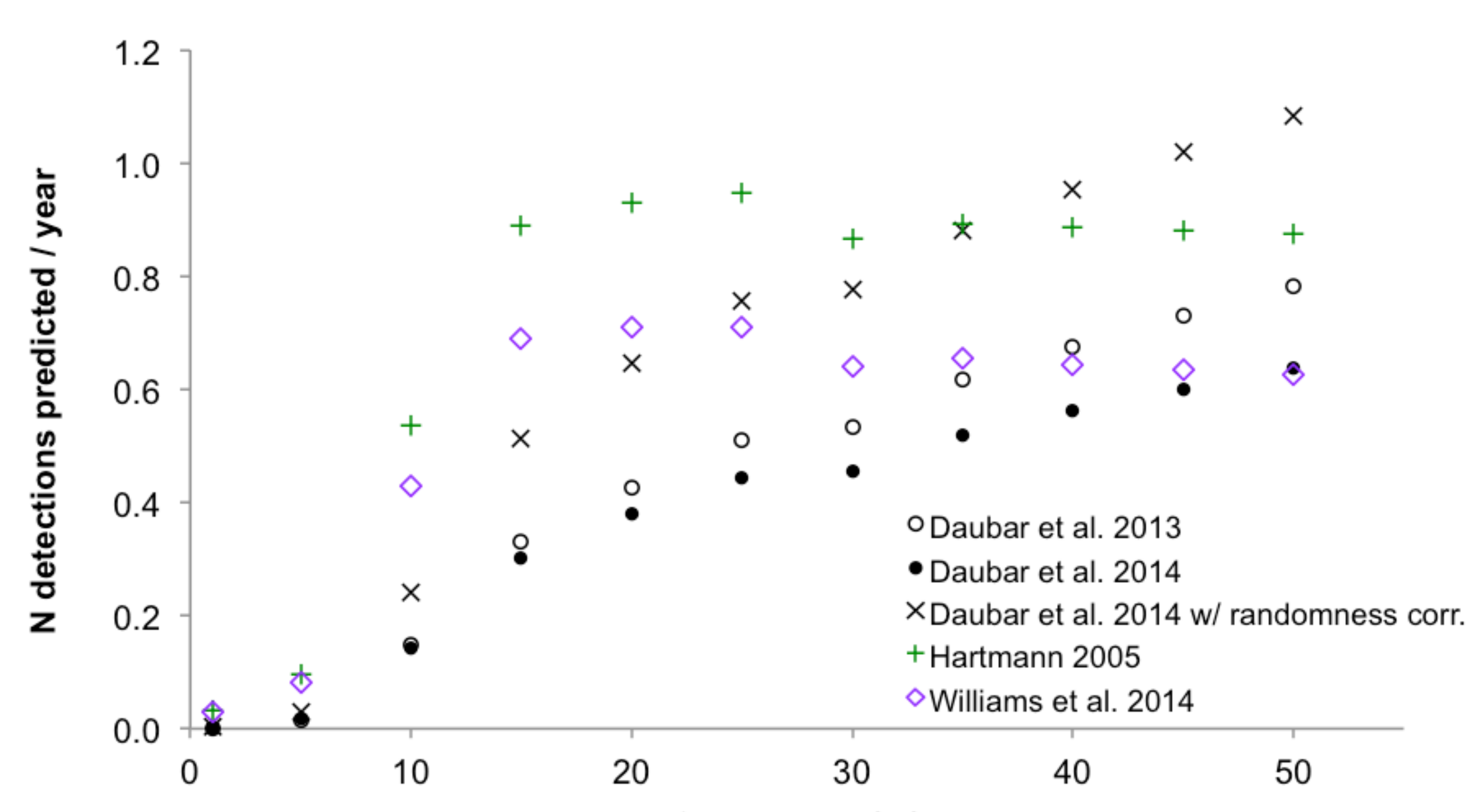

Figure 5 (above): *Predicted number of SEIS impact detections of craters of different sizes.*

- Minimum detectable crater size increases with increasing distance
- Detection limits + PFs [1, 2, 8, 14] (Fig. 4) → predicted number of impacts detected of a given size (Fig. 5): **~4-8 total impacts will be detected per Earth year (~8-16 in primary InSight mission)**
- ~Half new impacts are clusters – may reduce detectability
- *InSight will test these predictions and provide an independent measure of the current cratering rate at Mars*

National Aeronautics and Space Administration

Jet Propulsion Laboratory
California Institute of Technology
Pasadena, California

www.nasa.gov

References: [1] Daubar *et al.* (2013) *Icarus* 225, 506-516. [2] Daubar *et al.* (2014) *8th Mars Conf.*, Abs. 1007. [3] Banerdt *et al.* (2013) *LPSC*, Abs. 1915. [4] Malin *et al.* (2007) *JGR* 112, 5. [5] McEwen *et al.* (2007) *JGR* 112, 5. [6] Malin *et al.* (2006) *Science* 314, 1573-1577. [7] Ivanov (2001) *SSR* 96, 87-104. [8] Hartmann (2005) *Icarus* 174, 294-320. [9] Ruff and Christensen (2002) *JGR* 107, 5127. [10] Landis *et al.* (2014) *LPSC*, Abs. 2661. [11] Lognonné *et al.* (2000) *Planet. Space Sci.* 48, 1289-1302. [12] Schmerr *et al.* (2014) *GSA* Abs. 259-12. [13] Banks *et al.*, (2015) LPSC. [14] Williams *et al.* (2014) *Icarus* 235, 23-36. [15] Edwards *et al.* (2011) *JGR* 116, E10008.

Poster No. P-14

National Aeronautics and Space Administration

The International Space Station Microbial Observatory Experiment

Postdoctoral Fellow: Aleksandra Checinska (352N)
Principal Investigator: Kasthuri Venkateswawaran (352N)

Objectives

- The safety of the International Space Station (ISS) crewmembers and maintenance of hardware are the primary rationale for monitoring microorganisms in this closed habitat.
- National Research Council (NRC) recommended to utilize ISS – a closed habitat – and observe changes encountered due to the microgravity. Subsequently, NASA Space Biology program funded JPL to catalogue microbial diversity of ISS surfaces and atmosphere under NASA – Microbial Observatory Program.
- Molecular techniques were used to measure microbial burden and diversity associated with these samples that were previously.
- **This study provides the insight into microbial diversity of ISS using the state-of-the-art molecular techniques applied by JPL-352N group for the MARS exploration program.**

Sample Collection

Sample collection from 8 locations of Dragon capsule (SpaceX) using polyester wipes, contact slides, opsite tape and air sampling device. → Sample collection from 8 ISS locations using polyester wipes, contact slides, opsite tape and air sampling device. → Sample processing upon the arrival to JPL; the samples returned on Soyuz TM-14M and SpaceX CRS-6)

Sample Processing

Sample recovery and concentration →
- Propidium Monoazide (PMA) assay and DNA extraction → Viable population and microbial diversity (qPCR, Illumina based Next Generation Sequencing and Metagenomics)
- Microbial Bioburden Assessment measured by Adenosine Triphosphate (ATP) Assay
- Cultivable population (sample was split for incubation on R2A, PDA and Blood Agar)

Cultivable Bacterial Diversity

A

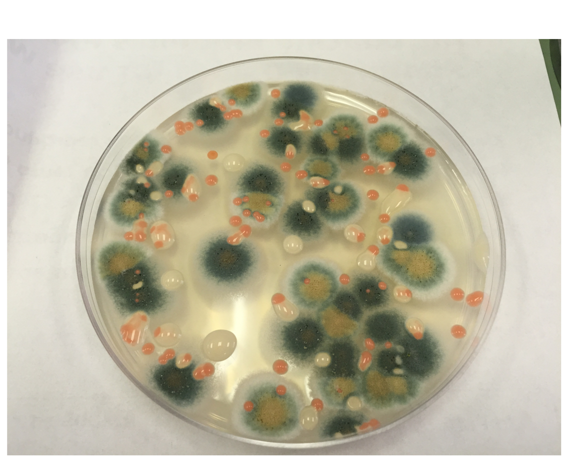

B

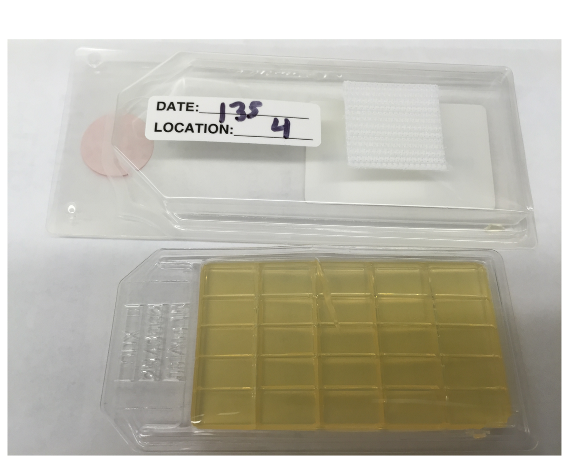

C

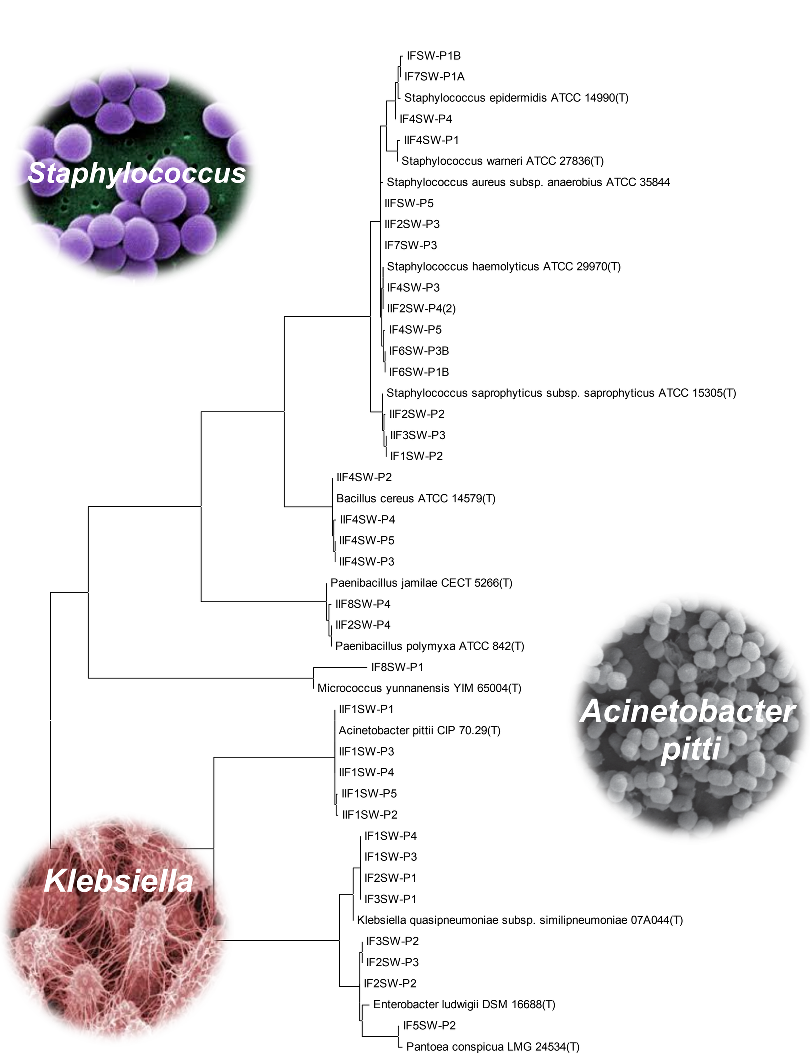

Fig. 1. Microbial population from ISS location no. 4 (dining table) on PDA plate (fungi promoting media) (A). The contact slide used for sampling the ISS location no. 4 (dining table) (B). Contact slides cover a surfaces of 25 cm^2 while a polyester wipes 1 m^2. Phylogenetic tree for the isolates collected from Blood Agar plates (potential pathogens); IF, IIF– first and second sampling on the ISS, respectively.

Cultivable/Viable, Bacterial Community

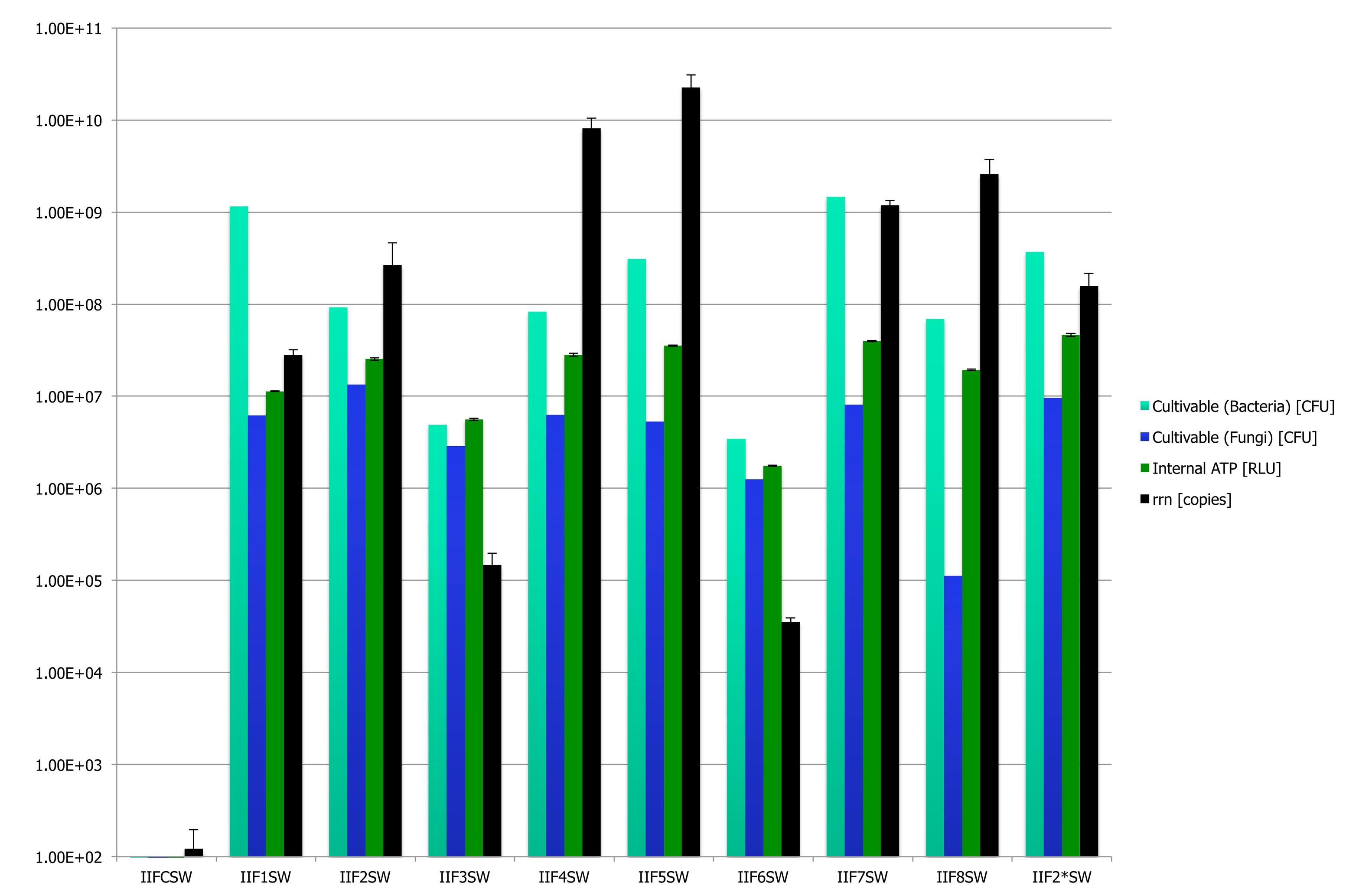

Fig. 2 Microbial population of various surface locations of ISS as measured by traditional and molecular methods.

Molecular Microbial Community Diversity Analysis

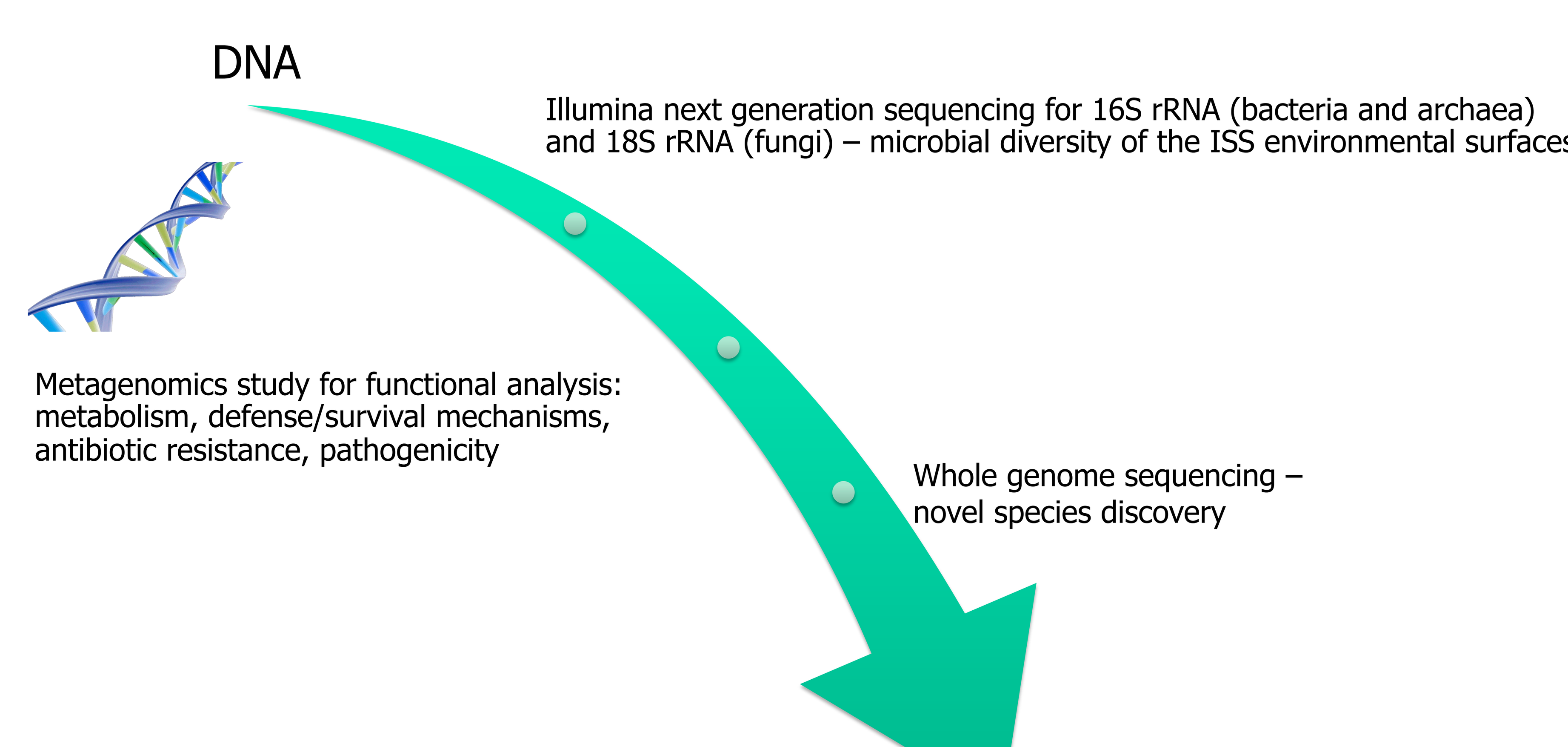

Data storage/accessibility:
1. ISS-MO – project database
2. GeneLab - NASA database for all genetic data
3. NCBI – worldwide database for biological data

Conclusions

- Two sampling campaigns revealed presence of diverse microbial population with some microbial species dominating in the ISS. The ongoing 16S rDNA Illumina sequencing will provide data on microbial diversity over time (subsequent months of sampling).
- The long-term goal of this project is aimed to develop practices for better cleaning and maintenance of the ISS, cataloguing and preserving beneficial microorganisms for future applications, and the general knowledge on microbial ecology of closed, environmentally controlled built systems.
- The microbial diversity study on the ISS will help to implement better practices for future robotic and human missions.

National Aeronautics and Space Administration
Jet Propulsion Laboratory
California Institute of Technology
Pasadena, California

Acknowledgments: Part of the research described in this publication was carried out at the Jet Propulsion Laboratory, California Institute of Technology, under a contract with NASA. This research was funded by a 2012 Space Biology NNH12ZTT001N grant # 19-12829-26 under Task Order NNN13D111T award to K. Venkateswaran. Government sponsorship acknowledged.

www.nasa.gov

Poster no. P-17